



MACQUARIE
University
SYDNEY · AUSTRALIA

Department of Biomedical Sciences
Faculty of Medicine and Health Sciences

*An investigation of systemic haemodynamic correlates of
intracranial pressure*

Julio Antonio Lara Hernandez (*M. Sc.*)

T H E S I S

Submitted in partial fulfilment of the requirements for the degree of
Master of Research in Biomedical Sciences

Supervisor:

Dr. Mark Butlin

Co-supervisor:

Dr. Alberto Avolio

July 2018

Abstract

Monitoring intracranial pressure (ICP) is vital to decide the appropriate clinical treatment of patients with conditions potentially causing high ICP (e.g. brain injury, cerebral tumor, and hydrocephalus). On the path for finding an alternative means to invasive ICP measurement, the only means to date for accurate ICP monitoring, this study investigates the relationship of ICP with systemic cardiovascular signals —heart rate (HR), aortic blood pressure (aBP), and carotid blood flow (cBF)— via rat experiments and signal analysis techniques. Whilst induced changes in aBP and cBF resulted in evident alterations of ICP magnitude, increases of mean ICP up to 49 mmHg showed minimal effect on HR, aBP, or cBF signals. Thus, a stepwise mixed-model regression proved that the cardiovascular parameters here studied have minimal but significant predictive value of ICP magnitude. Changes in HR were found to modify the waveforms observed in ICP, aBP, and cBF signals, without altering the magnitude or phase of transfer function models. The transfer function models were constructed as a function of mean ICP, mean aBP, and aBP or cBF waveforms, and they showed potential to reproduce the ICP waveform (Root Mean Square Error (RMSE) \leq 4 mmHg), being more accurate for mean aBP above 100 mmHg and mean ICP below 20 mmHg (RMSE \leq 0.5 mmHg). Likewise, estimation of pulse ICP showed a small error ($<1\pm 1.0$ mmHg) for mean ICP below 20 mmHg across a range of mean aBP (70–130 mmHg), proving considerable accuracy improvement in relation to previous studies.

Acknowledgements

I want to acknowledge Macquarie University for granting a full MRes scholarship for both tuition fees and living allowance. Without this funding my Master of Research would have been impossible. Special thanks to my supervisor, Mark Butlin, and my co-supervisor, Alberto Avolio, who gave me the opportunity of participating in their research group, trusting my academic ability. Likewise, thank you for conceding me knowledge, guidance, and support to complete my research project. Having developed my thesis with determination and commitment is perhaps the best way to thank you. I also would like to acknowledge Mi Ok Kim and Isabella Tan, who kindly instructed and helped me with signal and statistical analysis; your participation was key for the project. Fatemeh, Mahdiah, Alireza, Arthur and all the members of the research group thanks for making the office a friendly, warm, and supportive environment. Finally, thanks to my former supervisor, Jorge Zavala, and to my family who made my financial support and preparation (academic and personal) possible, so that I could travel to Sydney... friends and people from these and other places and times, thanks so much for building me up.

Statement of originality

Hereby I state that the current thesis has never been submitted before for a degree or diploma at any university. Likewise, to the best of my knowledge, the document has no previously published or written work from someone else, except where the appropriate reference is indicated; any contribution of others is explicitly acknowledged.

Julio Antonio Lara Hernandez
Department of Biomedical Sciences
Faculty of Medicine and Health Sciences
Macquarie University

10th July 2018

Declaration of contributions

Research project aims conceived by Professor Alberto P. Avolio and Dr. Mark Butlin. Review of current literature conducted by Julio A. Lara Hernández. The data used in this study comes from rat experiments performed by Dr. Mark Butlin. Data processing and analysis was carried out by Julio A. Lara Hernández. Interpretation of findings by Julio A. Lara Hernández with input from Professor Alberto P. Avolio and Dr. Mark Butlin.

Ethics approval

The work forming this thesis involves the analysis of data from rat experiments previously acquired and approved by the Macquarie University Animal Ethics Committee (Animal Research Authority 2016/005) (Appendix A).

Publications and conferences

Lara-Hernandez JA, Kim MO, Avolio AP, Butlin M (2018) Transfer function between intracranial pressure and aortic blood pressure and carotid blood flow. Conference paper and oral presentation at the 40th Annual International Conference of the IEEE Engineering in Medicine and Biology Society, Hawaii 17-21 July, 2018.

Lara-Hernandez JA, Tan I, Avolio AP, Butlin M (2018) Systemic cardiovascular inputs for estimating intracranial pressure magnitude and waveform. Poster presentation at ARTERY 18 Conference, Centro Cultural Vila Flor, Guimarães, Portugal 18-20 October, 2018.

TABLE OF CONTENTS

ABSTRACT	2
ACKNOWLEDGEMENTS	3
STATEMENT OF ORIGINALITY	4
DECLARATION OF CONTRIBUTIONS	5
ETHICS APPROVAL	6
PUBLICATIONS AND CONFERENCES	7
NOMENCLATURE	10
CHAPTER 1: INTRODUCTION	11
1.1. OBJECTIVES	12
1.1.1. <i>General</i>	12
1.1.2. <i>Specific</i>	12
1.2. HYPOTHESIS	13
CHAPTER 2: LITERATURE REVIEW	14
2.1. INTRACRANIAL DYNAMICS	14
2.1.1. <i>Intracranial content</i>	14
2.1.2. <i>Monro-Kellie hypothesis</i>	17
2.1.3. <i>Cerebral autoregulation</i>	18
2.1.4. <i>Intracranial pressure (ICP)</i>	19
2.1.5. <i>ICP waveform</i>	21
2.2. INVASIVE ICP MONITORING	22
2.2.1. <i>Intraventricular</i>	23
2.2.2. <i>Intraparenchymal</i>	24
2.2.3. <i>Epidural and subdural</i>	24
2.2.4. <i>Lumbar</i>	25
2.3. NON-INVASIVE ICP MONITORING	25
2.3.1. <i>Cardiovascular signals</i>	26
2.3.2. <i>Skull elasticity</i>	30
2.3.3 <i>Wave propagation</i>	31
2.3.4. <i>Ophthalmic</i>	33
2.3.5. <i>Otic</i>	36
2.3.6. <i>Fluid dynamics</i>	37
2.3.7. <i>Electrophysiologic</i>	38
2.3.8. <i>Morphology of intracranial structures</i>	40

CHAPTER 3: METHODS	42
3.1. DATA ACQUISITION	42
3.2. SELECTION OF DATA.....	46
3.3. STEPWISE MIXED-MODEL REGRESSION	46
3.4. FOURIER ANALYSIS	47
3.5. TRANSFER FUNCTION	49
3.6. MODEL ASSESSMENT.....	51
3.7. STATISTICAL TESTS	52
CHAPTER 4: RESULTS	53
4.1. STEPWISE MIXED-MODEL REGRESSION	53
4.2. FOURIER ANALYSIS	57
4.3. TRANSFER FUNCTION	62
4.4. MODEL ASSESSMENT.....	69
CHAPTER 5: DISCUSSION	73
5.1. INTRACRANIAL PRESSURE MAGNITUDE (MEAN AND PULSE)	73
5.2. INTRACRANIAL PRESSURE WAVEFORM	75
5.3. MODEL ASSESSMENT.....	79
5.4. LIMITATIONS AND POTENTIAL SOLUTIONS.....	81
5.5. PROJECT SIGNIFICANCE	83
5.6. FUTURE WORK	83
CHAPTER 6: CONCLUSION.....	85
REFERENCES.....	88
APPENDIX A: ETHICS APPROVAL FORM.....	120

Nomenclature

aBP	=	Arterial blood pressure
AF	=	Anterior fontanelle
cBF	=	Carotid blood flow
CPP	=	Cerebral perfusion pressure
CRV	=	Central retinal vein
CSF	=	Cerebrospinal fluid
CT	=	Computed tomography
ECG	=	Electrocardiogram
EEG	=	Electroencephalogram
HR	=	Heart rate
ICP	=	Intracranial pressure
IOP	=	Intraocular pressure
MRI	=	Magnetic resonance imaging
NIRS	=	Near infrared spectroscopy
OCT	=	Optical coherence tomography
ONS	=	Optic nerve sheath
oVEMPs	=	Ocular vestibular evoked myogenic potentials
PI	=	Pulsatility index
RMSE	=	Root mean square error
SE	=	Standard error
SLT	=	Scanning laser tomography
SMMR	=	Stepwise mixed-model regression
TCD	=	Transcranial doppler
TMD	=	Tympanic membrane displacement
VEPs	=	Visual-evoked potentials
VR	=	Ventilation rate

Chapter 1: Introduction

Intracranial pressure (ICP) is the sum of pressures exerted by the elements inside the skull (i.e. cerebral blood, cerebrospinal fluid, and brain tissue) (Partington & Farmery 2014). In normal conditions, ICP rhythmically fluctuates according to the cardiac and respiratory cycles, showing a mean value that ranges from 1.5–6 mmHg in infants up to 5–15 mmHg in adults (Andrews & Citerio 2004; Dunn *et al.* 2002). A close monitoring of ICP is particularly important for patients with conditions involving raised ICP, such as intracranial space occupying lesions, hydrocephalus or idiopathic hypertension, as even minor fluctuations in ICP may imply a different clinical management (Czosnyka *et al.* 1996b; Lavinio & Menon 2011; Davanzo *et al.* 2017; Gardner *et al.* 2017). The only accurate way so far for ICP monitoring is by direct measurement, which involves drilling a hole through the skull for placing a sensor inside the brain. This procedure is invasive and, consequently, it is associated with potential complications such as brain haemorrhage, infection, and catheter-tip drifting (Zhang *et al.* 2017).

To avoid the complications of invasive ICP monitoring, several non-invasive methods have been developed to estimate ICP from surrogate signals; however, none of them is accurate enough to be used clinically (Schmidt *et al.* 2002; Rosenberg *et al.* 2011; Bruce 2014; Nair 2016; Padayachy 2016; Robba *et al.* 2016; Khan *et al.* 2017; Zhang *et al.* 2017). Non-invasive estimation of ICP from cardiovascular signals, such as blood pressure and blood flow, seems one of the most promising approaches with the potential advantages of being economical and easy to use, while allowing bedside and continuous monitoring (Wagshul *et al.* 2011; Evensen *et al.* 2018). Since the use of cardiovascular signals as a mean for ICP estimation still requires further research, this Master of Research Project investigates, via rat

experiments and signal analysis techniques, the existence of predictive correlates from cardiovascular inputs including heart rate (HR), aortic blood flow (aBP) and carotid blood flow (cBF) to the magnitude and waveform of the ICP. This will set the basis for future studies on the development and testing of models that predict ICP from non-invasively acquired cardiovascular signals.

The objectives of this study are detailed in Section 1.1, followed by the study hypothesis in Section 1.2. A literature review focused on the intracranial dynamics and the invasive and non-invasive methods to monitor ICP is addressed in Chapter 2. Data acquisition and the procedures for data analysis are described in Chapter 3. The findings are reported in Chapter 4 and discussed in Chapter 5. Finally, the conclusion is presented in Chapter 6.

1.1. Objectives

1.1.1. General

To investigate the potential of cardiovascular signals (HR, aBP, and cBF) to be used for non-invasive ICP monitoring.

1.1.2. Specific

- To find predictors of ICP magnitude (mean and pulse) from parameters in cardiovascular signals.
- To find predictors of ICP waveform from cardiovascular signals.

1.2. Hypothesis

It is expected that cardiovascular signals can provide information on the magnitude and waveform shape of ICP because:

- 1) a potential physiological response to raised ICP, such as the Cushing Reflex at very high ICP, could be detected in the cardiovascular system.
- 2) reflected waves shaping the waveform of aBP or cBF may be influenced by ICP.
- 3) the pulsatility in the intracranial space has a cardiac origin.

Chapter 2: Literature Review

2.1. Intracranial dynamics

2.1.1. Intracranial content

The intracranial space is filled with three main nearly incompressible components: brain tissue, cerebral blood, and cerebrospinal fluid (CSF) (Galloon 1969; Tameen & Krowidi 2013; Partington & Farmery 2014; Oswal & Toma 2017). The human brain has a mass of about 1.4 kg, and it can be subdivided in three broad segments: forebrain, midbrain, and hindbrain. While the forebrain is responsible for higher functions such as memory and language, the hindbrain and midbrain are associated with basic life functions such as respiration and blood pressure. Additionally, brain tissue can be differentiated into gray matter (composed of unmyelinated neurons and other cells) and white matter (composed of myelinated axons) (Luria 1970; Donnelly 2014). Three layers (meninges) of connective tissue are responsible for wrapping and protecting the brain along with the spinal cord: dura mater (outer most layer), arachnoid, and pia mater (inner most layer) (Mack *et al.* 2009; Decimo *et al.* 2012).

Blood supply to the brain is via the internal carotid and vertebral arteries, which enter the skull via the carotid canals and foramen magnum, respectively (Takahashi & Mugikura 2010). Blood exits the cranial cavity through the internal jugular veins (Figure 1) (Tasker 2013). To provide an appropriate environment for neural activity, the blood is separated from the interstitial fluid of the brain by the blood-brain barrier created by tight junctions between capillary endothelial cells (Serlin *et al.* 2015; Gastfriend *et al.* 2017). Normal intracranial blood volume is around 150 mL, two thirds of which is in the venous system. Due to the high

brain energy demands, cerebral blood flow is large (700 mL/min) in comparison to the total blood in the cranium (150 mL) and accounts for more than 15% of total cardiac output (Partington & Farmery 2014; Oswal & Toma 2017). Additionally, cerebral blood is not uniformly distributed throughout the brain, being more abundant in grey matter than in white matter (Tasker 2013).

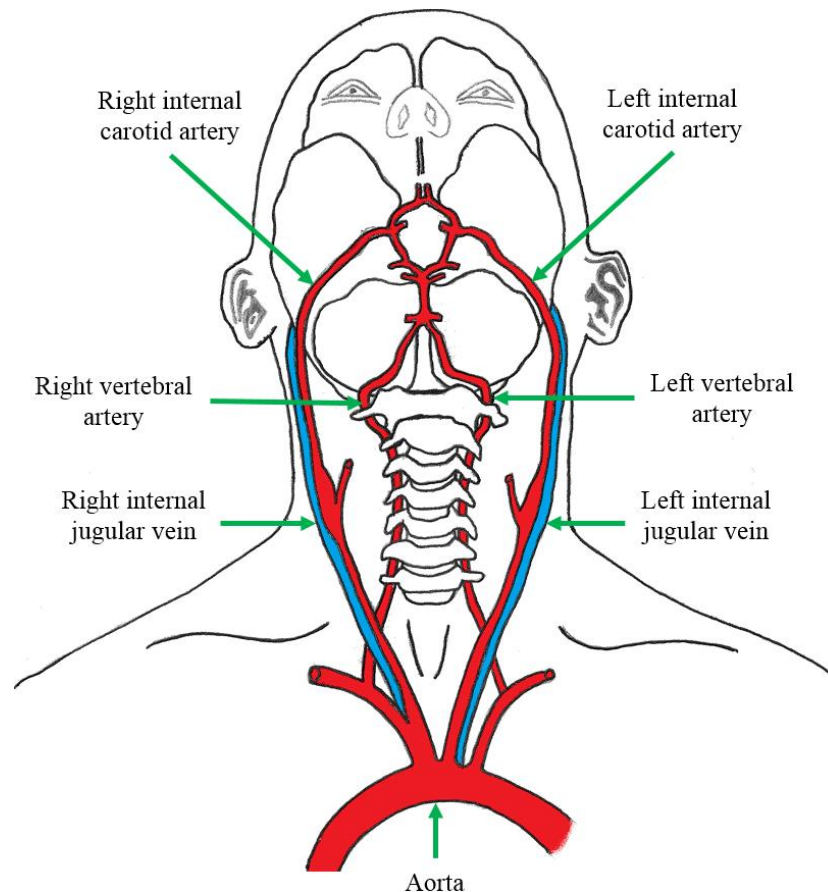


Figure 1. Pathways for inflow (arteries) and outflow (veins) of cerebral blood. Adapted and extended upon work of Morris (1997) and Scremin (2012).

CSF is a liquid composed of secretions from the choroid plexus (branched structures within specific regions of the cerebral ventricles) plus interstitial fluid from parenchymal capillaries and cellular metabolic processes. CSF is distributed in the ventricular system inside the brain, the cranial subarachnoid space around the brain, and the spinal subarachnoid space around the spinal cord (Figure 2), and it is separated from the vascular system by the blood-CSF

barrier (Cserr 1971; Milhorat *et al.* 1971; Tumani 2015a). The main functions of CSF are transport of materials (e.g. nutrients, waste products, hormones, antigenic material), protection by cushioning of the central neural system, and equilibrating the intracranial pressure (through CSF displacements between the cranial and spinal regions). CSF is mostly produced by the choroid plexus, and it is reabsorbed by arachnoid granulations of the venous system and brain capillaries (Tumani 2015b).

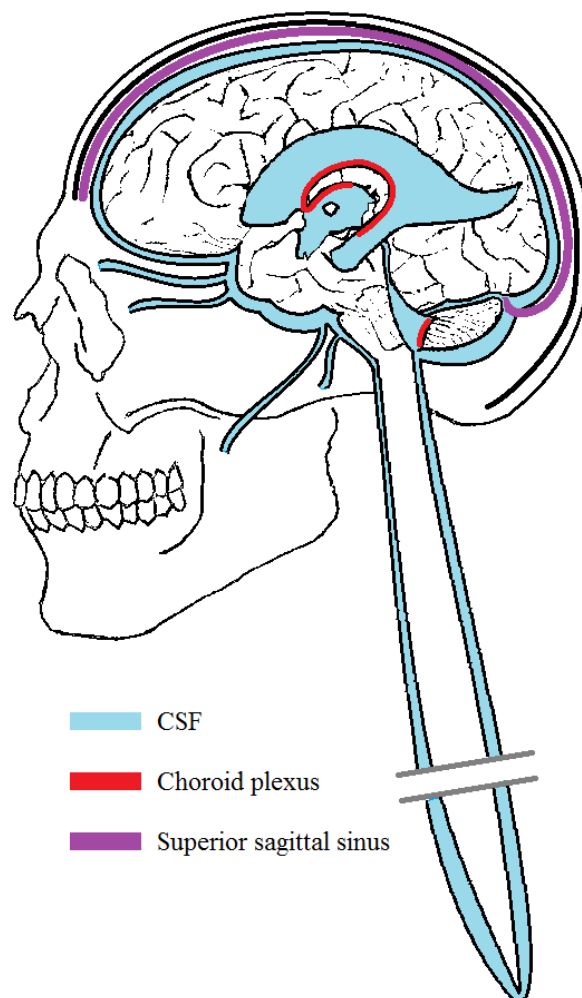


Figure 2. CSF surrounding the central neural system is mainly produced by the choroid plexus and reabsorbed by arachnoid granulations in the superior sagittal sinus. Adapted and extended upon work of Sakka *et al.* (2011).

2.1.2. Monro-Kellie hypothesis

The Monro-Kellie hypothesis (Monro 1783; Kellie 1824) states that if the skull is intact and rigid, then the sum of the volumes of brain, cerebrospinal fluid and intracranial blood is constant. Thus, considering that the intracranial contents are nearly incompressible, a volume increase in an intracranial component (e.g. blood) must cause a volume decrease in the other components (e.g. CSF) (Gallon 1969; Andrews and Citerio 2004; Partington & Farmery 2014). The Monro-Kellie hypothesis can be observed in the complex mechanisms that compensate for changes in intracranial blood volume caused by the cardiac cycle (Wilson 2016). Cardiac systole is associated with an expansion of the blood volume within elastic cerebral arteries, which leads to CSF displacement through the foramen magnum and an increase in venous outflow. In contrast, during diastole CSF re-enters the cranial compartment and venous outflow decreases. Arterial elasticity acts to dampen the arterial pulse pressure wave, and this contributes to the maintenance of a relatively stable ICP and cerebral blood flow (Oswal & Toma 2017). If the compensatory mechanisms fail, or the increase in volume of an intracranial component is too much, the inability of intracranial content to accommodate volume variations (low compliance) leads to raised ICP (Figure 3) (Rosner & Becker 1984; Partington & Farmery 2014).

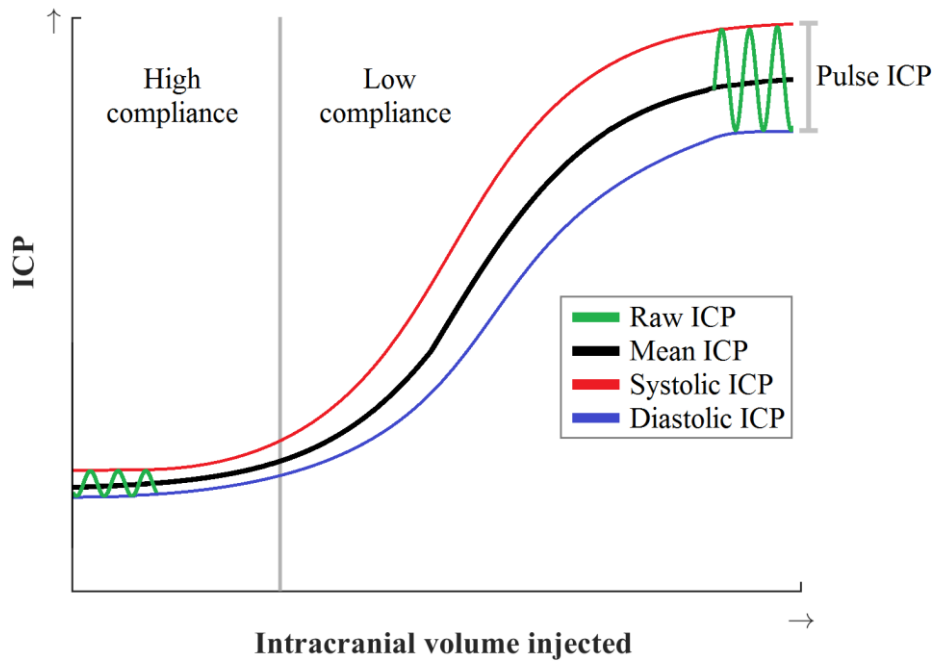


Figure 3. Pressure-Volume curve showing that injecting intracranial fluid after high-compliance exhaustion results in abrupt increments of both mean ICP and pulse ICP (systolic – diastolic ICP). Adapted and extended upon work of Oswal & Toma (2017).

2.1.3. Cerebral autoregulation

Blood flow to the brain is caused by the pressure gradient between ICP and arterial pressure. This pressure gradient is called cerebral perfusion pressure (CPP), and it is calculated by subtracting ICP from mean arterial blood pressure ($CPP = \text{mean arterial blood pressure} - ICP$). The high cerebral demand of oxygen and nutrients makes the brain intolerant to reduced blood inflow. For keeping the cerebral blood flow constant ($\sim 50 \text{ mL}/100 \text{ g}/\text{min}$) in an environment of changing arterial pressure and ICP, blood vessels react to oscillations of CPP in a process called cerebral autoregulation (Lang *et al.* 2002; van Beek *et al.* 2008).

Cerebral autoregulation involves adjustments in cerebrovascular resistance by actively dilating or contracting cerebral vessels through myogenic activity. Vascular smooth muscle constricts or dilates cerebral arterioles if CPP is, respectively, raised or reduced (van Beek *et al.* 2008; Oswal & Toma 2017). This intrinsic property of cerebral vessel resistance controls

downstream perfusion, independent of pressure, and limits the intraluminal pressure experienced by capillaries, whose thin walls are prone to injury. Vascular tone by local control mechanisms (e.g. release of dilator and constrictor substances) may also allow dynamic changes in the luminal diameter of vessels (Partington & Farmery 2014).

Autoregulation may have a detrimental effect under certain conditions of acutely raised ICP. For example, if ICP is raised by a haematoma, vasodilation due to autoregulation will be achieved to maintain cerebral inflow. Consequently, cerebral blood volume will increase, raising the already high ICP. Then, the higher ICP will promote vasodilation again, resulting in a vicious cycle (Giulioni & Ursino 1996; Powers *et al.* 2001; Partington & Farmery 2014; Oswal & Toma 2017).

2.1.4. Intracranial pressure (ICP)

ICP, the pressure inside the cranium, arises from the pressure exerted by the volumes of brain parenchyma (1200-1600 mL), cerebral blood (100-150 mL), and CSF (100-150 mL) within the skull (Partington & Farmery 2014). Under normal conditions, mean ICP varies with age (1.5-6 mmHg in infants, 3-7 mmHg in children, and 5-15 mmHg in adults; Figure 4) (Dunn *et al.* 2002) and fluctuates continuously according to the respiratory cycle and with a pulsatile cardiac component (Dardenne *et al.* 1969; Hamer *et al.* 1977; Kirkness *et al.* 2000; Andrews & Citerio 2004). Additionally, transient variations in ICP can be caused by posture, coughing, and straining (Alperin *et al.* 2005; Fan *et al.* 2008; Martin & Loth 2009; Oswal & Toma 2017).

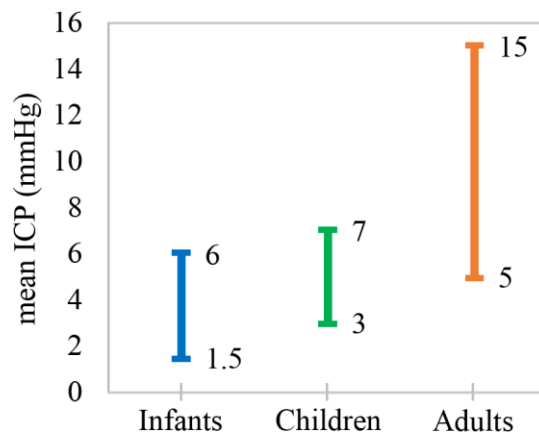


Figure 4. Normal range of mean ICP per group of age, according to Dunn *et al.* (2002).

An ICP higher than 15-25 mmHg is considered abnormally raised, and higher than 50 mmHg is likely to reduce the blood flow to the brain (Ryder *et al.* 1950; Dunn 2002; Roytowski & Figaji 2013; Bronzwaer *et al.* 2014; Lewis *et al.* 2016). If CPP falls below 15 mmHg through either an increase in ICP or decrease in blood pressure, a physiological response of the neural system, the Cushing reflex, is triggered, resulting in increased blood pressure, irregular breathing, and bradycardia (Cushing 1902, 1903). The Cushing reflex is usually seen in terminal stages of acute raised ICP, preceding brain herniation, global ischemia, and death (Kalmar *et al.* 2005; Wan *et al.* 2008). Some other symptoms of raised ICP include headache, papilloedema (swelling of the optic disc), vomiting, and deterioration in the conscious level (Carretero & Oparil 2000; Dunn 2002; Fan *et al.* 2008; Iencean & Ciurea 2008; Partington & Farmery 2014; Oswal & Toma 2017). Common pathologies causing raised ICP are space occupying lesions (e.g. traumatic haematomas, neoplasms, abscess, oedemas), overproduction or poor resorption of CSF (e.g. hydrocephalus), obstruction to the venous outflow (e.g. venous thrombosis), and possibly arterial hypertension (Kongstad & Grände 2001; Dunn *et al.* 2002). Possible procedures to relieve high ICP involve CSF drainage, elevation of the bedhead at 30° (improves jugular venous outflow), neuromuscular blockade (muscular activity may increase the intrathoracic pressure and obstruct cerebral outflow),

diuretics (remove fluid from the brain), and hyperventilation (induces vasoconstriction) (Dunn *et al.* 2002).

2.1.5. ICP waveform

Since the ICP waveform is synchronous with the arterial pulse (Figure 5), the origin of ICP pulsatility is thought to be mostly arterial (Dardenne *et al.* 1969; Cardoso *et al.* 1988; Wagshul *et al.* 2011; Kim 2014). Normally, an ICP pulse cycle shows three characteristic peaks (Figure 6): P1 (percussion wave), P2 (tidal wave), and P3 (dichotic wave). P1 originates from the pulsation of the choroid plexus; it is sharp and constant in amplitude. P2 represents the rebound after the initial arterial percussion; it is more variable in shape and amplitude than P1 is, and it ends in the dicrotic notch. P3 follows the dicrotic notch, and it has a venous origin. The dicrotic notch between P2 and P3 corresponds to the dicrotic notch of the arterial pulsation. As ICP increases, the amplitudes of P1 and P2 increases, then P2 exceeds P1, and finally all peaks become indistinguishable. This loss of the individual peaks produces a rounding appearance of the ICP waveform (Fan *et al.* 2008).

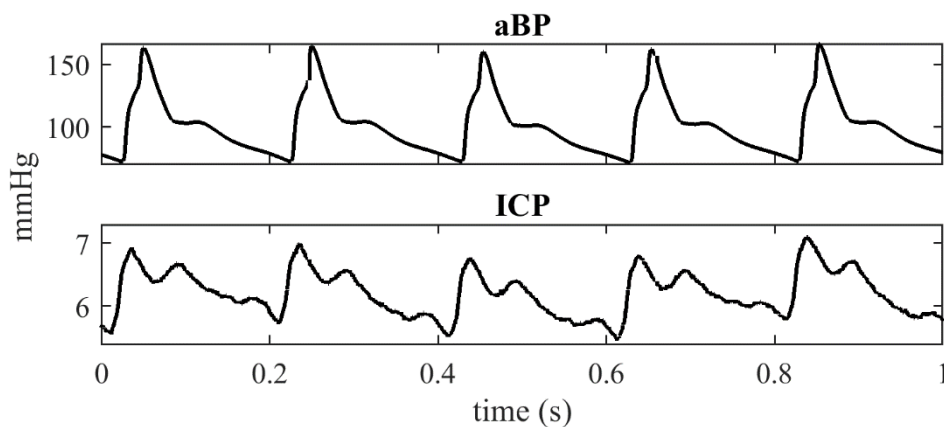


Figure 5. ICP and aortic blood pressure (aBP) recordings from the anaesthetized rat “female #3” considered in this study. The synchrony between these signals reflects the cardiac origin of ICP pulsatility.

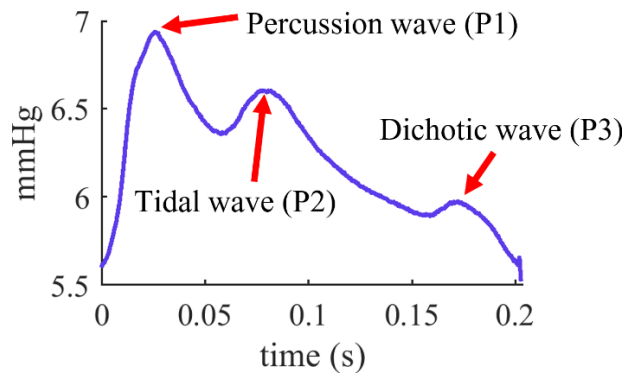


Figure 6. Average of 20 individual cycles from ICP recording of the anaesthetized rat “female #3” considered in this study.

Lundberg *et al.* (1965) described three types of minute-scale (i.e. smoothed, removing the cardiac pulsatile component) ICP waves in patients with raised ICP: A waves (also known as plateau waves), which show an increase from lower ICP to a mean ICP of 50–100 mmHg and last 5–20 min; B waves, recently redefined as slow waves and slow vasogenic waves, which reflect vasogenic activity of cerebral autoregulation (alterations in the timing of slow vasogenic waves may suggest reduced intracranial compliance), occur at a frequency of 0.33–3 cycles per minute with oscillations between a lower and higher ICP (up to 50 mmHg) (Momjian *et al.* 2004; Spiegelberg *et al.* 2016, 2018); and C waves, which last 4–5 min moving from a lower to a higher (up to 20 mmHg) ICP. C waves are of little clinical significance and may be present in normal people, B waves generally do not need any treatment, but A waves necessarily require interventions to reduce ICP and maintain CPP.

2.2. Invasive ICP monitoring

There are several modalities to invasively measure ICP, according to the place where the recordings are taken: intraventricular, intraparenchymal, epidural, subdural, and lumbar (Figure 7). These modalities generally require the opening of the skull for implantation of sensors with wires or catheters that pass through the skin to connect to monitors. Although telemetric, wireless, implantable microsensors constitute a promising and developing technology, they are not yet reliable and readily available (Zhang *et al.* 2017).

2.2.1. Intraventricular

In this method, considered the gold standard, measurements are obtained from inside the cerebral ventricles. The most accurate and reliable means for measuring ICP is by an intraventricular catheter coupled to a pressure transducer. The catheter is placed into one of the ventricles through a burr hole in the skull. The intraventricular method also allows CSF drainage as a therapeutic option when ICP is raised (The Brain Trauma Foundation 2000). However, four main shortcomings discourage intraventricular monitoring: (1) It may lead to CSF leakage, causing untrustworthy low readings (Zhang *et al.* 2017); (2) It is associated with infections and mechanical complications (Czosnyka *et al.* 1996a); (3) It may damage important cerebral tissue if placed incorrectly (Raboel *et al.* 2012); (4) It is a complicated and risky technique, especially when the ventricles are very small (Saladino *et al.* 2009).

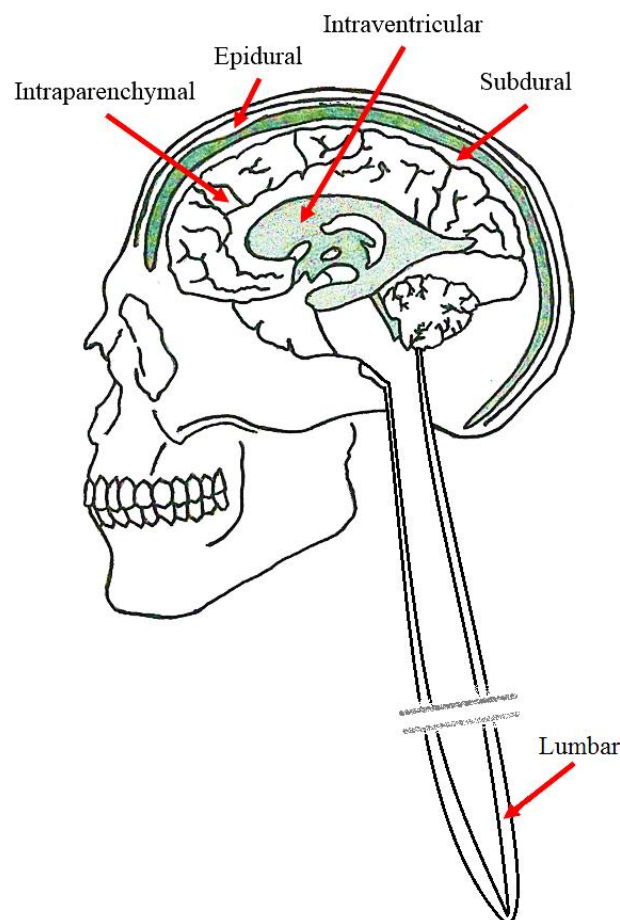


Figure 7. Places where ICP can be invasively measured. Redrawn from Ross & Eynon (2005).

2.2.2. Intraparenchymal

Measurements with this method are recorded inside the cerebral parenchyma (ideally 1-2 cm into the brain tissue), by microsensors based on optical fiber or electrical impedance (Zhang *et al.* 2017). These microsensors are accurate, minimally invasive, easy to place, and almost free of infections (Mack *et al.* 2003; Raboel *et al.* 2012). Thus, intraparenchymal measuring is the most frequent choice when ventricular drainage is not needed (Luerssen 1997; Wiegand & Richards 2007). Microsensors based on optical fiber need a wire kept in a straight line by a bolt (kinking the cable may produce bad recordings and disconnection; Stendel *et al.* 2003). On the other hand, microsensors based on electrical impedance can be inserted without a bolt (Anderson *et al.* 2004). The main disadvantage of the intraparenchymal technique is a small drift of the microsensors and the inability to drain CSF. Moreover, the local pressure detected by the sensors may be misleading since the ICP is not uniform within the brain (Zhang *et al.* 2017).

2.2.3. Epidural and subdural

For these methods pressure sensors are located between the skull and the dura (epidural) and between the dura and the brain (subdural). Since these methods do not invade the brain, they are less conducive to infections, haemorrhages, CSF leak, and seizures than the intraventricular method (Gaab *et al.* 1989; Raabe *et al.* 1998). A specific advantage of epidural sensors is the avoidance of dural penetration; however, they may be less accurate than intraventricular sensors (Bruder *et al.* 1995; Eide 2008). Subdural monitoring requires a large dural opening that involves the removal of a bone plate from the skull, plus it seems less reliable when measuring higher ICP. Both epidural and subdural measurements do not allow CSF drainage, and are almost unused (Zhang *et al.* 2017).

2.2.4. Lumbar

Measurements with this method involve puncture into the lumbar spinal CSF space. Lumbar puncture is not strictly an ICP measurement, but it accurately estimates ICP in patients whose CSF circulates freely through to the lumbar zone (Langfitt *et al.* 1964; Mertz *et al.* 2004; Speck *et al.* 2011). Lumbar puncture is the simplest and longest-standing ICP measurement method (Wiegand & Richards 2007); it is less risky than the other invasive methods, and it allows the drainage of CSF if needed (Tuettenberg *et al.* 2009; Speck 2011). However, lumbar puncture is not recommended when ICP is suspected to be high from a mass lesion because it may cause brain herniation (Kashif *et al.* 2012). Another drawback of the technique is that CSF in the lumbar spinal region may not reflect ICP in highly anaesthetised children (Wiegand & Richards 2007) or in case of an obstruction between the intracranial and intraspinal cavities (Eide & Brean 2006).

2.3. Non-invasive ICP monitoring

The association of invasive ICP monitoring with potential complications (e.g. anaesthesia, infections, haemorrhages, CSF leakage, obstruction, difficulty in placement) has prompted researchers to develop non-invasive techniques for ICP estimations. In general, non-invasive methods measure physiological variables that correlate with ICP; however, none of them has proved enough accuracy and ease of use for clinical monitoring (North 1997; Martínez-Mañas *et al.* 2000; Lang *et al.* 2003; Wiegand & Richards 2007; Shafi *et al.* 2008; Zhang *et al.* 2017). The existing non-invasive techniques to estimate ICP are described and critiqued below within eight categories according to their methodological origin: 1) cardiovascular signals, 2) skull elasticity, 3) wave propagation, 4) ophthalmic, 5) otic, 6) fluid dynamics, 7) electrophysiologic, and 8) morphology of intracranial structures.

2.3.1. Cardiovascular signals

System and signal analysis (Broughton & Kurt 2009; Perfetto *et al.* 2012; Alessio 2016; Giron-Sierra 2017a, 2017b) of cardiovascular parameters can be applied to estimation of ICP as has been previously done for arterial and venous blood flow and pressure (Karamanoglu *et al.* 1993; Chen *et al.* 1997; Silva *et al.* 2009; Avolio *et al.* 2009, 2010; Nayak *et al.* 2012; Butlin *et al.* 2013; Esper & Pinsky 2014; Gao *et al.* 2016), and constitutes a particularly promising and developing technology (Marmarou *et al.* 1978; Chopp & Portnoy 1980; Piper *et al.* 1990; Zou *et al.* 2008; Carrera *et al.* 2010; Golzan *et al.* 2012; Kao *et al.* 2013; Kim *et al.* 2017; Zhang *et al.* 2017). In this context cardiovascular signals have several advantages: 1) there is potential to estimate the whole complex ICP waveform, not only the mean value; 2) their potential to generate more accurate estimates is still high; 3) they are expected to allow a near-real-time monitoring on a beat-by-beat time scale; 4) they are relatively easy and inexpensive to obtain; and 5) specialized training would not be required and it is plausible that patient specific adjustments may not be required (Kashif *et al.* 2012; Kim 2014).

Jugular vein

Blood exits the intracranial space through the cerebral venous system. To keep the cerebral blood volume constant, a change in the arterial inflow to the brain would mean a change of the same magnitude in the venous outflow. If the venous outflow strives to match the arterial blood inflow (e.g. because of venous compression), accumulation of cerebral blood would lead to high ICP (Wilson 2016). It is well recognized that gentle pressure to the neck over the jugular veins (e.g. by using cervical collars) causes an ICP rise, and a linear relationship between jugular blood flow change rate and ICP has been reported (Allocca 1980; Verweij *et al.* 2001; Stone *et al.* 2010). Pranevicius *et al.* (2012) proposed a method to display jugular vein pressure value as an absolute value of ICP. The method measures the functional relationship between a jugular controlled occlusion and the blood pressure monitored in the

jugular vein. Rich *et al.* (2003) provided further evidence that venous outflow obstruction leads to elevated ICP, by finding significantly narrower jugular foramina in children with high ICP. The degree of compression of jugular veins assessed by ultrasound may also help in determining elevations in ICP. Through this imaging technique, it has been proved that cervical collars increase ICP through a mechanical effect on venous outflow from the brain (Stone *et al.* 2010; Zhang *et al.* 2017).

Arterial blood pressure

ICP is often expressed as a single mean value; however, ICP is inherently pulsatile, showing a complex oscillatory waveform through time. While respiratory- and vasomotor-induced oscillations contribute to ICP pulsatility, the main component is cardiovascular-induced pulsatility (Hamer *et al.* 1977; Cardoso *et al.* 1988; Greitz 2004; Tomycz *et al.* 2017). Each cardiac contraction produces an arterial blood pressure wave that propagates to the intracranial compartment, shaping the ICP wave. Since oscillation of ICP with the cardiac cycle is a result of the cardiac-driven variations in arterial blood pressure, estimating ICP from arterial blood pressure seems a reasonable proposition.

Dronkers (2011) used correlation techniques to study the association between ICP and blood pressure (mainly venous), and he concluded that little information about ICP can be extracted from blood pressure alone. However, his work suggests that other signals, such as blood flow, may reveal more information about ICP than pressure signals alone. One year later, Kashif *et al.* (2012) developed a model-based continuous estimation of ICP from cerebral blood flow velocity and arterial pressure, proving that non-invasive, continuous, calibration-free, and patient-specific estimation of ICP with clinically acceptable accuracy is feasible. However, their method still requires more accuracy and validation based on larger patient pools.

Kim *et al.* (2012) suggested that the cranial system absorbing arterial pulsations around the cardiac frequency (notch filter) (Kasuga *et al.* 1987; Zou *et al.* 2008; Wagshul *et al.* 2009, 2011) is probably an intrinsic property across species. This implies that results from animal experiments may be valid for humans, and that ICP could be potentially estimated by removing the cardiac frequency from arterial blood pressure. Kim *et al.* (2012) also recommend 1) to confirm the disappearance of the notch filter when cerebrospinal fluid is infused in rats; 2) assess the relative contribution of phase on the pressure transfer function spectra; and 3) investigate whether the transfer function spectra are consistently reproducible in the same animal across a range of heart rate frequencies. Johnston *et al.* (1972), Miller *et al.* (1973), Grubb *et al.* 1975, Beiner *et al.* 1997, and Eide (2016) have done some work on ventricular infusion testing along the lines of that proposed by Kim *et al.* (2012), though not in the context of examining the cardiac frequency (notch) filter characteristics.

More recent work supports the idea that the central aortic pressure wave, rather than the radial pressure wave, is a major determinant of the ICP waveform (Kim 2014; Kim *et al.* 2016a, 2017), except during very high ICP (Kim *et al.* 2015). Evensen *et al.* (2018) found that a transfer function approach to estimate the ICP waveform from the aBP waveform alone is not a reliable method for clinical use in idiopathic normal pressure hydrocephalus patients. However, it has been suggested that using arterial pressure waves in combination with arterial flow waves may provide a better estimate of ICP (Kim *et al.* 2015, 2016b; Lewis *et al.* 2016).

Cerebral blood flow velocity

Blood flow to the brain depends on the pressure gradient between the mean ICP (~10 mmHg) and the mean arterial pressure (~100 mmHg) exerted by the heartbeat. Thus, an increase in ICP may reduce this pressure gradient and consequently cerebral blood flow (Hanlo *et al.* 1995). However, when ICP is increased, the mean arterial pressure rises as a physiological response to maintain cerebral blood flow. Based on the former concepts, some studies have

attempted to estimate ICP from waveform analysis of cerebral blood flow velocity along with arterial pressure, obtaining from moderate to very high correlation between estimated and invasively measured ICP values (Schmidt *et al.* 2002; Xu *et al.* 2010; Kashif *et al.* 2012). It is this technique that forms the basis of a commercial non-invasive ICP monitoring system (ICM+, Division of Neurosurgery of the University of Cambridge, <https://icmplus.neurosurg.cam.ac.uk>).

The velocity of blood flow in cerebral vessels is measured by transcranial Doppler (TCD) sonography, a technique that detects the frequency shift between an emitted ultrasonic wave and the reflected wave from blood flowing in an artery in the intracranial space (Lupetin *et al.* 1995; Golzan *et al.* 2009; Popovic *et al.* 2009). This frequency shift directly correlates with the speed of blood (given a constant insonation angle), so that the analysis of an artery with TCD can be used to produce the waveform of the flow velocity in that artery. Since changes in the ICP may be reflected in the shape of the cerebral blood flow velocity waveform (Cardim *et al.* 2016), some studies have also attempted to estimate ICP from the cerebral blood flow velocity alone. In an adult study, the pulsatility index (PI, difference between systolic and diastolic flow velocity divided by the mean flow velocity) correlated well with ICP (correlation coefficient of 0.938, $p < 0.001$) (Bellner *et al.* 2004). A study in children with severe traumatic brain injury found the PI to be a less reliable indicator of absolute ICP values (Figaji *et al.* 2009). However, a subsequent study also in children found TCD to be an excellent examination for identifying patients likely to need invasive ICP monitoring (Melo *et al.* 2011). The inconsistencies among patient studies demand further research on the applicability of the cerebral blood flow velocity and arterial pressure to predict the ICP (Cardim *et al.* 2016).

2.3.2. Skull elasticity

Anterior fontanelle

Fontanelles are soft membranes that connect the bony plates of the infant skull in specific sections. The anterior fontanelle (AF), located at the top of the head, is the largest of all fontanelles, and it is usually closed when the infant is between seven and 20 months old (Aisenson 1950; Pindrik *et al.* 2014). In normal conditions, the AF of an infant is relatively firm and slightly curved inwards. An abnormal increase in the head circumference (possible because of the elastic nature of fontanelles) and an outward curving of a tense AF are typically good indicators of raised ICP (Padayachy 2016; Khan *et al.* 2017). In cases of very high ICP, the skull plates are sensed separated when touched, and distended veins are visible in the head (Wiegand & Richards 2007; Padayachy 2016).

Because the AF gives access to the intracranial compartment, several devices have been developed to assess the ICP via the AF. One of these devices is the fontogram (applanation transducer; Salmon *et al.* 1977), which has springs attached to a rod centered in a base plate. If a force is conducted across the AF, the rod experiments a relative displacement that can be used to measure and record the pulsations of the AF. Other devices such as the fontanometer (Davidoff & Chamlin 1959), which uses the principle of the Shiotz tonometer (a tool for estimating the intraocular pressure), and the Rotterdam Teletransducer (a resonator plus an electromagnetic coupled impedance measuring apparatus; Peters *et al.* 1995) have also been developed to estimate the ICP through the AF pulsations (Wiegand & Richards 2007). Recently, a technique using standard ICP probes secured against the AF was developed to epicutaneously measure transfontanelle ICP (Behmanesh *et al.* 2016). This novel method was reported as accurate as invasive epidural measurements; however, more studies supporting the results are needed. This method of ICP estimation is not available once the cranial plates are firmly fused (Padayachy 2016; Khan *et al.* 2017).

Bony deformities

Based on the hypothesis that the skull is not completely rigid, even after the closure of fontanelles, it has been proposed that tiny, but measurable, bony deformities of the skull can be used to estimate the ICP (Yue & Wang 2009). Pitlyk *et al.* (1985) devised and tested, on dogs and cadavers, an instrument to measure changes of the skull diameter in response to changes of ICP, concluding that their method should be sensitive enough to be used in clinical evaluation. Mascarenhas *et al.* (2012) confirmed that the consolidated skull of adults reflects a linear relation between the cranial deformation and ICP variations. Frigieri-Vilela *et al.* (2016) performed *in vivo* experiments to validate the method proposed by Mascarenhas *et al.* (2012), finding good agreement (Pearson's correlation coefficient $r = 0.8 \pm 0.2$, with a range of 0.31–0.99) between the measurements from deformation sensors glued onto the skull and direct ICP monitoring. However, the clinical applicability of this technique has yet to be evaluated (Khan *et al.* 2017).

2.3.3 Wave propagation

Mechanically induced waves

The vibration characteristics of a material (e.g. bone) changes according to the stress applied to it. Since the ICP generates stress in the skull bones, changes in the vibration characteristics of the skull imply changes in the ICP. If an input vibration (e.g. a vibration exciter transducer or impact hammer) is induced in some location of the skull, it creates a mechanical wave through the bone that can be detected (e.g. by an accelerometer, velocity sensor, or displacement sensor) as an output vibration in another part of the skull. Analyzing the differences (e.g. with a spectrum analyzer, a dynamic signal analyzer, or network analyzer) between repeated input and output vibrations can be used to estimate values of the ICP over time (Mick 1991, 1992; Sinha 2000). Li & Luo (2010) used finite element modelling to study the correlation between ICP and vibration responses of the head, finding that the ICP is the

only factor making a difference in the vibrational response. However, the vibrational responses were not equally sensitive to the changes of ICP.

Acoustically induced waves

The way in which an ultrasonic wave propagates through the skull depends on the acoustic properties of the intracranial content. Since these properties are influenced by the ICP (e.g. changes in the volume of any intracranial element affect transit time of ultrasonic waves; Ragauskas *et al.* 2003), it has been aimed to estimate the ICP by comparing the characteristics (e.g. speed and attenuation) of an ultrasonic input wave against its characteristics after travelling through the head (Ragauskas & Daubaris 1995; Michaeli & Rappaport 2002; Ragauskas *et al.* 2003; Fountas *et al.* 2005; Popovic *et al.* 2009). To emit and detect ultrasonic waves through the brain, two transducers are located on the cranium opposite walls, or a single transducer may be used for both generating the incident wave and measuring the reflected wave (Popovic *et al.* 2009).

Considering that the pulsatility of the ICP depends on the heartbeat, Michaeli *et al.* (2002) obtained an estimated ICP wave by digitally processing transcranial ultrasonic signals along with electrocardiogram measurement. In a preliminary clinical trial, the ICP wave estimated from their analysis showed a good correlation with that obtained from standard invasive methods (Michaeli *et al.* 2002). In addition, Ganslandt *et al.* (2017) found a strong positive linear relationship between invasively measured ICP and the ICP estimated from advanced signal analysis of acoustic waves propagating through the cranium. However, for most of ultrasonic transcranial methods, accuracy remains unclear and the validation for clinical use is scarce. The specific angles and locations of transducers influence ICP estimations, and this also decreases the reliability of the method. More research is also needed to evaluate how the measurements are affected by other factors such as brain shift or intracranial pathologic

masses (e.g. blood collections or tumors) (Schmidt *et al.* 1997; Levinsky *et al.* 2016; Khan *et al.* 2017; Zhang *et al.* 2017).

2.3.4. Ophthalmic

The optic nerve sheath

The optic nerve, which originates from the central neural system, is surrounded by CSF and then encased by a dural optic nerve sheath (ONS). Thus, an increase of ICP may push CSF around the optic nerve, causing an expansion of the ONS diameter (Helmke & Hansen 1996; Hansen & Helmke 1997). Changes in the ONS diameter can be visualised and measured with different imaging techniques such as optical coherence tomography (OCT), scanning laser tomography (SLT) and magnetic resonance imaging (MRI) (Robba *et al.* 2016; Padayachy *et al.* 2016). The assessment of the ONS diameter is a promising non-invasive method for the prediction of ICP since several studies have demonstrated a strong, almost direct, association between the distension of the ONS and ICP values (Geeraerts *et al.* 2008; Rajajee *et al.* 2011; Kimberly *et al.* 2008; Soldatos *et al.* 2008; Hansen & Helmke 1997; Wang *et al.* 2015). However, it does require expensive specialized equipment for measurement.

The central retinal vein

Since the optic nerve, which contains the central retinal vein (CRV), is immersed in CSF, both the nerve and the CRV are closely influenced by the ICP. As ICP rises, so does the resistance to retinal venous outflow; consequently, CRV pressure is enhanced to compensate the ICP effect on outflow resistance (Firshing *et al.* 2000, 2011; Querfurth *et al.* 2004, 2010; Morgan *et al.* 2012). In clinical practice, a suction cup (ophthalmodynamometer) surrounding the eye is used to increase the intraocular pressure until a collapse of the CRV is observed (the vein swells and lose tension in its wall) (Baurmann 1925). The pressure value at the

collapse point is the venous outflow pressure, and it has been found to linearly predict absolute ICP (Querfurth *et al.* 2010; Firshing *et al.* 2000, 2011).

In addition, the pulsations of the CRV (visible changes in the retinal vein calibre) are typically in phase with the ICP pulsations (Firshing *et al.* 2000; Golzan *et al.* 2012; Morgan *et al.* 2012). A reduction or absence of CRV pulsations may suggest an elevated ICP; however, 10% of normal people lack visible CRV pulsations (Levin 1978; Jacks & Miller 2003). To assess the CRV, the pupils must be dilated by an experienced ophthalmologist. Another disadvantage of the technique is that the cumbersome application of external ocular pressure can generate the oculo-cardiac reflex followed by hypotension, an undesired condition especially when ICP is increased (Padayachy 2016; Zhang *et al.* 2017).

The retina

The thickness of the retinal nerve fiber layer is usually altered (augmented) when the ICP is abnormally raised, and the degree of alteration has been found to correlate with ICP values (Hee *et al.* 1995; Heckmann *et al.* 2004; Savini *et al.* 2004; Scott *et al.* 2010; Driessen *et al.* 2014; Huang-Link *et al.* 2015). Imaging techniques such as optical coherence tomography (OCT) and scanning laser tomography (SLT) are very promising to quantify and evaluate the retinal morphology (Kruse *et al.* 1989; Rohrschneider *et al.* 1998; Trick *et al.* 1998; Anand *et al.* 2016; Swanson *et al.* 2017). However, the retina assessment through these techniques seems unreliable in patients with severe disk edema (optic disc swelling) or chronic high ICP previously treated (Skau *et al.* 2013; Bruce 2014). In addition, its clinical value in reliably predicting the ICP still demands further assessment (Padayachy 2016).

The pupil

It has been suggested that the change of the pupillary diameter as a response to light stimulation is affected by medical conditions involving high ICP (Chesnut *et al.* 1994; Chen

et al. 2011, 2014). Pupillometers are devices for accurately measuring the pupillary diameter during light stimulation (Larson & Muhiudeen 1995; Du *et al.* 2005; Meeker *et al.* 2005; Chen *et al.* 2011, 2014; John 2015; Couret *et al.* 2016). After the light stimulus, the pupillary diameter has been reported to decrease around 34% in normal people, 20% in head trauma patients (indicating high ICP), and 10% in patients with an ICP higher than 20 mmHg (Taylor *et al.* 2003). Thus, a reduction in the pupillary reactivity to light is associated to increased ICP values. Although the change of pupil diameter measured by a pupillometer reflects the ICP, some ocular and neurological conditions unrelated to ICP, as well as drugs, emotions, and the time of day, also influence pupillometry measurements (Fountas *et al.* 2006).

The intraocular pressure

Because of the anatomical proximity and direct communication between the eye and the intracranial space, several studies have been conducted to estimate the ICP by means of the intraocular pressure (Salman 1997; Lashutka *et al.* 2004). Additionally, the ease of use of tonometers, the devices that measure IOP, increased the interest in employing intraocular pressure as a quick indicator of high ICP (Lashutka *et al.* 2004; Padayachy 2016). Several studies have tested the correlation between intraocular pressure and ICP, and many of them conclude that intraocular pressure by itself is not an effective predictor of ICP due to its poor specificity and sensitivity (Sheeran *et al.* 2000; Lashutka *et al.* 2004; Sajjadi *et al.* 2006; Han *et al.* 2008; Spentzas *et al.* 2010; Golan *et al.* 2013; Chunyu *et al.* 2014; Khan *et al.* 2017). Nevertheless, intraocular pressure in conjunction with other physiological parameters such as blood pressure may provide better estimates of the ICP (Wang *et al.* 2014).

2.3.5. Otic

Tympanic membrane displacement

The ear is influenced by CSF due to the connection between the perilymph (a fluid like CSF) of the cochlea (the ‘hearing’ part of the inner ear) and the CSF of the posterior cranial fossa (part of the cranial cavity housing the cerebellum, medulla, and pons). The tympanic membrane is a thin and tense layer that displaces when receiving sounds, to transmit them to the inner ear. Tympanic membrane displacement (TMD) is transmitted through the ossicles (three small bones in the middle ear) to the fluid-filled cochlea. As the perilymph and CSF communicate through the cochlear aqueduct, changes in ICP may affect the direction and magnitude of TMD.

TMD may be assessed in response to sound stimulation (acoustic reflex) (Marchbanks 1984), and it has been found that an inward TMD is suggestive of high ICP, while an outward TMD is suggestive of normal or low ICP (Reid *et al.* 1990). While TMD assessment appears to be useful for detecting raised ICP, its limited accuracy prevents it from providing a quantitative estimate of ICP (Gwer *et al.* 2013). A further limitation is that it was not possible to perform a valid TMD measurement in approximately 60% of patients (Shimble *et al.* 2005), which raised doubts about the clinical value of the technique. TMD assessment is limited by poor intersubject reproducibility, and it is influenced by the permeability of the cochlear aqueduct, integrity of the tympanic membrane, and strength of the acoustic reflex (Padayachy 2016).

Otoacoustic emissions

Otoacoustic emissions are sounds produced by the cochlea of the inner ear in response to loud noises (Kemp 1978), and the otoacoustic emission characteristics (angles and magnitude) have been shown to vary with ICP (Avan *et al.* 1996; Voss *et al.* 2006; Olzowy *et al.* 2008). Thus, otoacoustic emissions have been considered a valuable tool for predicting

high ICP non-invasively (Bershad *et al.* 2014; Williams *et al.* 2016). However, several limitations are associated to this method: it cannot be applied on patients with sensorineural or conductive hearing deficits; it provides a detection of ICP changes, rather than absolute ICP values; and it has a large intersubject variability (Buki *et al.* 1996, 2009; Robba *et al.* 2016).

2.3.6. Fluid dynamics

Magnetic resonance imaging-based elastance index

Magnetic resonance imaging (MRI) can be used to calculate the change of intracranial volume by considering the arterial inflow and venous outflow in the brain, as well as the flow of CSF between the cranium and spinal compartment. These variables are then used to derive ICP via an elastance index, representing the ratio of pressure to volume change (Marmarou *et al.* 1975; Alperin *et al.* 2000, 2005; Raksin *et al.* 2003). Using a motion-sensitive technique, the flow during the cardiac cycle is calculated by multiplying the blood velocity by the cross-sectional areas of blood vessels obtained from static MRI scans (Popovic *et al.* 2009). Alperin *et al.* (2000) demonstrated a strong correlation between the MRI derived elastance index and invasively measured ICP. These results, however, were found to have poor repeatability in a subsequent study, due to technical errors in measurement and intra-individual variation, with the authors suggesting caution when interpreting individual measurements (Marshal *et al.* 2008). In another study, Glick *et al.* (2006) found that a normal ICP value derived from MRI in patients with hydrocephalus is a strong predictor of a good clinical outcome without the need of surgical intervention. In children with hydrocephalus, dynamic MRI correlated well with shunt valve opening pressure and symptom resolution (Muehlmann *et al.* 2013). MRI seems a promising technique that could potentially detect chronic disorders associated with increased ICP values. However, the method is expensive, cumbersome, and impractical for continuous monitoring of ICP (Padayachy 2016; Zhang *et al.* 2017).

Near infrared spectroscopy

Near infrared spectroscopy (NIRS), a technique based on the interaction between matter and near-infrared electromagnetic radiation, can be used to provide a continuous estimation of cerebral blood volume and flow by recording the concentration of deoxygenated and oxygenated haemoglobin in the cerebral blood. A decrease in cerebral oxygenation would imply a reduced cerebral blood flow and velocity, suggesting an increased ICP (Weerakkody *et al.* 2010; Zweifel *et al.* 2010). A strong relationship, which seems to change during peaks of ICP, between NIRS parameters and ICP has been found (Weerakkody *et al.* 2010, 2012). On the other hand, Davies *et al.* (2015) indicated that there is insufficient evidence to affirm that NIRS can detect significant changes in ICP as accurately as any invasive monitoring modality. In addition, the method is limited by NIRS equipment availability, it involves several hours of patient monitoring to obtain the required parameters, and it can only be reliably measured in about 50% of recordings (Zweifel *et al.* 2010). Future clinical tests are needed to validate the sensitivity of this method for detecting or predicting changes in ICP. Nonetheless, NIRS technology is developing and improving rapidly, being integrated with other imaging applications to obtain better results (Zhang *et al.* 2017; Khan *et al.* 2017).

2.3.7. Electrophysiologic

Electroencephalogram

Gradual increase of ICP will lead to a reduction in the cerebral blood flow, causing a shortage in the oxygen and glucose needed for cellular metabolism (to keep tissue alive). When this occurs, the patient experiences different levels of loss in consciousness (Balestreri *et al.* 2006). Electroencephalogram (EEG) power spectrum is a non-invasive technique involving signal analysis to monitor the electrical activity of the brain (Otto 2008; Czigler *et al.* 2008). Since this technique has been used to assess the level of consciousness and the depth of anaesthesia (Drummond *et al.* 2000), the estimation of ICP from EEG power spectrum has

also been proposed for detecting very high ICP. Chen *et al.* (2012) found a significant negative correlation between the intracranial pressure index (an index derived from EEG power spectrum analysis) and the ICP, suggesting that the analysis of specific parameters from EEG power spectrum may reflect the ICP. The existence of wireless, portable, and field deployable EEG systems encourages the application of this technique; however, its clinical utility still depends on validation through further research (Chen *et al.* 2012; Padayachy 2016). It is also unlikely to be sensitive to changes in the lower range of ICP.

Visual-evoked potential

Visual-evoked potentials (VEPs) are measurements of the electrical activity recorded at the scalp over the occipital cortex (visual processing centre of the brain) in response to light stimuli. They are used to detect electrical alterations of the visual pathways from the retina through the optic nerves up to the occipital cerebral cortex. Any disorder affecting the physiological function of visual pathways, including elevated ICP, can theoretically be detected as VEP alterations. VEPs are recorded with EEG electrodes while the patient is visually stimulated with flashing lights. The ICP is then estimated from elements of the recorded VEP waveform (York *et al.* 1981; Wu & Ji 2007). Several authors found good correlations between VEPs and ICP in both adults (Zhao *et al.* 2005) and children (York *et al.* 1981), suggesting that the VEP-based method can detect ICP with accuracy, safety, and ease. Despite the optimistic results, the method has also shown a wide inter- and intra-subject variability in the VEP waveform of healthy subjects. This variability may make the technique less reliable as a predictor of ICP (Andersson *et al.* 2012; Robba *et al.* 2016).

Ocular vestibular evoked myogenic potentials

Ocular vestibular evoked myogenic potentials (oVEMPs) are measurements of the electrical activity recorded at the inferior oblique muscle (near the anterior margin of the floor of the eyeball) in response to vestibular stimulation. It is used to assess the vestibular system (part

of the labyrinth of the inner ear), which provides the sense of balance. The vestibular stimulation used to generate electrical activity of extraocular muscles is recorded from the contralateral eye using surface electrodes. Jerin *et al.* (2015) found that increasing ICP systematically alters oVEMPs in terms of absolute amplitudes and frequency tuning characteristics. Thus, oVEMPs may have potential for non-invasive ICP monitoring; however, substantial research is still needed to evaluate the technique (Padayachy 2016).

2.3.8. Morphology of intracranial structures

The morphology of several elements in the intracranial space has been considered to predict elevated ICP: the midline shift (a shift of the brain past its centre line); the size of sulci (folds in the cerebral cortex); the morphology of cisterns (regions of the subarachnoid space where CSF accumulates, Eisenberg *et al.* 1990) and ventricles (cavities in the brain where CSF is produced, Eide 2003); the size of intracerebral hematoma (accumulated blood); and the presence of contusions or subarachnoidal blood. However, none of these findings has demonstrated sufficient reliability to assess increased ICP, and the discussion regarding which of the morphological parameters correlates best with raised ICP is still ongoing (Hiler *et al.* 2006; Robba *et al.* 2016; Rosenberg *et al.* 2011).

Computed Tomography (CT) scan has been the most widely used imaging technique for assessing the morphology of intracranial elements in patients with raised ICP, and its benefit in the context of traumatic brain injury has been broadly investigated (Toutant *et al.* 1984; Eisenberg *et al.* 1990; Hiler *et al.* 2006). Although CT scans are still a valuable diagnostic complement (when used alone, its low specificity is a major limitation) in the acute diagnosis of elevated ICP, a normal CT does not rule out a high ICP. Additionally, the patient must be exposed to radiation when subjected to a CT scan. Thus, the radiation effect over the lifetime of the patient must be considered, especially in children as the brain is still developing (Krille

et al. 2012; Pauwels & Bourguignon 2012). MRI could be safer and more reliable than CT, but its limited availability and long imaging time prevent its widespread use and like CT is not useful for continuous monitoring of ICP (Robba *et al.* 2016).

Despite several non-invasive methods for ICP monitoring have been developed, as described in previous sections, none of them is accurate enough for clinical use, most of them estimate mean ICP alone, they cannot provide continuous monitoring, or they are expensive and impractical. Thus, the focus of this study is to generate knowledge useful for estimating ICP from cardiovascular signals, a promising method with potential for continuous monitoring of the full ICP waveform while being inexpensive and easy to use.

Chapter 3: Methods

The study aimed to investigate the relationship between cardiovascular signals and mean and pulse ICP as well as the ICP waveform itself. Whilst it is aimed for the information to be used in human studies, animal studies were used due to the ability to control and manipulate both ICP through normal to pathologically high levels whilst also controlling and manipulating cardiovascular variables. Such studies are ethically impossible to perform in humans. The animal studies allowed measurement under controlled conditions across a wide physiological range of pressure, HR, and ICP levels to investigate the robustness of the relationship between cardiovascular signals and ICP.

3.1. Data acquisition

Data come from rat experiments (Figure 8) conducted to facilitate the identification of possible relationships between ICP and cardiovascular parameters (HR, aBP, and cBF). All the animal procedures were approved by the Macquarie University Animal Ethics Committee (Animal Research Authority 2016/005) (Appendix A).

Sprague-Dawley adult rats (6 females and 7 males, 12-20 weeks old) were anesthetized with intraperitoneal urethane (1.3 g/kg, 10% w/w solution), keeping body temperature at approximately 37 °C throughout the experiments using a heating mat regulated to rectal temperature. Rats were artificially ventilated via a tracheal tube (3 mg/kg of 2 mg/ml pancuronium i.v. at 0.2 ml/h was used to stop involuntary breathing), with variation of tidal volume for a target end tidal CO₂ of 4.0±0.5%.

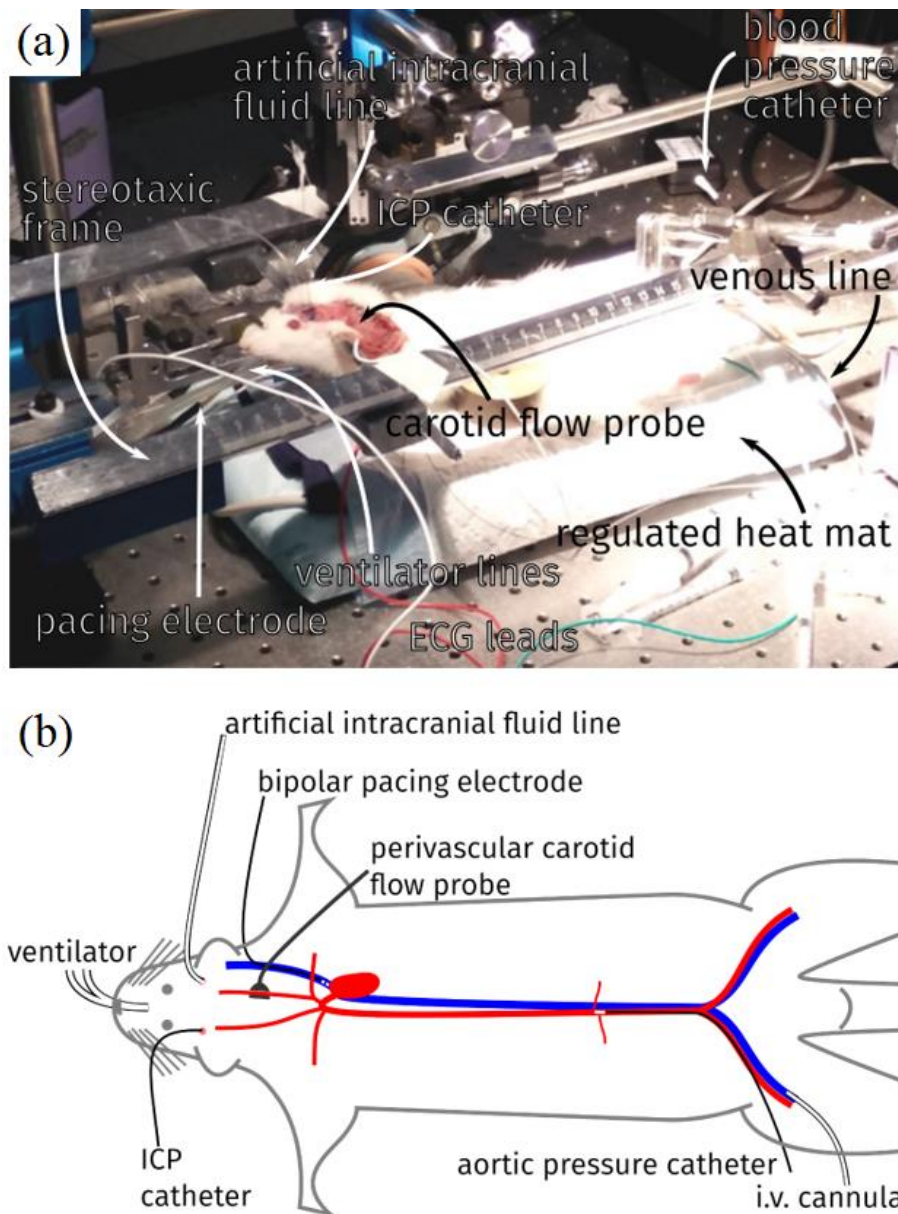


Figure 8. Photography (a) and schematic (b) of the experimental setup, showing positioning of stereotaxic frame, heat mat, ventilator, transducers for cBF, aBP and ICP and for lines for HR pacing and administering of fluids.

For ICP measurement, a 0.7 mm diameter hole was drilled through the skull (6 mm posterior to the bregma and 2.5 mm lateral of the midline, position obtained using a Kopf rodent stereotaxic frame coupled with an XYZ-micromanipulator) to place a 1.2 F high fidelity pressure sensor (Transonic Scisense) in the brain parenchyma (3-5 mm depth). A second 0.7 mm hole was drilled in the same position on the contralateral side to place a line into the CSF

fluid for infusion of artificial CSF. To measure aBP, another pressure sensor was inserted into the descending aorta via the femoral artery. cBF was measured with a perivascular ultrasound probe fitted to one common carotid artery (ventral approach). HR was measured with electrocardiogram limb leads in the lead II position. An inhouse manufactured bipolar pacing electrode was introduced adjacent to the right atrium via the right jugular vein for heart pacing. ICP, aBP, cBF, and electrocardiogram signals were continuously recorded at 5 kHz using (Figure 9) a Cambridge Electronic Design 1401 data acquisition system with Spike software (Version 7.09).

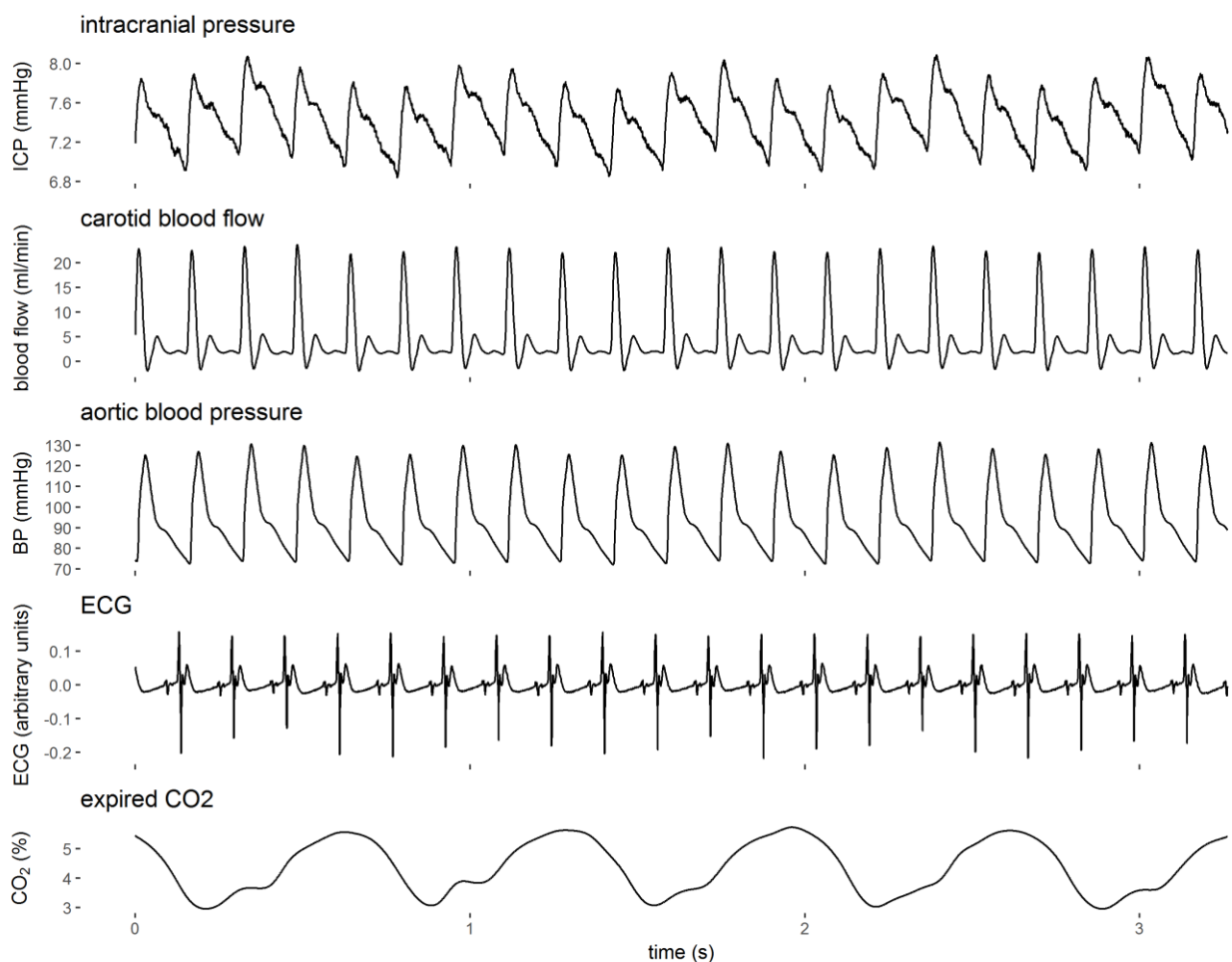


Figure 9. Example of physiological signals recorded during the rat experiments.

At the resting anaesthetized heart rate, measurements of the above signals were taken at ventilation rates (VRs) of 60 and 90 breaths/min. With VR returned to 90 breaths/min, intravenous ivabradine (2 mg/kg) was administered to lower HR, and then the heart was paced at 300, 350, 400, 450, and 500 bpm in a randomized order. HR pacing was triggered by driving an isolated pulse stimulator set to deliver a square pulse of 2 to 3 ms of amplitude 0.6 to 1.0 V adjusted as required. At each VR and pacing rate, mean arterial blood pressure was raised to approximately 130 mmHg and lowered to approximately 70 mmHg with intravenous injections of phenylephrine and sodium nitroprusside respectively.

In addition to these measurements at resting ICP (<10 mmHg mean ICP), ICP was raised by infusion of artificial CSF () at three levels: moderately high (10-15 mmHg mean ICP); high (15-20 mmHg mean ICP); and very high (>20 mmHg mean ICP). At each raised level of ICP the heart was paced at 400 and 500 bpm with blood pressure manipulation as previously described at each heart rate for each level of ICP. The permutations of mean ICP, VR, HR and mean aBP within the protocol are listed in Table I. The number of used rats could not be kept the same for all permutations due to technical setbacks related to intersubject variability (each rat was more or less susceptible to experimental treatments) and time availability for experimental procedures.

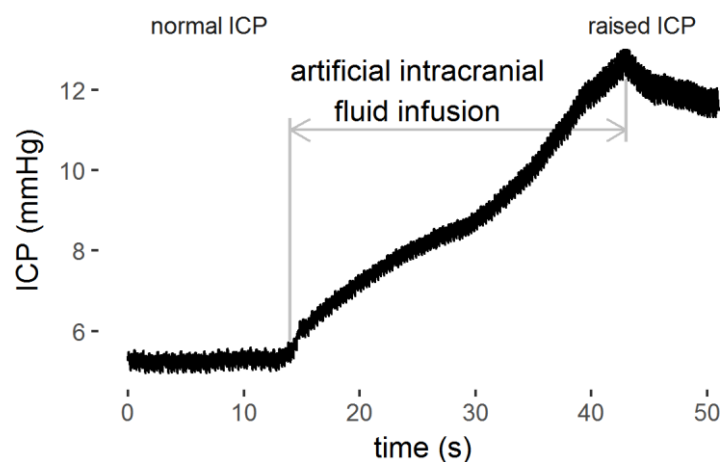


Figure 10. Artificial CSF was infused to raise ICP.

Table I. Experimental permutations and the number of rats measured at each permutation. This number could not be kept constant due to technical setbacks related to intersubject variability (each rat was more or less susceptible to experimental treatments) and time availability for experimental procedures.

Mean ICP	VR (breaths/min)	HR (bpm)	Mean aBP (mmHg)	Rats (n)
Resting (<10 mmHg)	Resting	Resting	Resting	13
	60	Resting	70, 100, 130	11
	90	Resting	70, 100, 130	11
	90	300	70, 100, 130	11
	90	350	70, 100, 130	11
	90	400	70, 100, 130	11
	90	450	70, 100, 130	11
	90	500	70, 100, 130	11
Moderately high (10-15 mmHg)	90	400	70, 100, 130	6
	90	500	70, 100, 130	6
High (15-20 mmHg)	90	400	70, 100, 130	7
	90	500	70, 100, 130	7
Very high (>20 mmHg)	90	400	70, 100, 130	8
	90	500	70, 100, 130	8

3.2. Selection of data

A time interval of twenty consecutive cardiac cycles of data were extracted for each rat at each permutation (Table I) to perform the subsequent statistical and signal processing analysis. The 20 cycle sets were selected making sure that the individual cycles were intact and free of artifacts. A length of 20 cycles was used as it was adequate for Fourier analysis, including enough data to resolve respiratory fluctuations, but still short enough to avoid substantial changes in mean aBP, the effect of the drugs used to manipulate aBP is transient.

3.3. Stepwise mixed-model regression

To find predictors of mean and pulse ICP, cardiovascular parameters –heart rate, mean aBP, minima aBP, maxima aBP, pulse aBP, mean cBF, minima cBF, maxima cBF, pulse cBF– were collected from the selected data at the four levels of mean ICP, a constant VR of 90 breaths/min (available for the four levels of mean ICP), paced HRs of 400 and 500 bpm (available for the four levels of mean ICP), and at the three levels of mean aBP (70, 100, and

130 mmHg) (Table I). Thus, this data subset was used as input for a stepwise mixed-model regression (SMMR) analysis performed with R (version 3.5.0). The analysis is a step-by-step iterative construction of a regression model, in which explanatory variables are selected by a combination of 1) adding independent variables in the regression model if they are linearly correlated with the response variable (ICP), and 2) including all the independent variables initially and then eliminating them if they show no linear correlation with the response variable (ICP) (Yan & Su 2009). The stepping criteria model selection was based on the Akaike information criterion.

3.4. Fourier analysis

The Fourier Series states that any periodic and continuous function can be expressed as the sum of sine or cosine functions, each of which has a specific amplitude, angle and frequency (Equation 1; Figure 11).

$$f(x) = \frac{a_0}{2} + \sum_{n=1}^{\infty} \left(a_n \cos \frac{2n\pi}{T} t + b_n \sin \frac{2n\pi}{T} t \right)$$

Equation 1

Where: a_n and b_n are Fourier coefficients; n = frequency component; T = period; t = time.

The fast Fourier Transform (*fft*) implementation in Matlab was used to find the first six cosine functions with peaks in amplitude (one at the respiratory frequency, one at the cardiac frequency, and four at subsequent harmonics of the cardiac frequency) conforming the signals of ICP, aBP and cBF at all the experimental permutations shown in Table I. These first six frequencies were adequate to represent and reconstruct the ICP, aBP, and cBF signals. The aBP signals from the 13 rats at resting conditions were then reconstructed, attenuating the component at the cardiac frequency. This was performed to test whether the aBP waveform without the cardiac frequency resembles more the ICP waveform, considering

that during resting conditions the intracranial system may act as a pulsation absorber of the cardiac frequency (Kasuga *et al.* 1987; Zou *et al.* 2008; Wagshul *et al.* 2009, 2011; Kim *et al.* 2012).

To investigate the possible relationship between mean ICP and the waveforms of ICP, aBP, and cBF, the mean amplitude (from up to 11 rats subjected to four mean ICP levels, a ventilation rate of 90 breaths/min, two paced HRs of 400 and 500 bpm, and three mean aBP levels) of the six cosine functions conforming ICP, aBP and CBF signals was graphed as a function of mean ICP and mean aBP. Finding the cosine functions comprising the ICP, aBP, and cBF waveforms is also necessary to construct transfer function models, as explained next in Section 3.5.

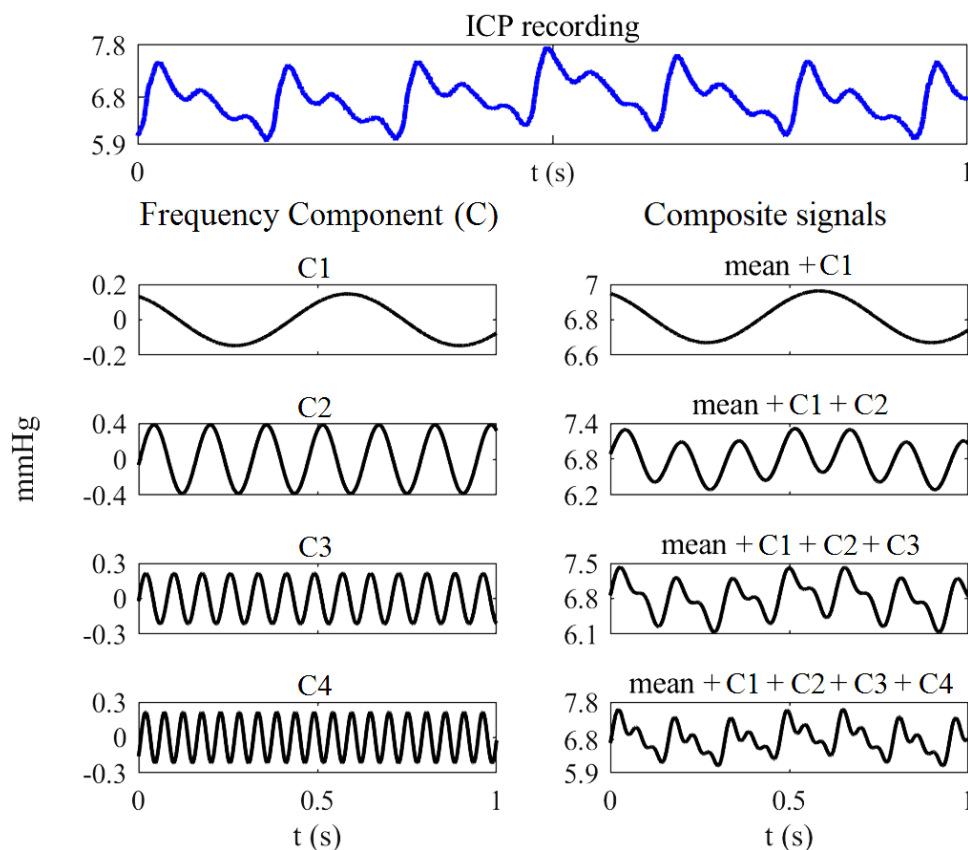


Figure 11. Schematic to show that a periodic and continuous function, such as an ICP signal, can be expressed as a sum of sine or cosine functions, which amplitudes, angles, and frequencies can be found with the Fourier Transform. In the example of an ICP signal, the frequency components with high amplitude and thus contributing significantly to the reconstructed signal are at the respiratory frequency (C1), at the heart rate frequency (C2), and at harmonics of the heart rate frequency (C3 – C4).

3.5. Transfer function

In signal analysis, a transfer function is a mathematical algorithm that transforms an input signal into an output signal. To investigate the relationship between blood pressure and flow waveforms and the ICP waveform, two transfer function models were considered for this study: both models considered ICP as the output signal, but the first model used aBP as the input signal, while the second model used cBF as the input signal (Figure 12).

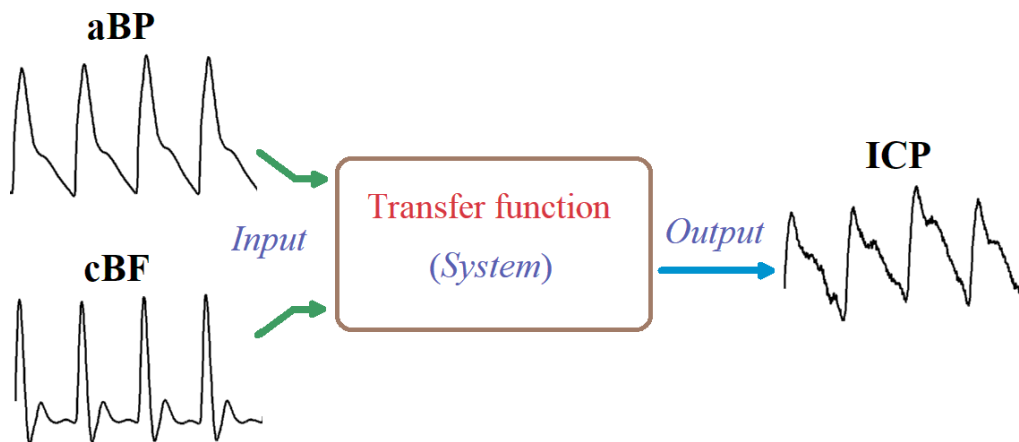


Figure 12. Transfer function models used as systems transforming cardiovascular input signals (aBP or cBF) into ICP as output signal.

The transfer function models are mathematical functions applied to the magnitude and phase of the frequencies of the input signal to obtain the magnitude and phase of the frequencies of the output signal. The transfer function approach has proved adequate for estimating aBP waveforms from brachial or radial blood pressure waveforms (Chen *et al.* 1997; Gao *et al.* 2016). In this study, the magnitude of the transfer function was computed as the amplitude (average from up to 11 rats) of the six main cosine functions conforming the ICP (mmHg) signals (see Section 3.4) divided by the amplitude of the six main cosine functions of the aBP (mmHg) or cBF (mL/min) signals (Equation 2). Thus, the magnitude of the first model is dimensionless (mmHg/mmHg), while the amplitude of the second is in mmHg/mL/min. The phase of the transfer functions is computed as the mean angle (radians) of the six main cosine

functions of the ICP waveform minus the mean angle (radians) of the six main cosine functions of the aBP or cBF waveforms (Equation 3). Thus, at each frequency component, the magnitude of the transfer functions can be multiplied by the amplitude of a cardiovascular signal (aBP or cBF) to obtain an estimated ICP amplitude (Equation 4). Similarly, at each frequency component, the phase of the transfer functions can be added to the phase of a cardiovascular signal (aBP or cBF) to obtain an estimated ICP phase angle (Equation 5). Finally, an ICP waveform can be reconstructed by adding the cosine functions corresponding to each frequency component (Equation 6).

$$TF\ mag(fc) = \frac{1}{n} * \sum_{n=1}^{n \leq 11} \left(\frac{obs.\ ICP\ amp(n, fc)}{obs.\ CVS\ amp(n, fc)} \right)$$

Eq. 2

$$TF\ pha(fc) = \frac{1}{n} * \sum_{n=1}^{n \leq 11} (obs.\ ICP\ pha(n, fc) - obs.\ CVS\ pha(n, fc))$$

Eq. 3

$$est.\ ICP\ amp(fc) = TF\ mag(fc) * obs.\ CVS\ amp(fc)$$

Eq. 4

$$est.\ ICP\ pha(fc) = TF\ pha(fc) + obs.\ CVS\ pha(fc)$$

Eq. 5

$$est.\ ICP\ waveform = \sum_{fc=1}^{fc=6} (est.\ ICP\ amp(fc) * \cos(t * 2\pi * Hz(fc) + est.\ ICP\ pha))$$

Eq. 6

Where: *TF* = Transfer function; *mag* = magnitude; *amp* = amplitude; *pha* = phase; *Hz* = frequency in Hertz; *obs.* = observed; *est.* = estimated; *CVS* = cardiovascular signal (aBP or cBF); *n* = rat subjects; *fc* = frequency component; *t* = time in seconds.

To highlight the effect of the respiration rate, the transfer function from 11 rats with normal ICP, resting HR and three mean aBP levels was graphed at two VRs: 60 and 90 breaths/min. Similarly, to highlight the effect of the HR, the transfer function from 11 rats with normal ICP, a VR of 90 breaths/min and three mean aBP levels was graphed at five HRs: 300, 350, 400, 450, and 500 bpm. The transfer function models used to predict ICP waveform, from mean ICP, mean aBP, and waveforms of aBF of cBF were constructed considering up to 11 rats at four mean ICP levels (<10, 10-15, 15-20, and >20 mmHg), two HRs (400 and 500 bpm), and three levels of mean aBP (70, 100, and 130 mmHg).

3.6. Model assessment

A cross validation approach was used to test the ability of the transfer function models to reproduce the ICP waveform and to predict pulse ICP. The approach consisted in subtracting one rat from the model construction, and then applying the model to the subtracted rat; this procedure was repeated for each of the up to 11 rats at four mean ICP levels, a VR of 90 breaths/min (VR available for the four mean ICP levels), HRs of 400 and 500 bpm (HRs available for the four mean ICP levels), and the three mean aBP levels (Table I). The Root Mean Square Error (RMSE) was computed as an index of the resemblance degree between the observed and predicted pulse ICP waveforms. The smaller the RMSE, the better the estimation of the waveform. Additionally, the pulse ICP estimated from the up to 11 rats was averaged and compared versus the observed values as a function of mean aBP and mean ICP. Then, the error between the observed and modelled pulse ICP was computed (modelled minus observed) as a function of mean aBP and mean ICP.

3.7. Statistical tests

A mixed model analysis was performed to find significant differences in the amplitude of the frequency components of ICP, aBP and cBF signals, as a function of frequency, HR, mean aBP, and mean ICP. Similarly, the mixed model analysis was used to determine the effect of frequency, VR, HR, mean aBP and mean ICP on the magnitude and phase of the transfer functions at each frequency component. Post hoc paired t-tests were used to compare the differences in magnitude and phase of between levels of VR, HR, and mean ICP at each frequency component, with Holm or Tukey correction applied. For assessment of the transfer function models via cross validation, mixed model analysis was used to find: 1) significant differences between observed and modelled values of ICP waveform and pulse, 2) the effect of mean aBP, mean ICP, and HR on model performance, and 3) differences between both transfer function models (the one using aBP vs the one using cBF). The variables of frequency, VR, HR, mean aBP, and mean ICP were modelled as categorical variables. A p-value less than 0.05 was considered statistically significant.

Chapter 4: Results

4.1. Stepwise mixed-model regression

The cardiovascular predictor variables of mean and pulse ICP considered for the SMMR analysis (Figure 13, Figure 14) proved minimal but significant predictive value (Table II and Table III). Maxima, mean and minima of aBP as well as maxima and minima of cBF had significant predictive value for mean ICP ($p < 0.001$, $R^2 = 0.25$) (Table II). HR ($p < 0.05$), maxima and mean aBP ($p < 0.001$), maxima ($p < 0.001$), mean ($p < 0.05$) and minima ($p < 0.01$) cBF had some significant predictive value for pulse ICP ($R^2 = 0.35$) (Table III). However, aBP and cBF parameters showed a slightly stronger relationship with pulse ICP ($R^2 = 0.35$) than with mean ICP ($R^2 = 0.25$). Additionally, pulse ICP was more related with aBP parameters (mean $R^2 = 0.1821$) than with cBF parameters (mean $R^2 = 0.0075$). On the other hand, notwithstanding very low correlation coefficients, mean ICP was more related with cBF parameters (mean $R^2 = 0.0081$) than with aBP parameters (mean $R^2 = 0.00095$).

The parameter most related to mean ICP was mean cBF ($R^2 = 0.015$) (Figure 13), while the parameters most related to pulse ICP were minima and mean aBP ($R^2 = 0.23$) (Figure 14). An inversely proportional relationship was observed between pulse ICP and aBP (minima, maxima, mean and pulse); pulse ICP is smaller when aBP is higher. From visual inspection of data, it could be observed that intravenous injection of phenylephrine (used to raise aBP) usually caused an evident increase in mean ICP and a small reduction of pulse ICP. Similarly, intravenous injection of sodium nitroprusside (used to reduce aBP) usually caused a very marked increase in both mean and pulse ICP (Table IV). On the other hand, the intracranial injection of CSF (used to raise ICP) was not observed to cause any change in aBP or cBF.

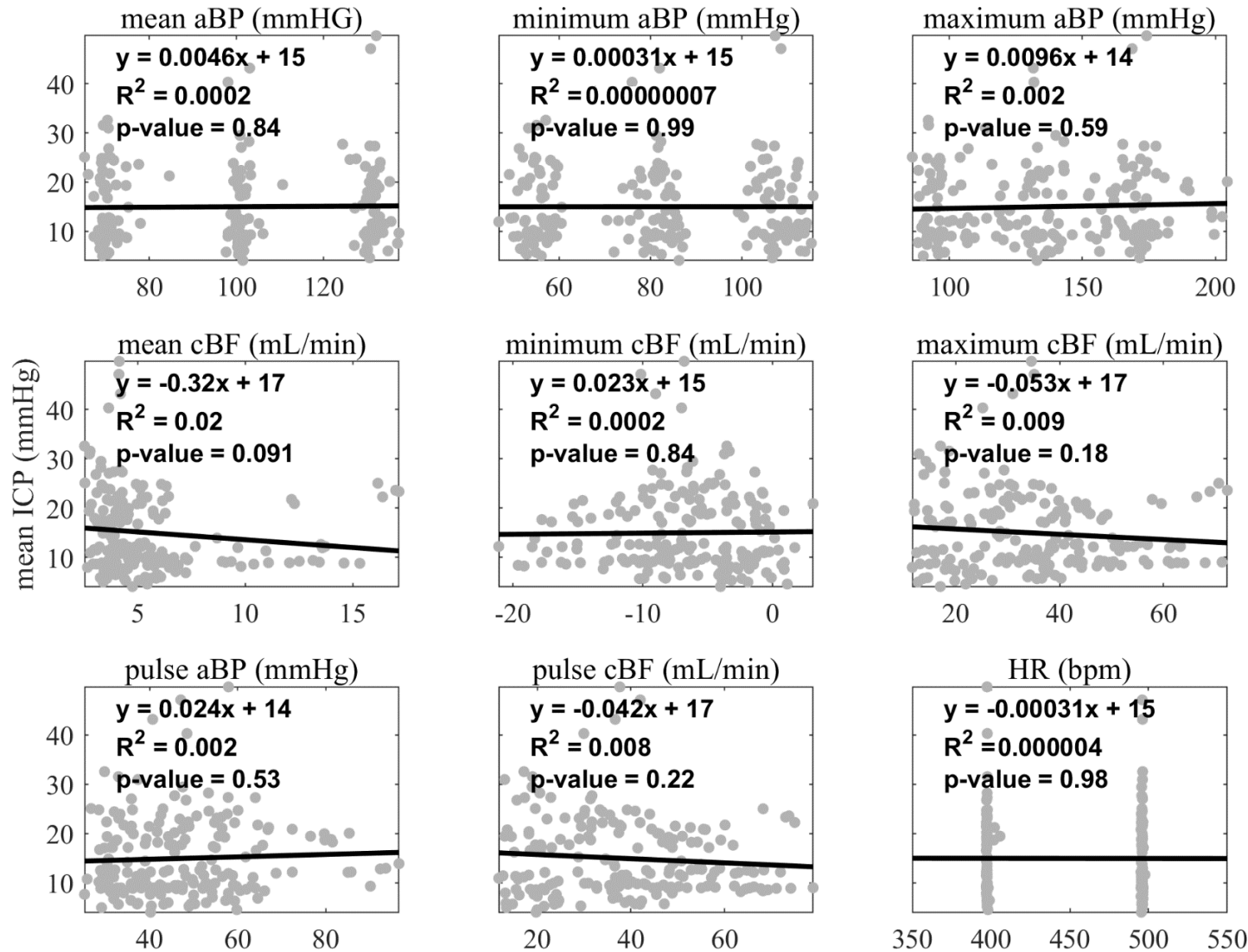


Figure 13. Scatter graphs of cardiovascular parameters versus mean ICP, fitting a linear trendline. Data come from up to 11 rats at four mean ICP levels (>10, 10-15, 15-20, >20 mmHg), two heartrates (400 and 500 bpm), three mean aBP levels (70, 100, 130 mmHg), and ventilated at 90 breaths/min.

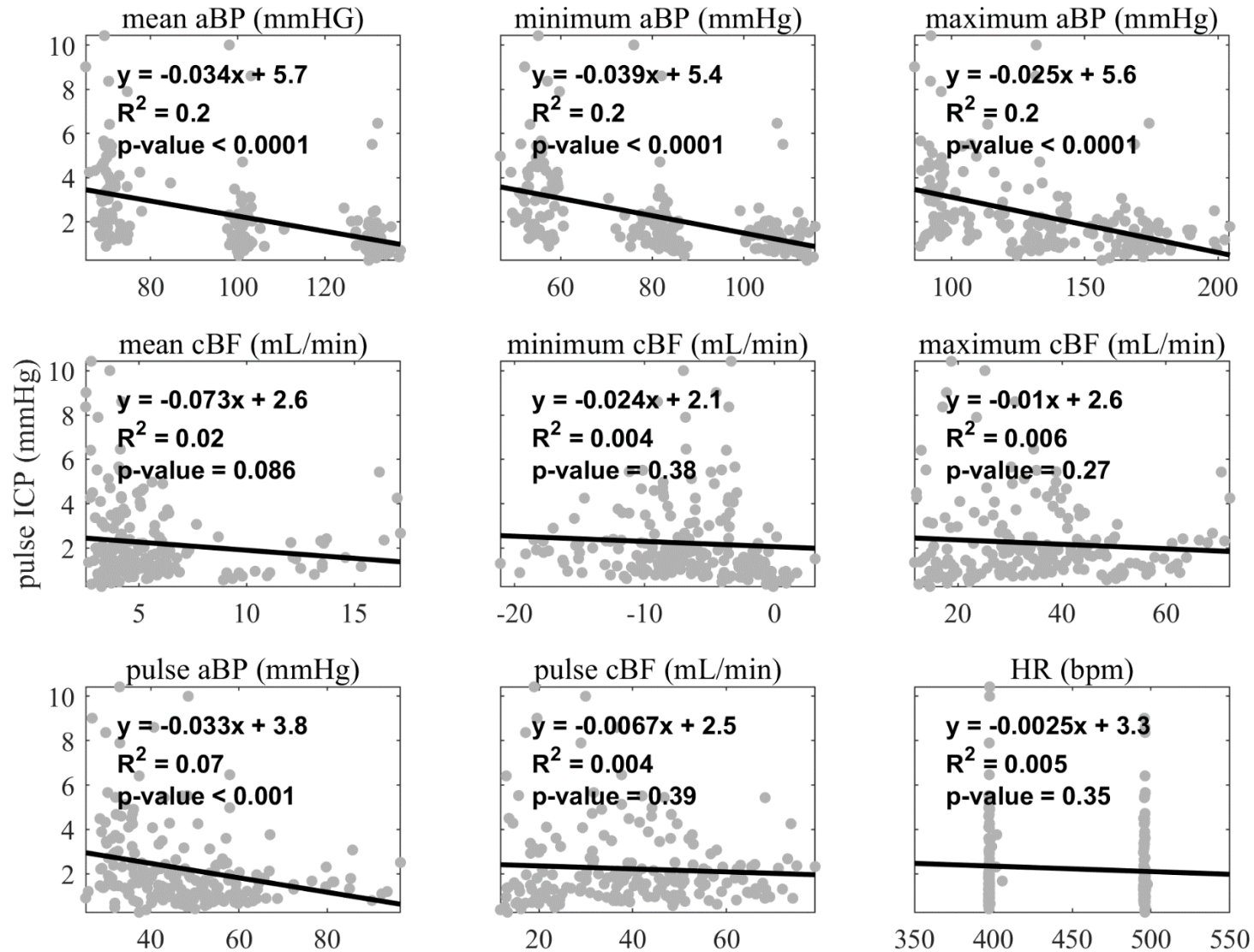


Figure 14. Scatter graphs of cardiovascular parameters versus pulse ICP, fitting a linear trendline. Data come from up to 11 rats at four mean ICP levels (>10, 10-15, 15-20, >20 mmHg), two heartrates (400 and 500 bpm), three mean aBP levels (70, 100, 130 mmHg), and ventilated at 90 breaths/min.

Table II. Predictors of mean ICP according to the stepwise mixed-model regression. The next five (out of nine) cardiovascular parameters showed significant predictive value of mean ICP.

Predictor	Slope	P
Maxima blood pressure (mmHg/mmHg)	0.33±0.05	<0.001
Mean blood pressure (mmHg/mmHg)	-0.75±0.14	<0.001
Minima blood pressure (mmHg/mmHg)	0.41±0.11	<0.001
Maxima blood flow (mmHg/ml/min)	-0.39±0.04	<0.001
Minima blood flow (mmHg/ml/min)	-0.30±0.05	<0.001

Table III. Predictors of pulse ICP according to the stepwise mixed-model regression. The next six (out of nine) cardiovascular parameters showed significant predictive value of pulse ICP.

Predictor	Slope	P
Heart rate (mmHg/bpm)	0.002±0.001	<0.05
Maxima blood pressure (mmHg/mmHg)	0.07±0.01	<0.001
Mean blood pressure (mmHg/mmHg)	-0.12±0.01	<0.001
Maxima blood flow (mmHg/mmHg)	-0.08±0.02	<0.001
Mean blood flow (mmHg/ml/min)	-0.12±0.06	<0.05
Minima blood flow (mmHg/ml/min)	-0.04±0.02	<0.01

Table IV. Observed effect (occurrence percentage) on mean and pulse ICP as a consequence of increasing aBP (by phenylephrine injection) and decreasing aBP (by sodium nitroprusside injection). 100% corresponds to all the times that 13 rats were injected with phenylephrine (increased aBP) or sodium nitroprusside (decreased aBP).

		Increased aBP (phenylephrine injection)	Decreased aBP (sodium nitroprusside injection)
Mean ICP	Increased	86%	71%
	Decreased	3%	22%
	Unaltered	11%	7%
Pulse ICP	Increased	5%	95%
	Decreased	57%	1%
	Unaltered	38%	4%

4.2. Fourier analysis

From data of up to 11 rats at four levels of mean ICP, two HRs, one VR, and three mean aBP levels, the amplitude of the six main frequency components corresponding to ICP waveforms was found to significantly decrease as mean aBP increases ($p < 0.0001$), being the second frequency component (component at the cardiac frequency) the largest component of ICP waveforms at any mean aBP (Figure 15). Conversely, the amplitude of the frequency components corresponding to aBP waveforms was found to significantly increase as mean aBP increases ($p < 0.0001$), but the second frequency component conserved the biggest amplitude (Figure 16). Despite there was a significant effect of mean aBP on the amplitude of the frequency components corresponding to cBF waveforms as mean aBP increases ($p < 0.01$), no obvious trend was observed, but the third frequency component was usually bigger than the second one at most mean aBP levels (Figure 17). In the three signals (ICP, aBP, and cBF; Figure 15 - Figure 17) the amplitude of the frequency components was significantly dependent on frequency ($p < 0.0001$), corresponding the largest amplitudes to the second, third and fourth frequency components. Nevertheless, the amplitudes of the first frequency component (component at the breathing frequency) were relatively big, comparable to the amplitudes of the fourth frequency component, in ICP signals (Figure 15).

In ICP signals, the amplitude of frequency components was significantly influenced ($p < 0.0001$) by mean ICP –the larger the mean ICP, the larger the amplitude–, mainly when mean ICP exceeds 20 mmHg (Figure 15). In addition, there was a significant interaction effect between mean aBP and mean ICP ($p < 0.0001$), meaning that the effect of mean aBP on the amplitude of ICP frequency components depends on the mean ICP level. In aBP signals, the amplitude of the frequency components was not significantly influenced by any level of mean ICP (Figure 16). In cBF signals, the amplitude of the frequency components was not

significantly influenced by mean ICP ($p=0.695$); however, a reduction in the amplitude of the frequency components may be observed when mean ICP is 10-15 mmHg (Figure 17). HR was found to significantly influence the waveform of aBP signals ($p<0.0001$), but not ICP ($p=0.3184$) or cBF ($p=0.8401$). Nevertheless, in cBF signals at a mean aBP of 130 mmHg, the second frequency component is usually the highest at 400 bpm while the third frequency component is usually the highest at 500 bpm (Figure 17).

From data of 13 rats at resting conditions, reconstructing aBP waveforms by attenuating the cardiac frequency (Figure 18, Figure 19) less than 25% resulted in a slightly increased resemblance between the aBP and ICP waveforms. However, an attenuation beyond 25% resulted in less resemblance between the waveform of both signals. As the attenuation of the cardiac frequency level increases, two peaks in the aBP waveform become more prominent, usually being the first one bigger than the second one; however, the number of peaks (usually three) observed in the ICP waveform was not achieved with this method (Figure 18) in any rat.

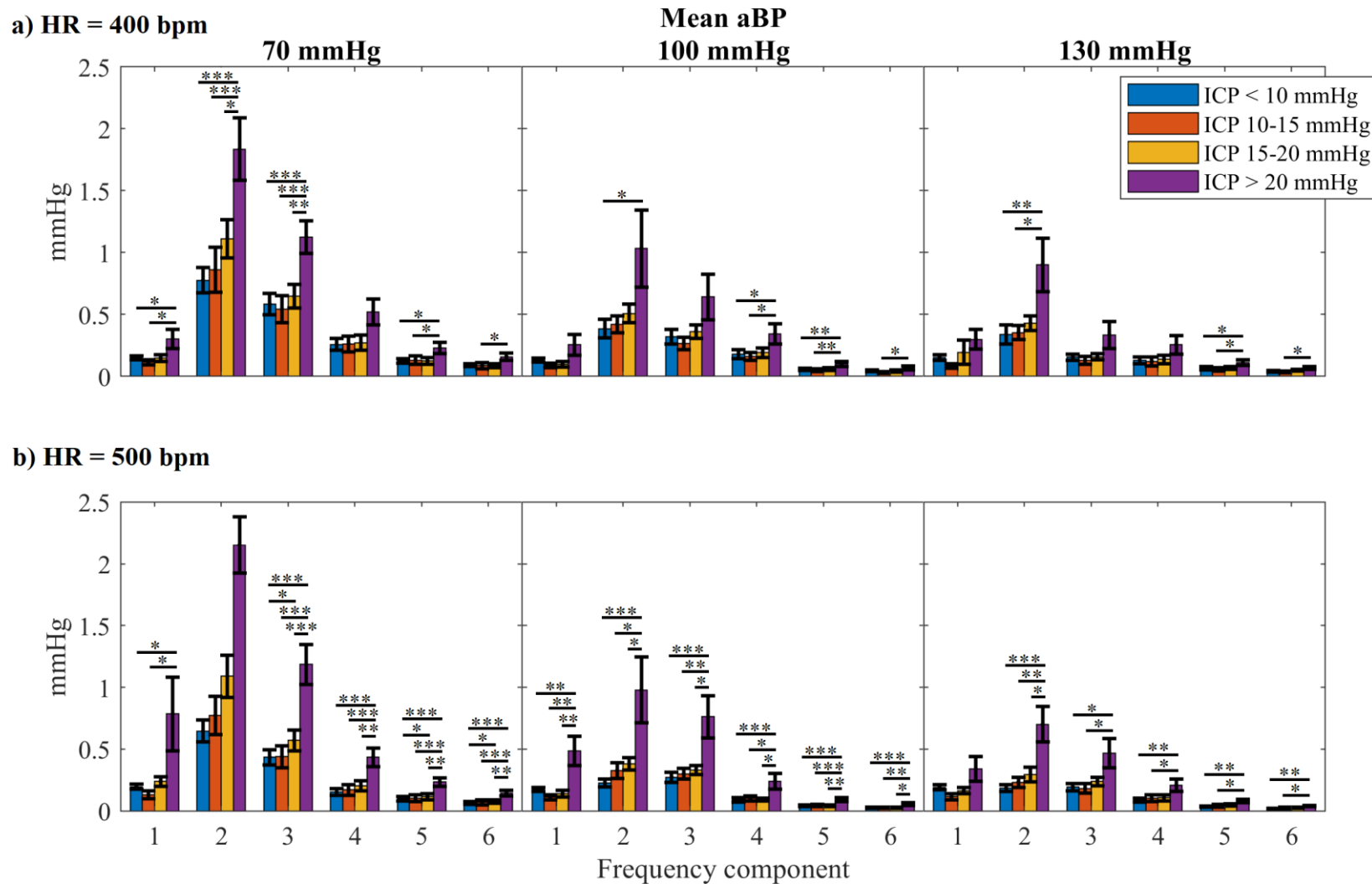


Figure 15. Amplitude (mean±SE), at a) 400 bpm and b) 500 bpm, of the six main frequency components of ICP signals from up to 11 rats (11 for ICP<10; six for ICP 10-15; seven for ICP 15-20; eight for ICP>20 mmHg) ventilated at 90 breaths/min. Frequency components found with Fourier Transform. There is a main effect of frequency, mean aBP, mean ICP, and interaction effect aBP×ICP ($p<0.0001$) on the amplitude of frequency components. * = $p<0.01$; ** = $p<0.001$; *** = $p<0.0001$.

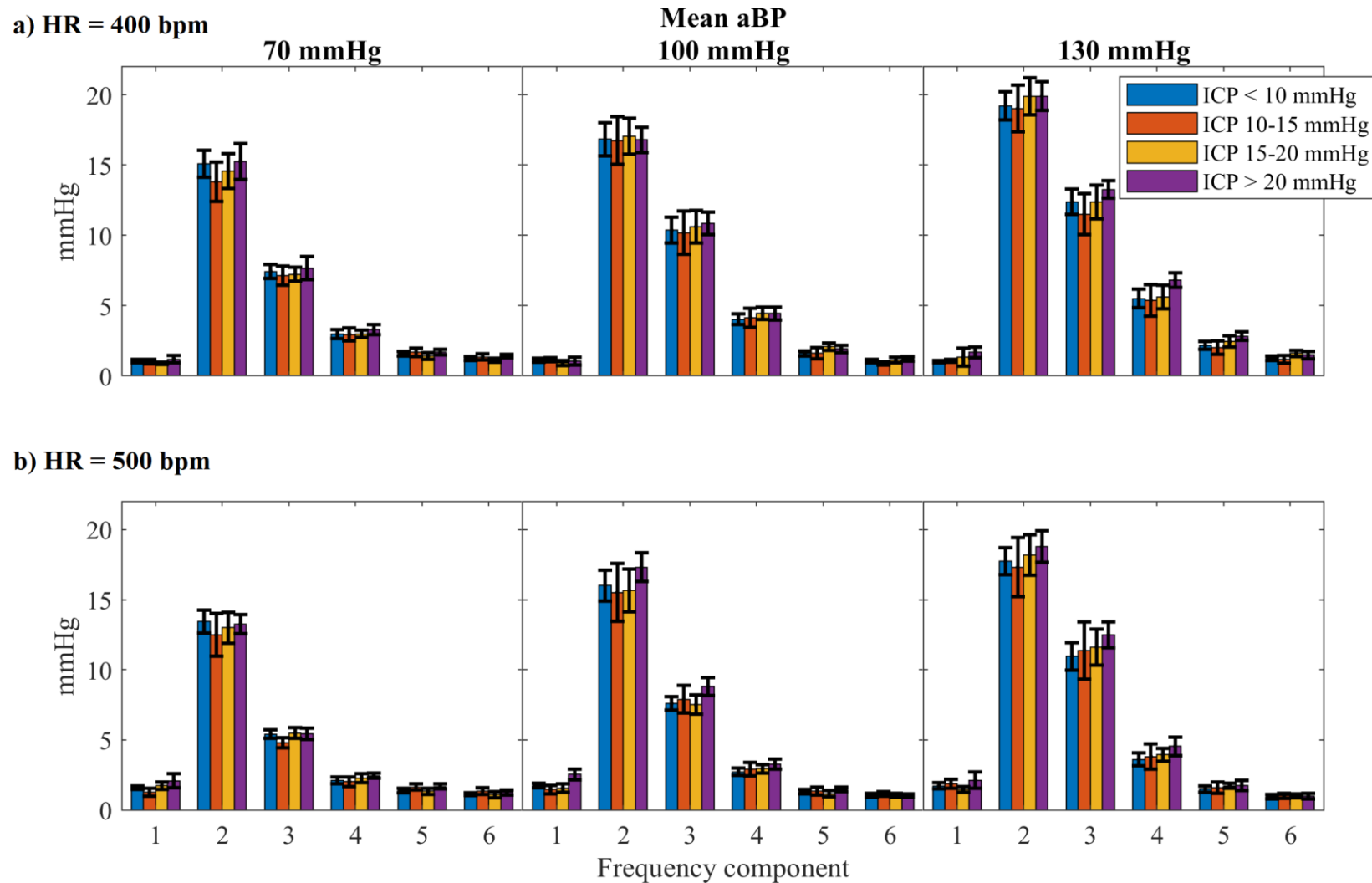


Figure 16. Amplitude (mean±SE), at a) 400 bpm and b) 500 bpm, of the six main frequency components of aBP signals from up to 11 rats (11 for ICP<10; six for ICP 10-15; seven for ICP 15-20; eight for ICP>20 mmHg) ventilated at 90 breaths/min. Frequency components found with Fourier Transform. There is a main effect of frequency, mean aBP, and HR ($p<0.0001$) on the amplitude of frequency components.

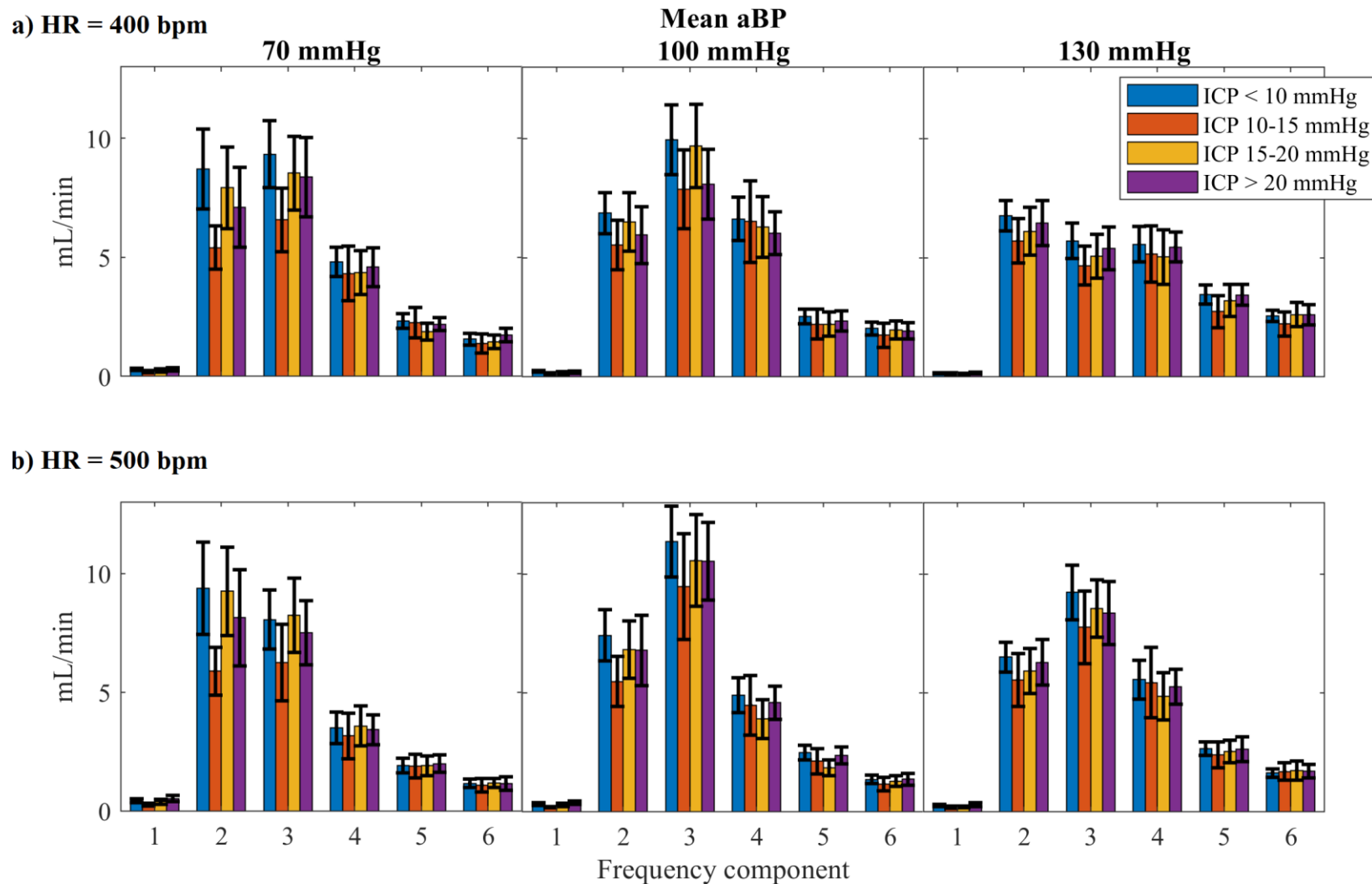


Figure 17. Amplitude (mean \pm SE), at a) 400 bpm and b) 500 bpm, of the six main frequency components of cBF signals from up to 11 rats (11 for ICP<10; six for ICP 10-15; seven for ICP 15-20; eight for ICP>20 mmHg) ventilated at 90 breaths/min. Frequency components found with Fourier Transform. There is a main effect of frequency ($p<0.0001$) and mean aBP ($p<0.01$) on the amplitude of frequency components.

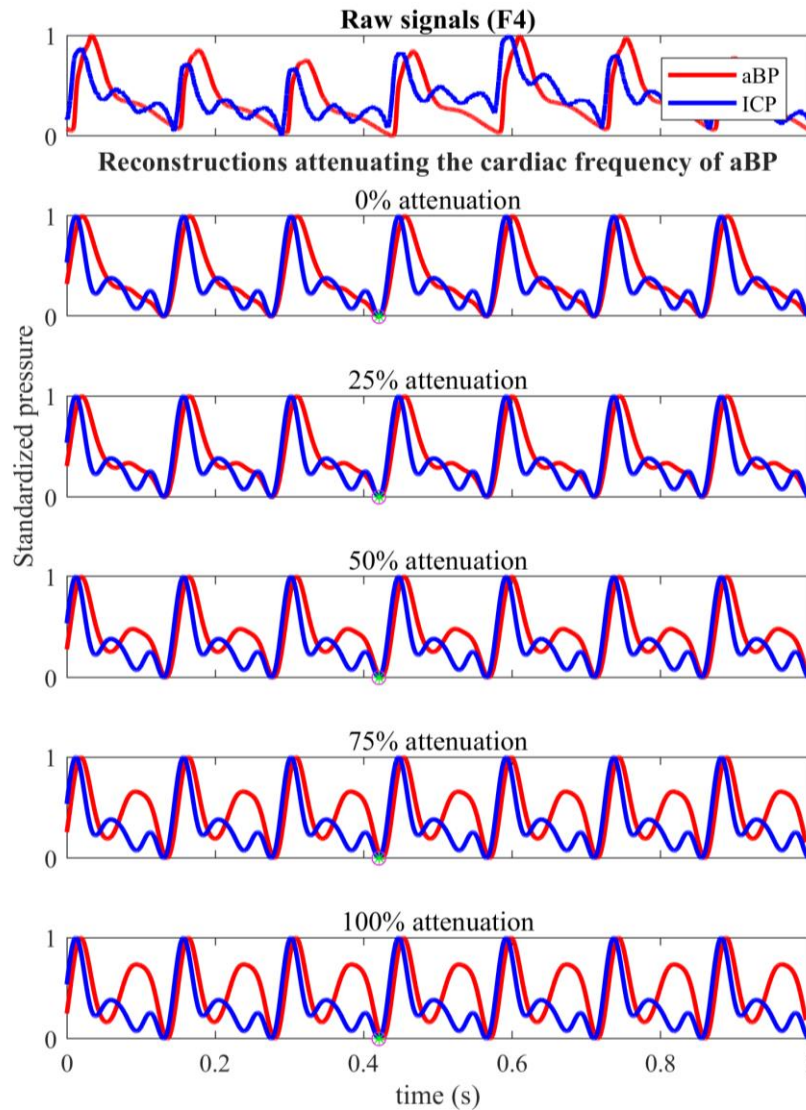


Figure 18. Comparison of standardized waveforms from 0 to 1 of aBP and ICP signals, at different attenuation levels of the cardiac frequency component in aBP. Attenuations greater than 25% resulted in less resemblance between the waveform of aBP and ICP. The example shown corresponds to the anaesthetized rat F4 under resting conditions.

4.3. Transfer function

The transfer function analyses (Figure 20 - Figure 25) consistently showed that the magnitude of the transfer functions (both mean and SE) is significantly reduced as mean aBP increases ($p < 0.0001$). This change in magnitude is higher from mean aBP of 70 to 100 mmHg than from mean aBP of 100 to 130 mmHg. The transfer function showed the highest magnitude values at the respiratory frequencies, but they were not consistent in the mean and had the highest SE, so that a trend could not be identified. Thus, data at respiratory frequency are not

shown in graphs (Figure 20 - Figure 25) to better visualize differences at the cardiac-related frequencies. From data of 11 rats at normal mean ICP, resting HR, three mean aBP levels, and two VRs (60 and 90 breaths/min), it was proved that VR has no significant effect on the shapes of the transfer function curves ($p > 0.54$; Figure 20, Figure 21). From data of 11 rats at normal mean ICP, five HRs (300, 350, 400, 450 and 500 bpm), three mean aBP levels, and one VR (90 breaths/min), it was found a significant main effect of HR on the magnitude ($p = 0.001$) and phase ($p = 0.008$) of the transfer function; however, when compared within the same mean aBP levels, HR was no longer significant effect ($p = 0.841$ and 0.77 at 70 mmHg; $p = 0.524$ and 0.622 at 100 mmHg; $p = 0.124$ and 0.934 at 130 mmHg for magnitude and phase, respectively) (Figure 22, Figure 23). Thus, dots to the same curves are added when different VRs and HRs are considered. Nevertheless, VR and HR showed a slightly greater influence on the magnitude of the transfer functions when mean aBP is below 100 mmHg, and on the phase of the transfer function that considers aBP as input (Figure 20, Figure 22).

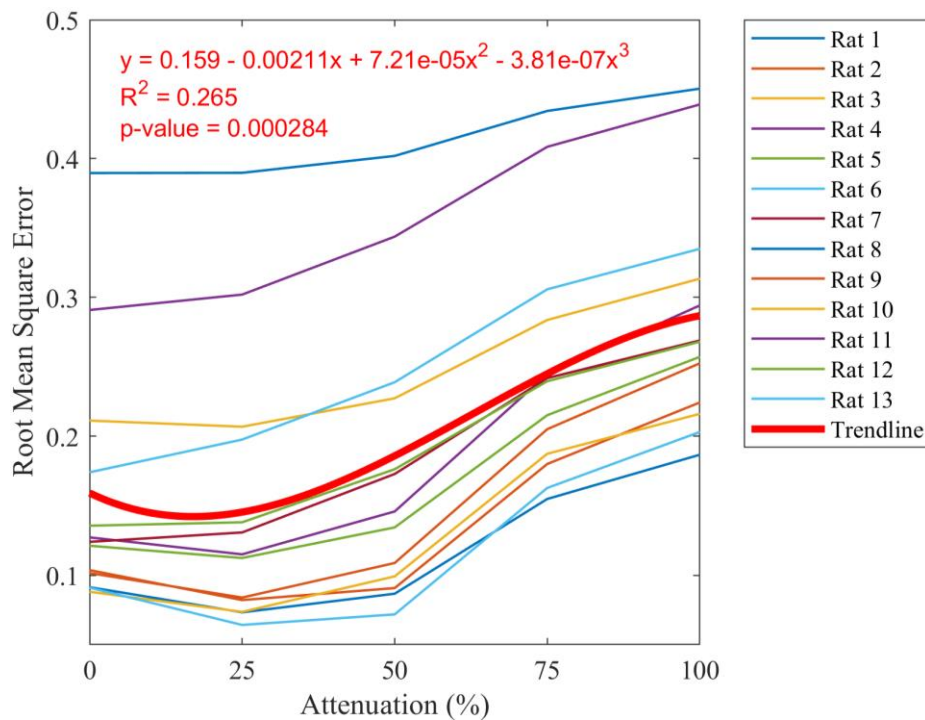


Figure 19. Root Mean Square Error comparing ICP and aBP waveforms standardized from 0 to 1, at different attenuation levels of the cardiac frequency component of aBP. Data come from 13 anaesthetized rats at resting conditions. Attenuations above 25% reduces the resemblance between aBP and ICP waveforms.

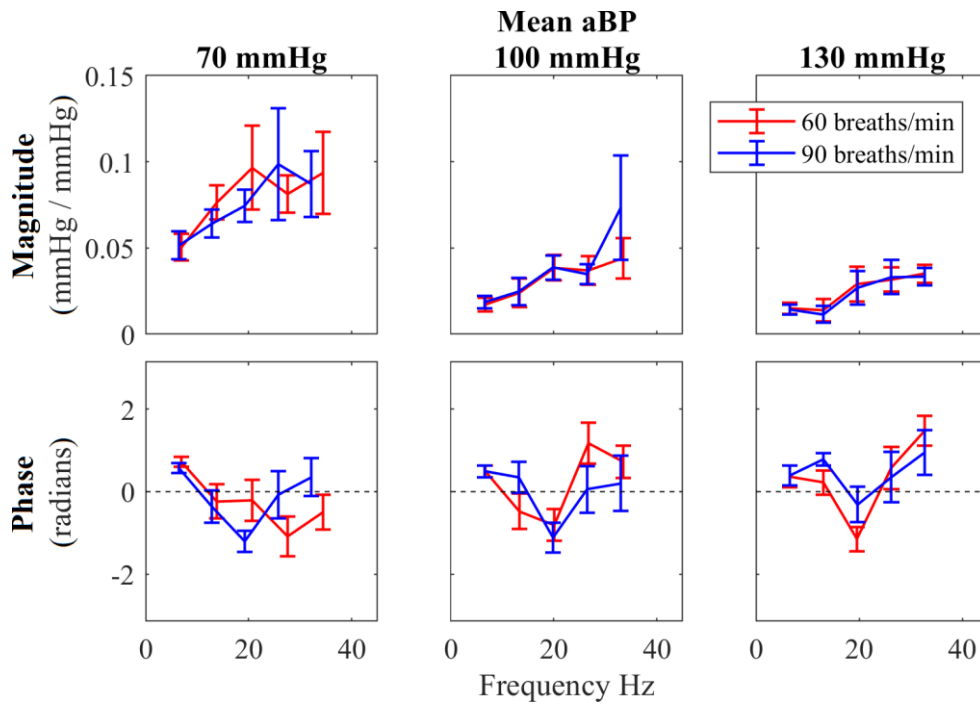


Figure 20. Effect of VR on the magnitude and phase of the transfer function (mean \pm SE) from aBP to ICP, considering 11 rats at normal ICP and resting HR. Data at the respiratory frequency are not shown to better visualize differences at cardiac-related frequencies. There is a main effect of frequency ($p < 0.0001$) and mean aBP ($p < 0.01$) on both magnitude and phase of the transfer function; VR had no significant effect on magnitude ($p = 0.982$) or phase ($p = 0.949$).

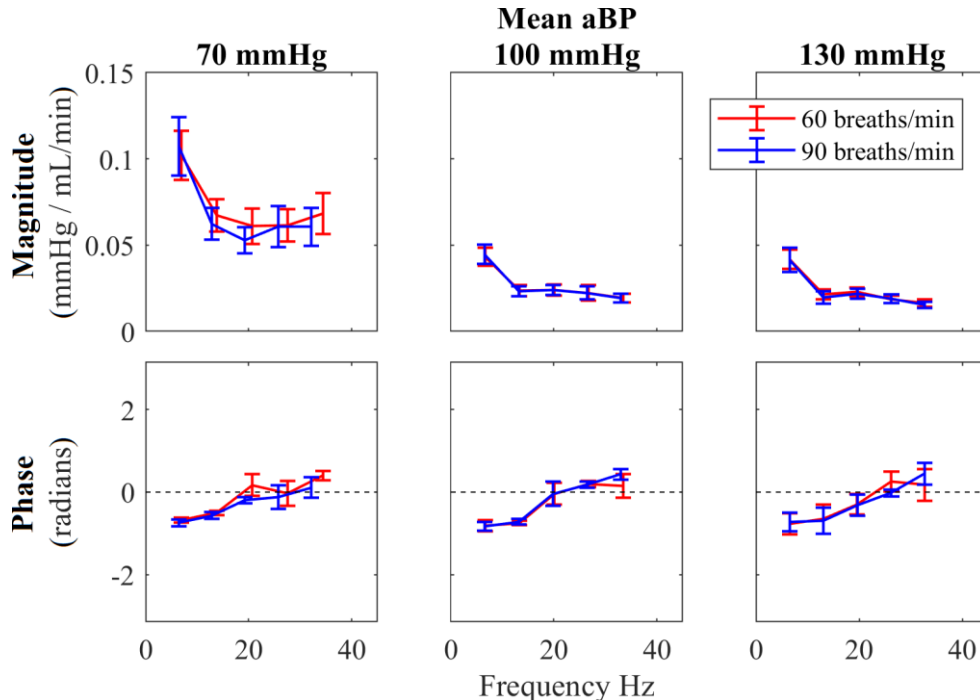


Figure 21. Effect of VR on the magnitude and phase of the transfer function (mean \pm SE) from cBF to ICP, considering 11 rats at normal ICP and resting HR. Data at the respiratory frequency are not shown to better visualize differences at cardiac-related frequencies. There is a main effect of frequency on both magnitude and phase ($p < 0.0001$) of the transfer function; mean aBP had a significant effect on the magnitude ($p < 0.0001$) but not on the phase ($p = 0.873$); VR had no significant effect on magnitude ($p = 0.541$) or phase ($p = 0.577$).

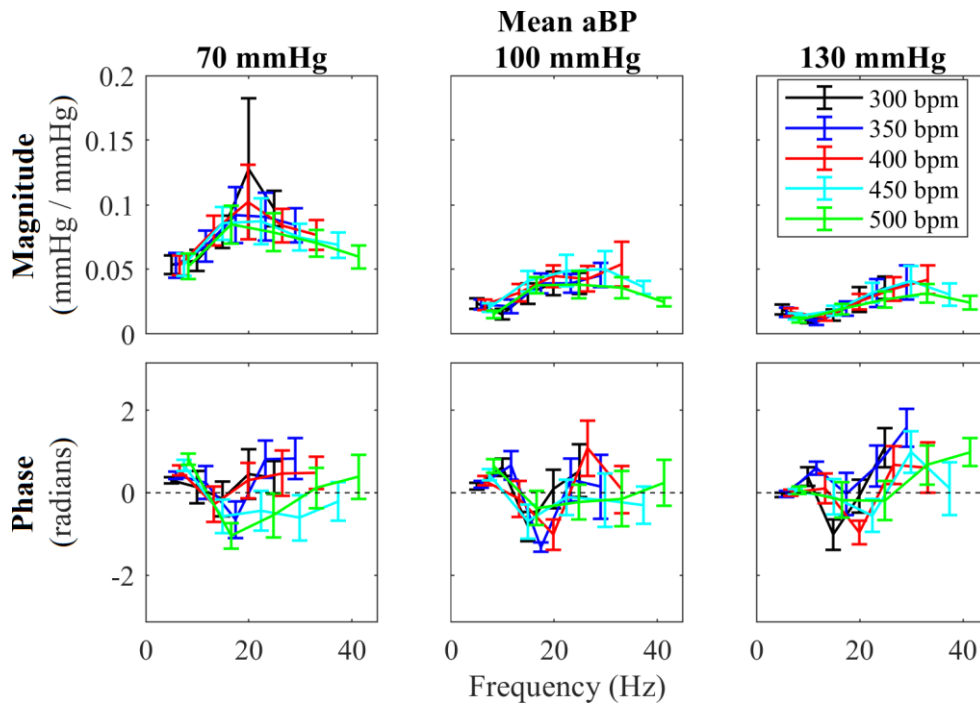


Figure 22. Effect of HR on the magnitude and phase of the transfer function (mean \pm SE) from aBP to ICP, considering 11 rats at normal ICP and a VR of 90 breaths/min. Data at the respiratory frequency are not shown to better visualize differences at cardiac-related frequencies. There is a main effect of frequency ($p < 0.0001$); mean aBP had a significant effect on magnitude ($p < 0.0001$) but not on phase ($p = 0.214$); HR had no significant effect on magnitude ($p = 0.217$) or phase ($p = 0.128$).

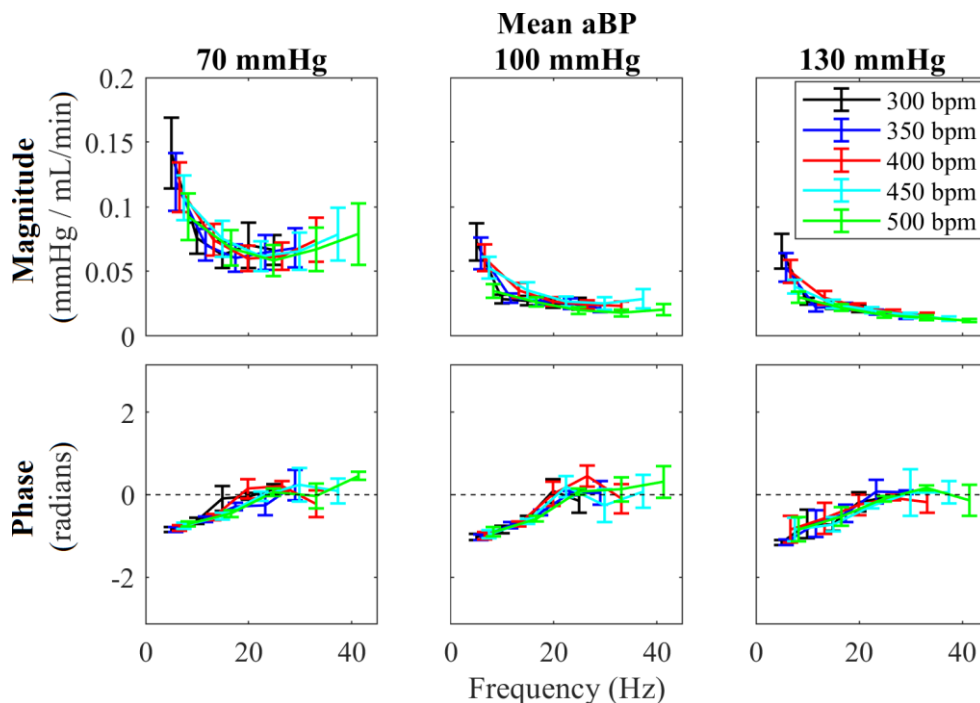


Figure 23. Effect of HR on the magnitude and phase of the transfer function (mean \pm SE) from cBF to ICP, considering 11 rats at normal ICP and a VR of 90 breaths/min. Data at the respiratory frequency are not shown to better visualize differences at cardiac-related frequencies. There is a main effect of frequency ($p < 0.0001$); mean aBP had a significant effect on magnitude ($p < 0.0001$) and ($p < 0.05$); HR had a significant main effect on magnitude ($p = 0.001$) and phase ($p = 0.008$), but when compared within

the same mean aBP levels, HR was no longer significant ($p=0.841$ and 0.77 at 70 mmHg; $p=0.524$ and 0.622 at 100 mmHg; $p=0.124$ and 0.934 at 130 mmHg for magnitude and phase, respectively).

From data of up to 11 rats at four mean ICP levels, two HRs, one VR and three mean aBP levels, Figure 24 and Figure 25 show the two transfer function models constructed to estimate the ICP waveform from aBP (Figure 24) and cBF (Figure 25) waveforms. In both models, it can be observed that the three mean ICP levels below 20 mmHg have similar but significantly different ($p<0.01$) magnitude curves: the magnitude of the frequency components raises as mean ICP increases. A prominent raise in the magnitude curve is observed when mean ICP exceeds 20 mmHg. The phase of the transfer functions does not show a clear dependence on mean ICP, but it seems to be smaller as mean ICP raises.

In the case of the transfer function model considering aBP waveforms (Figure 24), the magnitude for mean ICP >20 mmHg and mean aBP <130 mmHg forms a concave-down curve with the maximum value at about 20 Hz. At mean aBP of 70 mmHg, the peak of the magnitude curve is observed at about 30 Hz. Frequency ($p<0.05$), Mean aBP ($p<0.001$), mean ICP ($p<0.001$) and the interaction aBP \times ICP ($p<0.05$) had a significant effect on the magnitude at 400 and 500 bpm. Only frequency significantly influenced ($p<0.0001$) the phase at 400 and 500 bpm. The magnitude curve of the transfer function considering cBF waveforms (Figure 25) displays a shape more consistent across mean ICP and mean aBP levels. The peak of the magnitude curve is found at about 7 Hz, and then it decreases as frequency increases. The phase curve is also more consistent across mean ICP and mean aBP levels for the transfer function considering cBF waveforms. The phase is initially negative, and it increases gradually until it fluctuates around zero at frequencies greater than 20 Hz. HR does not affect significantly the transfer function models. Frequency ($p<0.0001$), Mean aBP ($p<0.0001$), mean ICP ($p<0.0001$) and the interaction aBP \times ICP ($p<0.01$) had a significant effect on the magnitude at 400 and 500 bpm. Frequency ($p<0.0001$) and mean aBP ($p<0.01$)

influenced the phase at 400 bpm, while frequency ($p<0.0001$) and mean ICP ($p<0.05$) influenced the phase at 500 bpm.

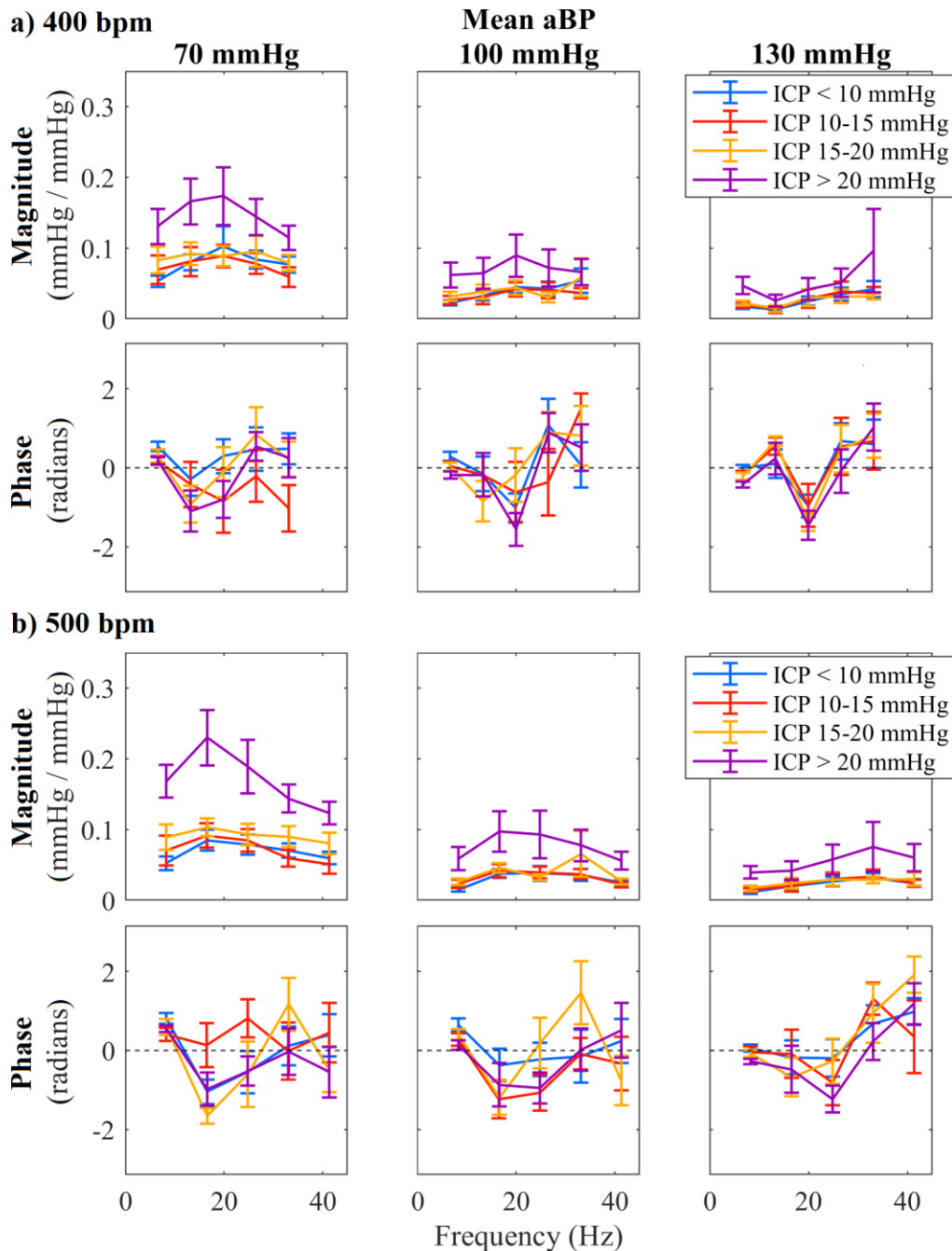


Figure 24. Magnitude and phase of the transfer function model (mean±SE) used to estimate ICP waveforms from aBP waveforms, considering up to 11 rats (11 for ICP<10; six for ICP 10-15; seven for ICP 15-20; eight for ICP>20 mmHg), with a VR of 90 breaths/min, and paced at a) 400 bpm and b) 500 bpm. Data at the respiratory frequency are not shown to better visualize differences at cardiac-related frequencies. Frequency ($p<0.05$), mean aBP ($p<0.001$), mean ICP ($p<0.001$) and the interaction aBP×ICP ($p<0.05$) had a significant effect on the magnitude at 400 and 500 bpm. Only frequency significantly influenced ($p<0.0001$) the phase at 400 and 500 bpm.

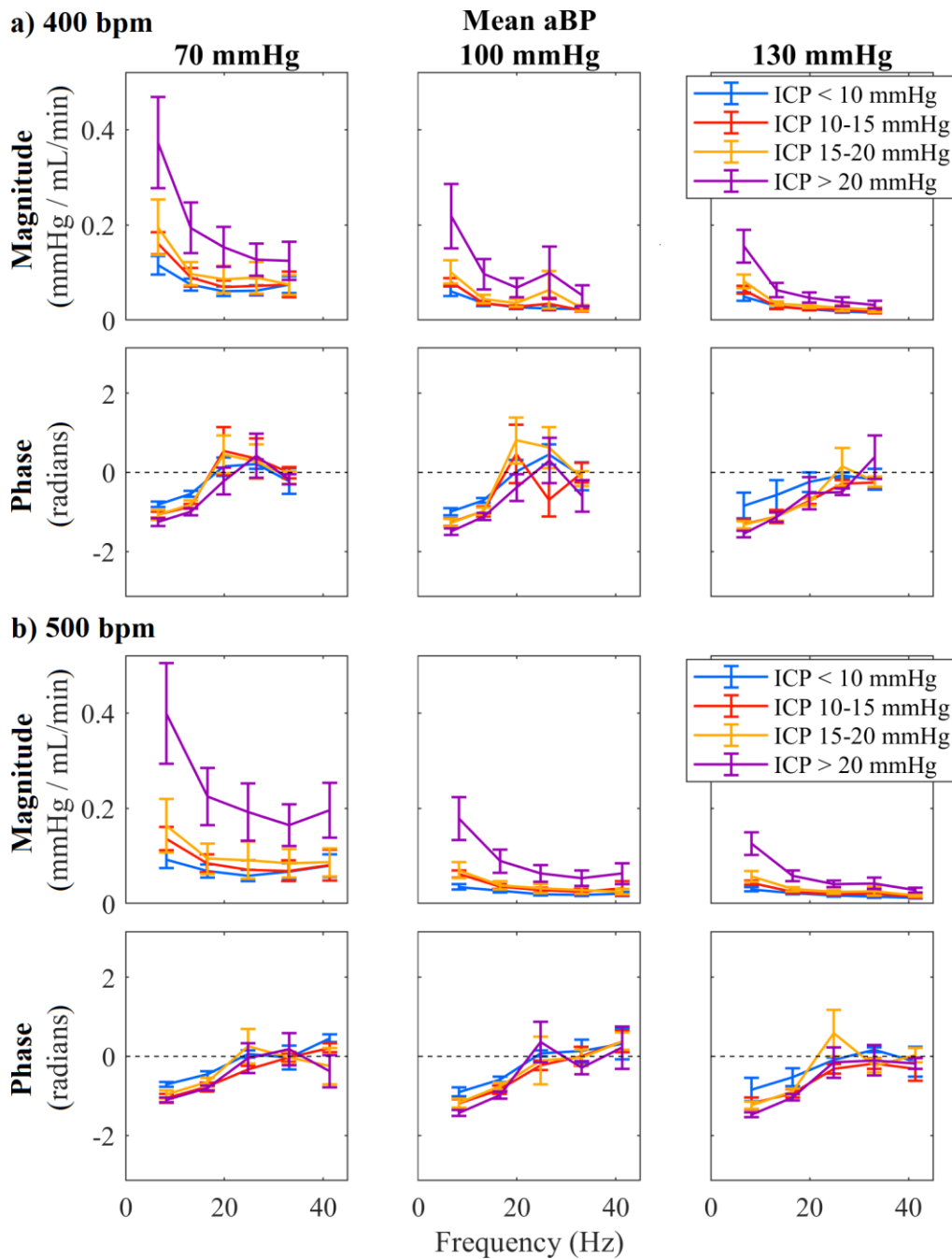


Figure 25. Magnitude and phase of the transfer function model (mean±SE) used to estimate ICP waveforms from cBF waveforms, considering up to 11 rats (11 for ICP<10; six for ICP 10-15; seven for ICP 15-20; eight for ICP>20 mmHg), with a VR of 90 breaths/min, and paced at a) 400 bpm and b) 500 bpm. Data at the respiratory frequency are not shown to better visualize differences at cardiac-related frequencies. Frequency ($p<0.0001$), mean aBP ($p<0.0001$), mean ICP ($p<0.0001$) and the interaction aBPxICP ($p<0.01$) had a significant effect on the magnitude at 400 and 500 bpm. Frequency ($p<0.0001$) and mean aBP ($p<0.01$) influenced the phase at 400 bpm, while frequency ($p<0.0001$) and mean ICP ($p<0.05$) influenced the phase at 500 bpm.

4.4. Model assessment

Considering up to 11 rats at four mean ICP levels, two HRs, one VR, and three mean aBP levels, the reconstructed ICP waveforms from aBP or cBF waveforms (e.g. Figure 26) showed more accuracy for mean aBP above 100 mmHg and mean ICP below 20 mmHg (RMSE \leq 0.5 mmHg) (Figure 27). For mean ICP higher than 20 mmHg, the RMSE ranged from 0.5 to 4 mmHg. Similarly, the SE associated to the RMSE is increased as mean aBP reduces. Mean ICP and mean aBP significantly influenced ($p<0.0001$) the model performance at both HRs. Although no significant differences were found between the estimates of both transfer function models, at mean aBP of 70 mmHg and mean ICP higher than 20 mmHg the observed ICP waveform is more like the ICP waveform estimated from aBP waveform (RMSE \approx 2.5 \pm 0.2 mmHg) than to the ICP waveform estimated from cBF waveform (RMSE \approx 3.5 \pm 0.6 mmHg).

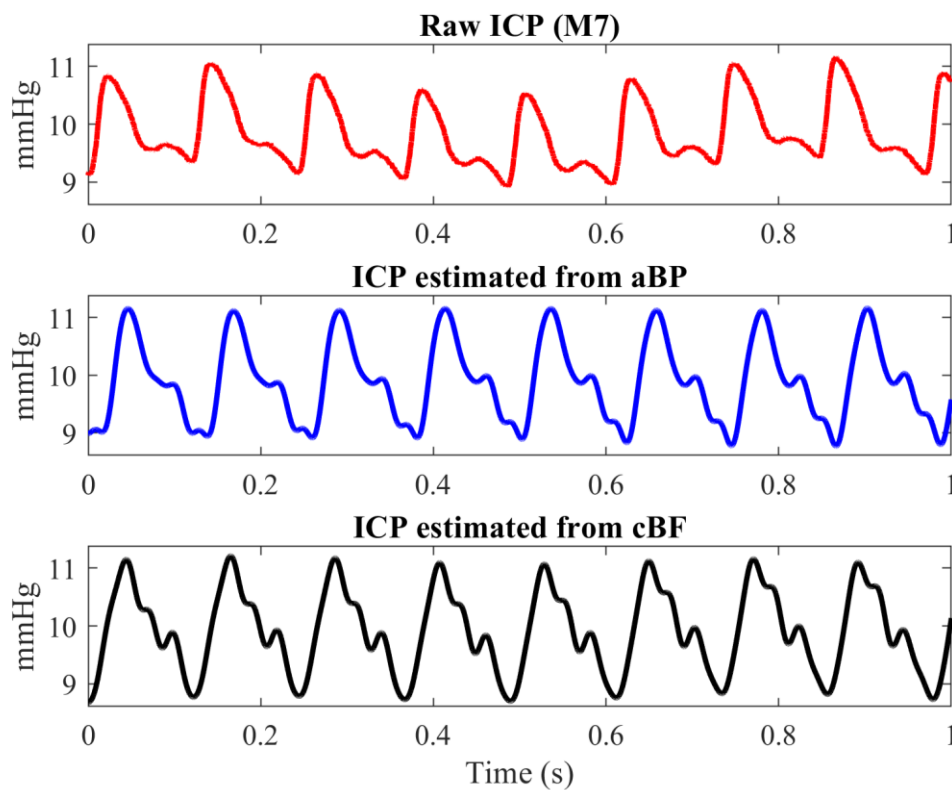


Figure 26. Reconstructions of ICP waveform from aBP and cBF waveforms. The example shown corresponds to rat M7 at resting ICP, HR of 500 bpm, mean aBP of 70 mmHg, and VR of 90 breaths/min. The reconstructions come from the transfer function models excluding this rat.

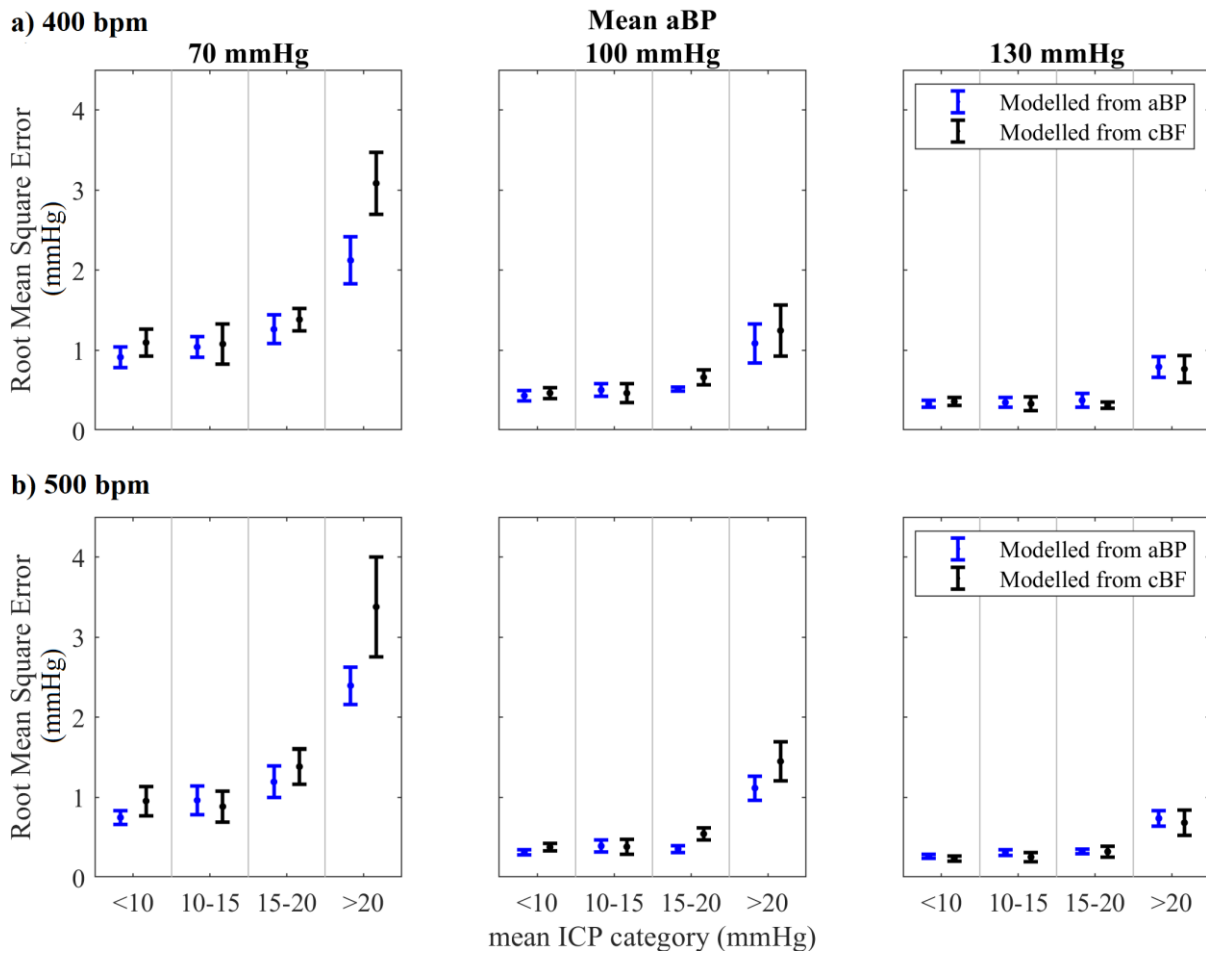


Figure 27. Root Mean Square Error (mean±SE) from cross-validation of ICP waveform estimated with the transfer function models, considering up to 11 rats (11 for ICP<10; six for ICP 10-15; seven for ICP 15-20; eight for ICP>20 mmHg) with a VR of 90 breaths/min, and paced at a) 400 bpm and b) 500 bpm. Mean ICP and mean aBP significantly influenced ($p<0.0001$) the model performance at both HRs; no significant differences were found between the estimates of both transfer function models.

Observed pulse ICP was also very similar to the pulse ICP estimated with the two transfer function models (Figure 28); however, this similarity is reduced as mean aBP reduces and mean ICP increases. Mean ICP and mean aBP significantly influenced ($p<0.0001$) the model performance at both HRs. Although no significant differences were found between the observed and the estimated values, at mean aBP of 70 mmHg and mean ICP>20 mmHg, aBP model seems better (estimated pulse ICP $\approx 6\pm 0.2$ mmHg) than cBF model (estimated pulse ICP $\approx 9\pm 2$ mmHg), which apparently overestimates the observed pulse ICP (6 ± 0.4 mmHg). A

closer view of the error between the observed and modelled pulse ICP (Figure 29) showed that only mean aBP has a significant effect ($p < 0.05$) on the error at 500 bpm (the larger the mean aBP, the smaller the error), and that the estimates from both models are not significantly different. Although the differences are not significant, cBF model seems to overestimate pulse ICP at mean aBP lower than 100 mmHg, while the error from aBP model is generally closer to zero. A larger but not significant error may be observed at mean ICP above 20 mmHg.

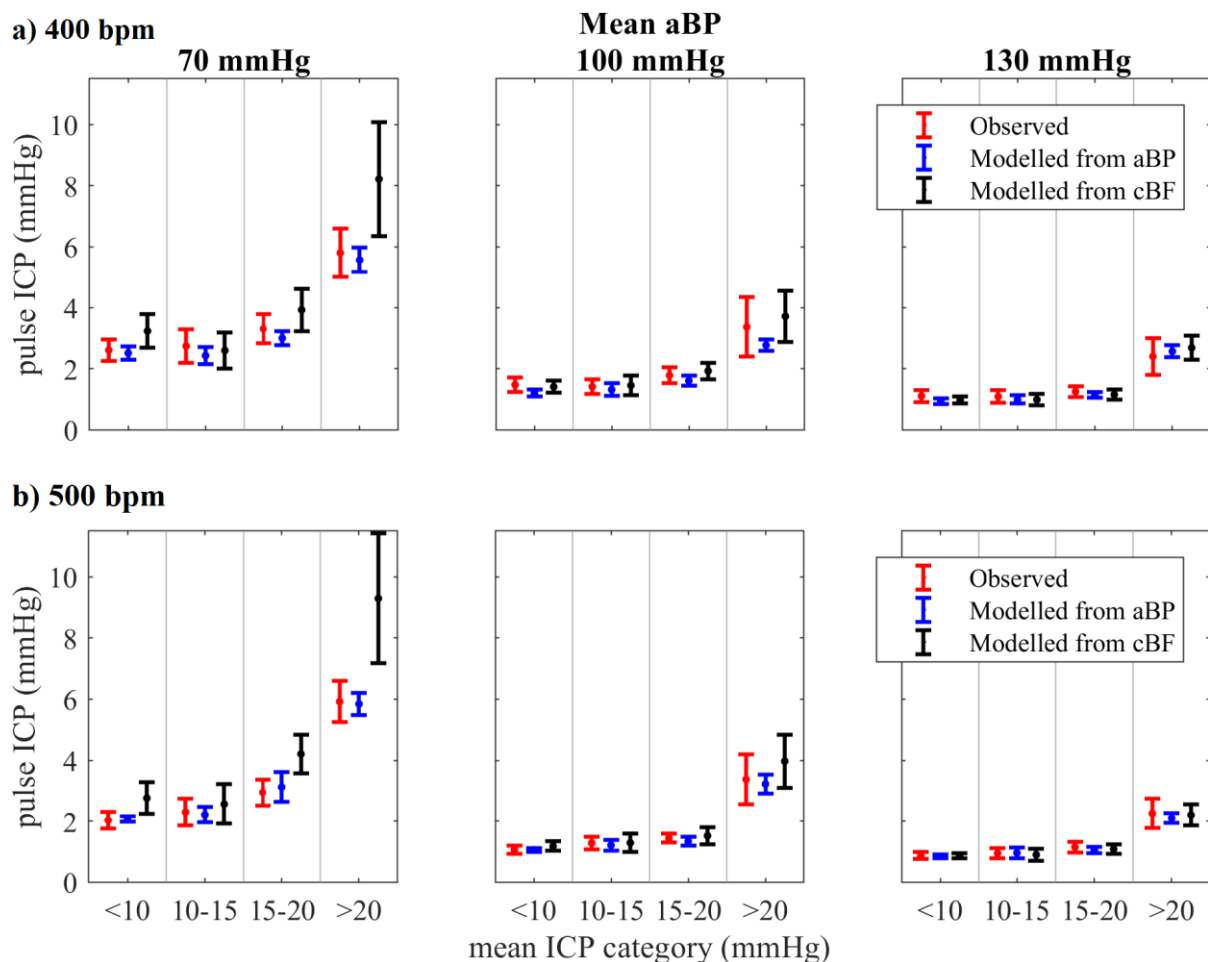


Figure 28. Comparisons between observed and modelled pulse ICP (mean \pm SE) from cross-validation technique, considering up to 11 rats (11 for ICP<10; six for ICP 10-15; seven for ICP 15-20; eight for ICP>20 mmHg) with a VR of 90 breaths/min, and paced at a) 400 bpm and b) 500 bpm. Mean ICP and mean aBP significantly influenced ($p < 0.0001$) the model performance at both HRs; no significant differences were found between the observed and the estimated values.

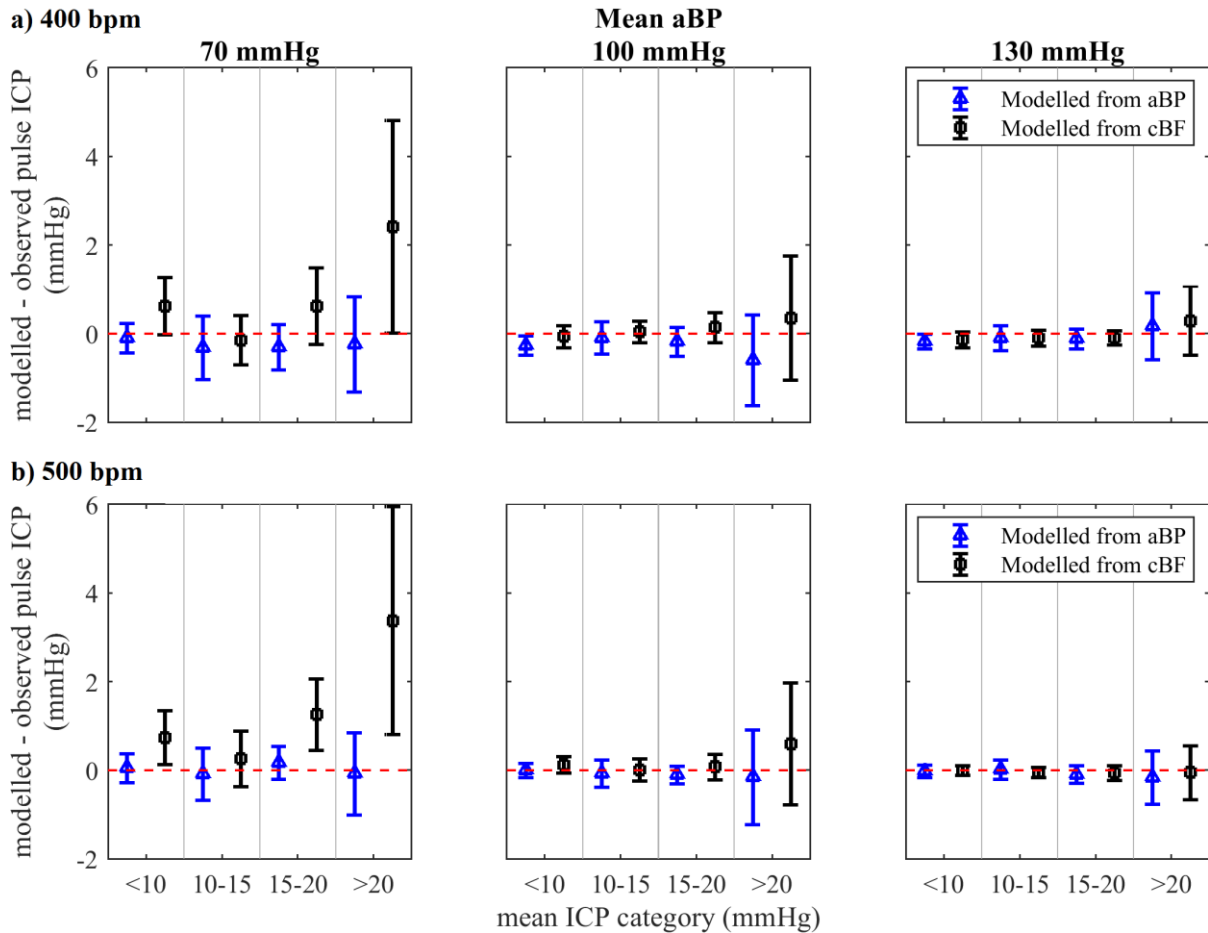


Figure 29. Error (mean±SE) between modelled and observed pulse ICP, from cross-validation of the transfer function models, considering up to 11 rats (11 for ICP<10; six for ICP 10-15; seven for ICP 15-20; eight for ICP>20 mmHg) with a VR of 90 breaths/min, and paced at a) 400 bpm and b) 500 bpm. Only mean aBP showed a significant effect ($p<0.05$) on the error at 500 bpm.

Chapter 5: Discussion

5.1. Intracranial pressure magnitude (mean and pulse)

The SMMR analysis showed minimal but significant value of cardiovascular parameters to predict ICP magnitude. Thus, the response observed in cardiovascular signals as a consequence of raised ICP below 50 mmHg could be due to 1) reflected waves from ICP shaping aBP or cBF waveforms –it is known that central aBP waveform is affected by wave reflection from peripheral body (O'Rourke & Yaginuma 1984; Nichols *et al.* 2008)– and 2) a neural response to raised ICP potentially shaping aBP or cBF waveforms before the Cushing reflex –sympathetic activity has been linked to raised ICP below 39 mmHg (Schmidt *et al.* 2018)– (Figure 30). Nevertheless, further research is needed to accept or reject these two possibilities.

More specifically, the SMMR analysis showed a higher predictive value for pulse ICP than for mean ICP. The correlation between mean ICP and cardiovascular signals is not straightforward largely because of cerebral autoregulation, which is responsible for maintaining a constant cerebral blood inflow despite changes in mean ICP and arterial pressure (Lang *et al.* 2002; van Beek *et al.* 2008); thus, ICP *pulsatility*, rather than mean ICP, may be more related to cardiovascular signals. While aBP parameters were slightly more related to pulse ICP, cBF parameters were more related to mean ICP, indicating that mean ICP may be more influenced by the amount of blood flow entering the brain than by the force (pressure) causing blood flow. It was observed that the lower the mean aBP, the higher the pulse ICP: lowering aBP (i.v. injection of sodium nitroprusside) caused a very marked increase in both mean and pulse ICP, while raising mean aBP caused a less marked effect.

Therefore, ICP pulsatility could be more affected by loosening, rather than stiffening, of arterial vessels.

The lack of a strong physiological response manifested in cardiovascular parameters as a consequence of raised mean ICP below 50 mmHg could be explained by the absence of baroreceptors –natural “blood pressure sensors” in the aortic arch, carotid sinus, and afferent arterioles of kidneys (Koeppen and Stanton 2013)– in the intracranial space. Thus, the Cushing reflex occurs at terminal phases of acute ICP when cerebral ischemic death is imminent (Kalmar *et al.* 2005; Wan *et al.* 2008). Since the correlation between mean ICP and cardiovascular parameters was rather small and no dependency of cardiovascular signals on mean ICP was observed from visual inspection of raw data, the estimation of mean ICP was not conducted as part of the Master of Research project. Additionally, previous research has been primarily focused on non-invasive estimates of mean ICP (Khan *et al.* 2017; Zhang *et al.* 2017), lagging the research on non-invasive estimates of ICP waveform.

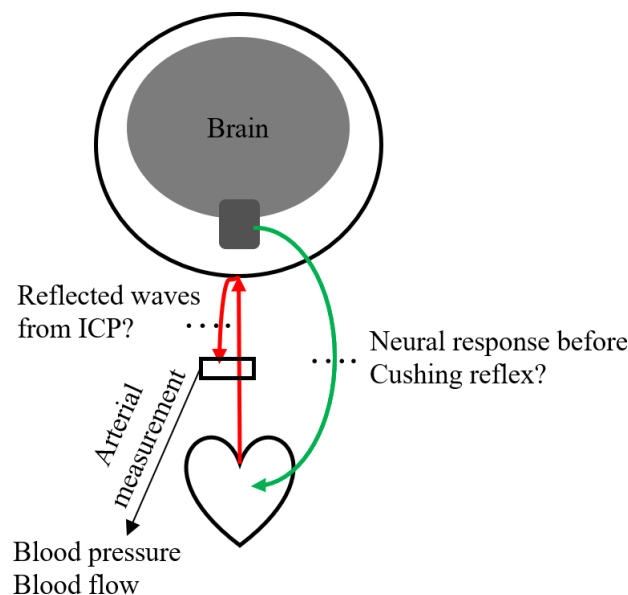


Figure 30. This study suggests that information from cardiovascular signals is transmitted to ICP, but considerably less information is transmitted from ICP to cardiovascular signals. This information (ICP→cardiovascular signals), despite minimal, may come from 1) reflected waves from ICP shaping the waveforms of aBP or cBF, and 2) a neural response to raised ICP before the Cushing reflex.

5.2. Intracranial pressure waveform

The magnitude of the frequency components in ICP signals is gradually raised as mean ICP increases (i.e. the higher the mean ICP, the higher the pulse ICP), showing a larger rise when mean ICP exceeds 20 mmHg. Additionally, there is an interaction effect aBPxICP on the magnitude of the frequency components (Figure 15). This means that a specific waveform and pulse may correspond to a specific range of mean ICP, with greater differences between the waveform and pulse of mean ICP above 20 mmHg. The directly proportional relationship between pulse ICP and mean ICP agrees with previous studies (Oswal & Toma 2017); however, this relationship may not be linear since pulse ICP changes more steeply when mean ICP exceeds 20 mmHg (Figure 31).

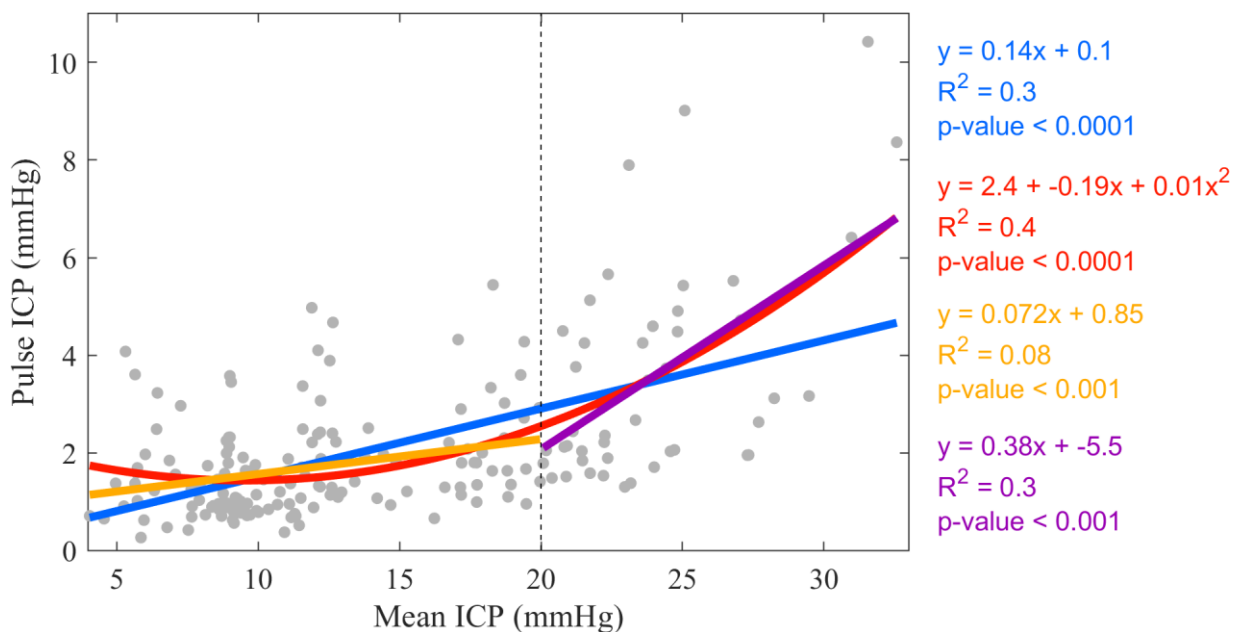


Figure 31. Observed mean ICP versus observed pulse ICP. The rate of change associated with pulse ICP is five times higher for mean ICP above 20 mmHg (purple line) than for mean ICP below 20 mmHg (yellow line). Thus, the quadratic model (red line) has a better fit than the linear model (blue line). Data come from 11 rats ventilated at 90 breaths/min, paced at 400 and 500 bpm, and subjected to several levels of mean ICP (<10, 10-15, 15-20, >20 mmHg) and mean aBP (70, 100, 130 mmHg).

Unlike ICP, aBP did not show a substantial change in the magnitude of frequency components as a function of mean ICP (Figure 16), this suggests that aBP waveforms are not modified by mean ICP at the studied range of mean ICP. The magnitudes of frequency components in cBF showed a significant but less strong dependence on mean ICP (Figure 17); being the second (cardiac frequency) and the third (first harmonic of cardiac frequency) frequency components reduced for mean ICP of 10-15 mmHg. Although the reduction was not significant, there is the possibility that a particular cBF waveform, with lower pulse amplitude, occurs when mean ICP is 10-15 mmHg; further research with a larger sample size is needed.

Attenuation below 25% of the cardiac frequency in aBP signals resulted in slightly more resemblance between ICP and aBP waveforms at resting conditions (Figure 19). This is consistent with previous research suggesting that the intracranial space filters arterial pulsatility around the cardiac frequency (Kasuga *et al.* 1987; Zou *et al.* 2008; Wagshul *et al.* 2009, 2011; Kim *et al.* 2012). The theory is that this feature may protect cerebral microvessels from mechanical damage by reducing the transmission of the pulse to those vessels. However, an attenuation higher than 25% diminished the resemblance between the waveforms. This indicates that, despite the intracranial space dampening some of the arterial pulsatility, subtracting the cardiac frequency of aBP waveforms may be an over simplistic approach to approximate ICP waveforms. Additionally, this approach cannot be used directly to estimate pulse ICP as it provides estimation of the waveform shape, but not the calibration of that ICP waveform.

HR and VR showed no significant effect on the magnitude and phase of the transfer functions other than adding further data to the same curves: the system compliance is not changed, but different sections of the curve are being sampled by modifying the HR (Figure 20 - Figure

23). This implies that transfer function models can be applied to any subject regardless of the individual HR or respiration rate. On the other hand, changing the cardiac frequency changes the period or duration of the cardiac pulses in ICP, aBP and cBF signals (the higher the HR, the shorter the individual pulse), and it may change the waveforms as well. For example, the magnitude of the transfer function considering cBF at the cardiac frequency is higher for HR paced at 300 bpm than for HR paced at 500 bpm (Figure 23); this implies that, in this case, the pulse of ICP and/or cBF was altered by HR. Analysis of the amplitude of the frequency components in the signals showed that exclusively aBP waveforms are significantly altered by HR, which is consistent with previous studies (Wilkinson *et al.* 2002; Tan *et al.* 2012). On the other hand, VR is not likely to change the period, pulse, or waveform of ICP, aBP, and cBF signals because the wave at the respiratory frequency is in a higher temporal scale, just “carrying” the individual cardiac pulses.

A reduction in the magnitude of the transfer functions (ratio ICP/aBP or ICP/cBF) implies a reduction of magnitude in the frequency components of ICP with respect to those of aBP or cBF. Thus, the smaller the transfer function magnitude, the more dampening of ICP frequency components. Both transfer function models (Figure 24, Figure 25) may suggest that as mean ICP increases, there is a significant reduction in the ability of the intracranial space to dampen arterial pressure pulsatility. This ability is more sharply reduced when mean ICP reaches 20 mmHg; 20 mmHg may be the threshold from which the intracranial space can no longer maintain intracranial pulsatility within a healthy range. Consistently, other studies and the clinical practice have considered 20 mmHg as the upper limit for normal mean ICP (Dunn 2002; Roytowski & Figaji 2013).

An inverse relationship was observed between mean aBP and the magnitude of the transfer function models (Figure 24, Figure 25). This magnitude reduction is due to both the reduction in ICP pulsatility (Figure 15) and the increase of aBP pulsatility (Figure 16) as mean aBP

raises. The transfer function model considering aBP waveforms (Figure 24) indicates that ICP frequency components are less dampened at frequencies around 20 Hz for mean aBP of 70 and 100 mmHg. For aBP of 130 mmHg, the least dampening occurs at frequencies around 35 Hz. Like previous research (Kasuga *et al.* 1987; Zou *et al.* 2008; Wagshul *et al.* 2009, 2011; Kim *et al.* 2012), this study shows dampening of the ICP waveform (with respect to aBP waveform) at the main cardiac frequency (6.5-8.5 Hz). However, at mean aBP of 70 and 100 mmHg, a higher dampening was found at frequency components above 30 Hz; previous studies did not consider frequencies higher than 30 Hz. The transfer function model considering cBF waveforms (Figure 25) shows the general trend that magnitude of frequency components is reduced as frequency increases, suggesting that ICP pulsatility is attenuated as a function of frequency. This pulsatility dampening, as previously suggested (Kasuga *et al.* 1987; Zou *et al.* 2008; Wagshul *et al.* 2009, 2011; Kim *et al.* 2012), may be a mechanism to prevent damage of thin cerebral capillaries potentially caused by the pulsatile force of the heartbeat.

The phase of the transfer function model considering aBP (Figure 24) was exclusively affected by frequency, but no clear trend could be identified; this may be due to noise or actual intersubject variability. On the other hand, the phase of the transfer function model considering cBF is more consistent, and it was significantly correlated with frequency, mean aBP (for HR=400 bpm), and mean ICP (for HR=500 bpm) (Figure 25). An increasing trend from negative values up to values around zero could be identified. Negative values indicate that the phase of cBF frequency components is greater than the phase of ICP frequency components and, consequently, that the ICP wave at that frequency occurs after the cBF wave. That the cardiac cycle observed in cBF waveforms occurs before the cardiac cycle observed in ICP waveforms (Figure 25) matches the notion that ICP pulsatility has an arterial origin (Cardoso *et al.* 1988; Wagshul *et al.* 2009, 2011). However, in some cases ICP waves

seem to occur before aBP or cBF waves (e.g. positive phase at the cardiac frequency of the transfer function from aBP to ICP; Figure 24), this phenomenon has also been reported in previous studies (Zou *et al.* 2008), and a possible explanation is that the observed ICP cycle is not caused by the nearest aBP or cBF cycle but by the previous one, respecting the idea that aBP or cBF pulsatility occurs before ICP pulsatility. It was also observed that the larger the mean ICP, the larger the absolute value of phase of the transfer function from cBF to ICP (mainly at the cardiac frequency) (Figure 25). This means an increasing time lag of the ICP waveform with respect to the aBP waveforms as mean ICP increases.

Evensen *et al.* (2018) used a transfer function approach to estimate the ICP waveform from arterial blood pressure in hydrocephalus patients with normal ICP, concluding that the approach is not reliable for use in clinical practice. However, their transfer function model was constructed from a single subject at resting conditions. The transfer function models in this study (Figure 24, Figure 25) are more comprehensive by coming from several subjects (up to 11 rats), not only one, and by considering several levels of mean ICP, mean aBP, HR and VR (different states of the system). This consideration of different states of the system, coupled with the fact that mean ICP (model input) correlates with pulse ICP (Figure 31), enhances the potential of transfer function models to predict the ICP waveform from aBP or cBF waveforms.

5.3. Model assessment

By knowing the mean ICP value (from invasive measurement), it was possible to use transfer function models to estimate the pulse and waveform of ICP because: 1) the models consider different mean ICP levels and 2) there is a strong relationship between mean and pulse ICP (Figure 31). These estimations of ICP, both pulse and waveform, were more accurate and consistent (smaller SE) for mean aBP above 100 mmHg (Figure 27-Figure 29). A possible

explanation is that the system becomes stiffer as mean aBP raises (blood vessels are constricted), thus reducing the magnitude and variability of pulsations. Similarly, the estimations were more accurate and consistent for mean ICP below 20 mmHg. This may be due to the fact that the upper limit of the category mean ICP>20 mmHg was not strictly limited, 49 mmHg being at the highest value; the other mean ICP categories comprise an interval of only 5 mmHg. Additionally, this reduced ability to estimate ICP pulse and waveform at mean ICP>20 mmHg could be due to intersubject variability; some individuals may be more resilient to raised ICP. Despite the transfer function model considering cBF showed slightly more overestimation of pulse ICP at mean aBP of 70 mmHg (Figure 29), the performance of both transfer function models (the one considering aBP waveforms and the one considering cBF waveforms) was statistically equal. This was expected since blood flow is a consequence of blood pressure.

The transfer function model in Evensen *et al.* (2018) used to estimate pulse ICP from aBP waveform at normal mean ICP proved an error of 1.6 ± 1.0 mmHg. The transfer function models in this study showed an error below 1 ± 1.0 mmHg for mean ICP<10 mmHg (Figure 29), proving accuracy improvement. The RMSE associated to ICP waveform estimation is relatively small (Figure 27); however, the correct number and position of peaks observed in ICP waveforms were not usually reproduced by the models. Thus, estimations of pulse ICP may be more readily achievable whereas full characterisation of the ICP waveform may require further inputs. These inputs could come in the form of non-invasive intracranial signals that were not able to be measured in the rodent model due to size limitations, such as transcranial Doppler assessment of intracranial arterial vessel flow.

5.4. Limitations and potential solutions

Despite the benefits of rodents as animal models of human physiology, the circulatory system of humans and rats is not an exact match (e.g. differences in size, architecture, and HR). Thus, the generalization of findings to human physiology must be taken with caution. Once a sufficiently robust transfer function model is developed to estimate ICP in rats, new studies in humans should be carried out, as far as ethically possible, to validate its applicability in humans.

The rat experiments developed for this project consider several levels of mean aBP. However, the drugs used to lower (sodium nitroprusside) or raise (phenylephrine) mean aBP act by expanding or constricting blood vessel, including cerebral vessels. Thus, there is uncertainty whether the ICP alterations observed after drug injections were due to changes in the systemic blood pressure alone or also direct drug effects on vascular smooth muscle, changing cerebral arterial vessel diameters. Whilst the effect of sodium nitroprusside and phenylephrine in the infusion rates used has been shown to have minimal effect on large artery stiffness in the rat (Butlin *et al.* 2015), similar studies have not yet been carried out for intracranial vessels.

Since the relationships between ICP and cardiovascular signals do not match exactly with linear models, the conclusions derived from the stepwise mixed-model regression analysis are not definitive. The use of more robust, nonlinear techniques should be considered to corroborate the current conclusions. Mean ICP was not estimated because of minimal predictive potential shown in multiple linear regression model, consequently, the estimation of ICP waveform and pulse from the transfer function models required the invasive measurement of mean ICP. However, mean ICP could be provided from other promising non-invasive methods estimating mean ICP such as measurement of optic nerve sheath

diameter, pupillometry, and intraocular pressure (Section 2.3.4. Ophthalmic). Complementing non-invasive methods good at estimating the ICP waveform (e.g. cardiovascular signals) with methods good at estimating mean ICP may be key for better non-invasive estimation of ICP.

The Fourier transform is applicable for periodic time series; however, ICP and cardiovascular signals may not always show a well-defined periodic behavior, hindering their reconstruction via Fourier transform. This could have a detrimental effect on the accuracy of transfer function models. This theoretical limitation can be addressed by considering each cardiac cycle in isolation and conducting analysis on that cardiac period assuming infinite repeat of the waveform (for the purposes of analysis). Wavelets is another mathematical transform, which has shown accuracy for signal reconstruction and does not depend on the theoretical assumption of infinite periodicity. Wavelet transforms may be an alternative to the Fourier Transform. The two mathematical approaches, despite having different assumptions and working in different domains (frequency and time), generally arrive at the same conclusion. However, the wavelet method may provide more rapid processing of data.

Despite the inter-subject variability reflected in the transfer functions was small (consistency in the mean value and small SE, particularly at mean aBP > 70 mmHg and mean ICP < 20 mmHg) (Figure 24, Figure 25), the use of generalized transfer functions (average from several individuals) may be overlooking intrasubject variability, explaining why the estimated waveforms were not always reproducing the number of peaks observed in invasive ICP waveforms. In other words, the transfer function models consider that two subjects with the same mean aBP, mean ICP, and HR will have the same ICP waveform, which does not necessarily have to be true. Thus, more inputs such as jugular flow and pressure, blood flow in cerebral arteries, CSF flow, body weight, age, and sex could be used to consider individual specificity in transfer function models.

5.5. Project significance

This research is the first of its kind based on comprehensive experiments with an animal model, Sprague-Dawley rat, considering wide but still physiological ranges of ICP, aBP, HR, and VR. Therefore, the transfer function models are more complex than those in previous studies, showing that estimation of ICP waveform from cardiovascular signals is possible, and that it could still be improved by adding more inputs into the models. Additionally, the new experimental information provided is highly valuable in the sense that it could not be derived from human experimentation due to ethical restrictions. The findings presented here contribute to shortening the accuracy gap between invasive and non-invasive ICP monitoring. Although non-invasive modalities are not yet a substitute of invasive monitoring, they could help to decide whether invasive monitoring is necessary or not, and they could provide ICP estimates when invasive techniques are unavailable or contraindicated.

5.6. Future work

Estimating mean ICP from cardiovascular signals and adding the estimation into transfer function models constitute a next step to investigate. The multiple mixed-model showed minimal predictive value of mean ICP. However, if this predictive value is sufficient to differentiate between mean ICP above or below 20 mmHg, the estimations of ICP pulse and waveform could retain their degree of accuracy because the transfer function curves are very similar when mean ICP is below 20 mmHg. The effect of other categories of mean ICP above 20 mmHg (e.g. 20-25, 25-30, 30-35) should also be evaluated. Analyzing data at larger timescales (e.g. minute-timescale) could reveal more information between the relationships of ICP and cardiovascular signals. Additionally, the use of more comprehensive signal decomposition techniques, e.g. wavelets, could be considered instead of the Fourier Transform.

Considering more inputs into the models constitutes a priority. One input could be the venous component (e.g. jugular blood pressure and flow) (Figure 32), which is known to shape the diastolic wave (P3) of normal ICP waveform (Fan *et al.* 2008), and the entire waveform when there is impairment of cerebral autoregulation or acute venous hypertension (Dereymaeker *et al.* 1971; Pettorossi *et al.* 1978). Analyzing the differences between venous waveforms and arterial waveforms could be explored as an approach analogous to the wave propagation method described in Section 2.3.3., with the difference that it would not be required to induce artificial waves. Blood flow in cerebral arteries, CSF flow, body weight, age and sex could also be considered. More rat experiments will be performed to achieve this task. Finally, similar transfer function models should be constructed from available human data, assessing their accuracy for potential clinical use.

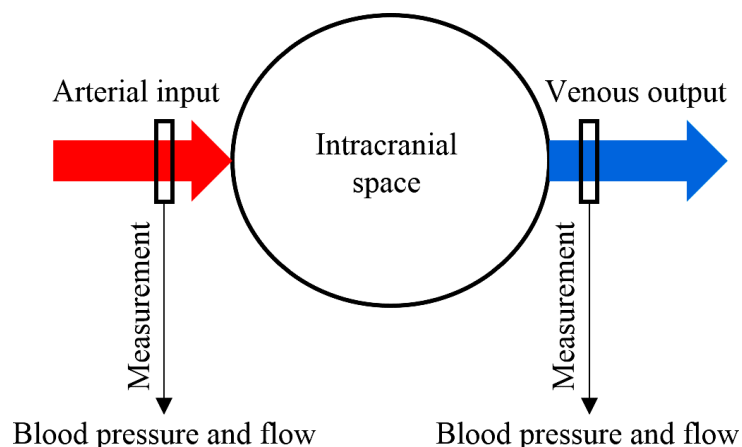


Figure 32. Analyzing the differences between venous waveforms and arterial waveforms is proposed as an approach for future studies aiming to estimate ICP from cardiovascular signals. This approach would be analogous to the wave propagation method described in Section 2.3.3., with the difference that it would not be required to induce artificial waves.

Chapter 6: Conclusion

The pressure inside the skull (ICP) is the sum of pressures exerted by the intracranial components (i.e. brain, blood, and CSF). Since the skull is a rigid compartment, to maintain a constant intracranial volume, a rise in volume of an intracranial component (e.g. blood) should match a reduction in volume of at least one other intracranial component (e.g. CSF). If the intracranial elements strive to match the rise of an intracranial element, the tendency towards the increase of intracranial volume (matter being pushed harder towards the intracranial space) is reflected as a rise in ICP. Cerebral autoregulation (active dilation or constriction of cerebral vessels) is responsible for maintaining a relatively constant cerebral blood inflow across a variable but limited range of CPP (mean arterial blood pressure – mean ICP). Since raised ICP may lead to severe health complications such as reduced cerebral blood inflow, brain herniation and death, monitoring ICP is vital during the management of neurological patients.

The most accurate way to measure ICP is via an intraventricular pressure sensor; however, this is an invasive procedure not always available and associated to risks. To avoid potential drawbacks, several non-invasive techniques have been proposed, but so far none of them has demonstrated enough ease of use and accuracy to reliably predict ICP during clinical monitoring. Estimating ICP from cardiovascular signals, such as arterial pressure and flow, constitutes a particularly attractive method because they are easy and inexpensive to obtain, their continuous monitoring would favor real-time estimation of the whole ICP waveform, and their potential to generate more accurate estimates is still high.

The present research investigated the adequacy of using cardiovascular signals –heart rate (HR), aortic blood pressure (aBP) and carotid blood flow (cBF)– as inputs for transfer function models to estimate ICP magnitude (pulse and mean) and waveform as an alternative means to invasive ICP measurement. To do so, comprehensive animal experiments involving manipulations of ICP (sequentially raised from resting ICP to 30-40 mmHg with infusions of artificial intracranial fluid), aBP (lowered with sodium nitroprusside and raised with phenylephrine, 30 µg/kg/min, across a physiological range), HR (paced at 400 and 500 bpm), and breathing rate (artificial ventilation at 60 and 90 breaths/min) were performed in 11 anaesthetised Sprague Dawley rats. Data were analyzed via linear regression models and signal analysis techniques, and the main findings are summarized below:

- Manipulations of cardiovascular signals produced an evident effect on ICP magnitude (mean and pulse), while increasing mean ICP had minimal effect on cardiovascular signals. Thus, SMMR analysis showed that cardiovascular parameters have minimal but significant predictive value of ICP magnitude, mainly pulse ICP.
- As mean aBP increases due to vasoconstriction, ICP pulsatility decreases, aBP pulsatility increases, and cBF pulsatility slightly decreases.
- HR influences the amplitude of aBP, but not the amplitude of cBF or ICP waveforms. Mean ICP influences ICP waveforms, but not aBP or cBF waveforms.
- Attenuating the cardiac frequency of aBP waveforms did not provide accurate estimates of ICP waveforms.
- Neither the VR nor the HR showed a significant effect on the transfer function models, indicating that the models can be applied to any subject regardless the individual VR or HR.
- The magnitude of the transfer function models was similar for the three categories of mean ICP below 20 mmHg, but considerably higher for mean ICP > 20 mmHg.

- As mean aBP increases due to vasoconstriction, the magnitude of the transfer function models is reduced (ICP pulsatility is dampened in relation to aBP and cBF pulsatility).
- The phase of the transfer function model considering cBF depends on mean ICP: the larger the mean ICP, the larger the absolute value of the phase (larger lag of ICP waveforms in relation to cBP waveforms).
- The transfer function models showed the same potential to reproduce ICP waveforms (Root Mean Square Error (RMSE) ≤ 4 mmHg), being more accurate as mean aBP increases and for mean ICP below 20 mmHg (RMSE ≤ 0.5 mmHg).
- The transfer function models provided good estimates of pulse ICP, particularly for mean ICP below 10 mmHg (Error = 1 ± 1.0 mmHg), proving accuracy improvement in relation to previous studies (e.g. Evensen *et al.* 2018).
- Systemic cardiovascular measures have predictive value in estimating the ICP magnitude and waveform, but other inputs may be necessary to improve accuracy in estimating ICP across the full physiological range.

References

- Aisenson MR (1949) Closing of the anterior fontanelle. *PEDIATRICS* 6: 223-226.
- Alessio SM (2016) Digital signal processing and spectral analysis for scientists: concepts and applications. Springer International Publishing Switzerland, DOI: 10.1007/978-3-319-25468-5.
- Allocca JA (1980) Method and apparatus for non-invasive monitoring of intracranial pressure US Patent 4,204,547.
- Alperin NJ, Lee SH, Loth F, Raksin PB, Lichtor T (2000) MR-intracranial pressure (ICP): a method to measure intracranial elastance and pressure noninvasively by means of MR imaging: baboon and human study. *Radiology* 217: 877-85.
- Alperin N, Hushek SG, Lee SH, Sivaramakrishnan A, Lichtor T (2005) MRI study of cerebral blood flow and CSF flow dynamics in an upright posture: the effect of posture on the intracranial compliance and pressure. *Acta Neurochir Suppl* 95: 177-181.
- Anand A, Pass A, Urfy MZ, Tang R, Cajavilca C, Calvillo E, Suarez JI, Venkatasubba Rao CP, Bershada EM (2016) Optical coherence tomography of the optic nerve head detects acute changes in intracranial pressure. *J Clin Neurosci* 29: 73-76.
- Anderson RC, Kan P, Klimo P, Brockmeyer DL, Walker ML, Kestle JR (2004) Complications of intracranial pressure monitoring in children with head trauma. *J Neurosurg* 101: 53-58.
- Andersson L, Sjolund J, Nilsson J (2012) Flash visual evoked potentials are unreliable as markers of ICP due to high variability in normal subjects. *Acta Neurochir(Wien)* 154: 121-127.

- Andrews PJD, Citerio G (2004) Intracranial pressure Part one: Historical overview and basic concepts. *Intensive Care Med* 30: 1730-1733.
- Asiedu DP, Lee KJ, Mills G, Kaufmann EE (2014) A review of non-invasive methods of monitoring intracranial pressure. *J Neurol Res* 4: 1-6.
- Aaslid R, Markwalder TM, Nornes H (1982) Noninvasive intracranial Doppler ultrasound recording of flow velocity in basal cerebral arteries. *J Neurosurg* 57: 769-774.
- Avan P, Büki B, Lemaire JJ, Dordain M, Chazal J (1996) Otoacoustic emissions: a new tool for monitoring intracranial pressure. *Hear Res* 94: 125-129.
- Avolio AP, Van Bortel LM, Boutouyrie P, Cockcroft JR, McEniery CM, Protogerou AD, Roman MJ, Safar ME, Segers P, Smulyan H (2009) Role of pulse pressure amplification in arterial hypertension: experts' opinion and review of the data. *Hypertension* 54 375-83.
- Avolio AP, Butlin M, Walsh A (2010) Arterial blood pressure measurement and pulse wave analysis—their role in enhancing cardiovascular assessment. *Physiol Meas* 31: R1–R47.
- Balestreri M, Czosnyka M, Hutchinson P, Steiner LA, Hiler M, Smielewski P, Pickard JD (2006) Impact of intracranial pressure and cerebral perfusion pressure on severe disability and mortality after head injury. *Neurocrit Care* 4: 8-13.
- Baurmann M (1925) On the origin and clinical significance of retinal venous pulse. *Zusammenkunft Deutschen Ophthalmologie* 45: 53-59.
- Behmanesh B, Setzer M, Noack A, Bartels M, Quick-Weller J, Seifert V, Freiman TM (2016) Noninvasive epicutaneous transfontanelle intracranial pressure monitoring in children under the age of 1 year: a novel technique. *J Neurosurg Pediatr* 27:1-5.

- Beiner JM, Olgivy CS, DuBois AB (1997) Cerebral blood flow changes in response to elevated intracranial pressure in rabbits and bluefish: a comparative study. *Comp Biochem Physiol* 116A: 245-252.
- Bellner J, Romner B, Reinstrup P, Kristiansson KA, Ryding E, Brandt L (2004) Transcranial Doppler sonography pulsatility index (PI) reflects intracranial pressure (ICP). *Surg Neurol* 62: 45-51.
- Bershad EM, Urfy MZ, Pechacek A, McGrath M, Calvillo E, Horton NJ, Voss SE (2014) Intracranial pressure modulates distortion product otoacoustic emissions: a proof-of-principle study. *Neurosurgery* 75: 445-454; discussion 54-55.
- Brain Trauma Foundation (2000) The American Association of Neurological Surgeons. The Joint Section on Neurotrauma and Critical Care. Recommendations for intracranial pressure monitoring technology. *J Neurotrauma* 17: 497-506.
- Bronzwaer A-SGT, Stok WJ, Westerhof BE, van Lieshout JJ (2014) Arterial pressure variations as parameters of brain perfusion in response to central blood volume depletion and repletion. *Frontiers in Physiology* 5: 1-12.
- Broughton SA, Kurt B (2009) Discrete Fourier analysis and wavelets: applications to signal and image processing. John Wiley & Sons, Inc., DOI: 10.1002/9781118032442.
- Bruce BB (2014) Noninvasive assessment of cerebrospinal fluid pressure. *J Neuroophthalmol* 34: 288-294.
- Bruder N, N'Zoghe P, Graziani N, Pelissier D, Grisoli F, François G (1995) A comparison of extradural and intraparenchymatous intracranial pressures in head injured patients. *Intensive Care Med* 21: 850-852.
- Bouma GJ, Muizelaar JP, Bandoh K, Marmarou A (1992) Blood pressure and intracranial pressure-volume dynamics in severe head injury: relationship with cerebral blood flow. *J Neurosurg* 77: 15-19.

- Buki B, Avan P, Lemaire JJ, Dordain M, Chazal J, Ribari O (1996) Otoacoustic emissions: a new tool for monitoring intracranial pressure changes through stapes displacements. *Hear Res* 2: 125-139.
- Buki B, Giraudet F, Avan P (2009) Non-invasive measurements of intralabyrinthine pressure changes by electrocochleography and otoacoustic emissions. *Hear Res* 2: 51-59.
- Butlin M, Qasem A, Battista F, Bozec E, McEniery CM, Millet-Amaury E, Pucci G, Wilkinson IB, Schillaci G, Boutouyrie P, Avolio AP (2013) Carotid-femoral pulse wave velocity assessment using novel cuff-based techniques: comparison with tonometric measurement. *J Hypertens* 31: 2237-2243.
- Butlin M, Lindsay G, Viegas KD, Avolio AP (2015) Pressure dependency of aortic pulse wave velocity in vivo is not affected by vasoactive substances that alter aortic wall tension ex vivo. *Am J Physiol Heart Circ Physiol* 308: H1221-H1228.
- Cardim D, Robba C, Donnelly J, Bohdanowicz M, Schmidt B, Damian M, Varsos GV, Liu X, Cabeleira M, Frigieri G, Cabella B, Smielewski P, Mascarenhas S, Czosnyka M (2016a) Prospective study on noninvasive assessment of intracranial pressure in traumatic brain-injured patients: comparison of four methods. *J of neurotrauma* 33: 792-802.
- Cardim D, Robba C, Bohdanowicz M, Donnelly J, Cabella B, Liu X, Cabeleira M, Smielewski P, Schmidt B, Czosnyka M (2016b) Non-invasive monitoring of intracranial pressure using transcranial Doppler ultrasonography: is it possible? *Neurocrit Care* 25: 473-491.
- Cardoso ER, Rowan JO, Galbraith S (1983) Analysis of the cerebrospinal fluid pulse wave in intracranial pressure. *J Neurosurg* 59: 817-821.
- Cardoso ER, Reddy K, Bose D (1988) Effect of subarachnoid haemorrhage on intracranial pulse waves in cats. *J Neurosurg* 69: 712-718.

- Carrera E, Kim D-J, Castellani G, Zweifel C, Czosnyka Z, Kasproicz M, Smielewski P, Pickard JD, Czosnyka M (2010) What shapes pulse amplitude of intracranial pressure? *J Neurotrauma* 27: 317-324.
- Carretero OA, Oparil S (2000) Essential hypertension part I: definition and etiology. *Circulation* 101: 329-335.
- Chen C-H, Nevo E, Fetcs B, Pak PH, Yin FCP, Maughan WL, Kass DA (1997) Estimation of central aortic pressure waveform by mathematical transformation of radial tonometry pressure: validation of generalized transfer function. *Circulation* 95: 1827-1836.
- Chen JW, Gombart ZJ, Rogers S, Gardiner SK, Cecil S, Bullock RM (2011) Pupillary reactivity as an early indicator of increased intracranial pressure: the introduction of the neurological pupil index. *Surg Neurol Int* 2: 82.
- Chen JW, Vakil-Gilani K, Williamson KL, Cecil S (2014) Infrared pupillometry, the Neurological Pupil index and unilateral pupillary dilation after traumatic brain injury: implications for treatment paradigms. *SpringerPlus* 3: 548.
- Chen H, Wang J, Mao S, Dong W, Yang H (2012) A new method of intracranial pressure monitoring by EEG power spectrum analysis. *Can J Neurol Sci* 39: 483-487.
- Chesnut RM, Gautille T, Blunt BA, Klauber MR, Marshall LE (1994) The localizing value of asymmetry in pupillary size in severe head injury: relation to lesion type and location. *Neurosurgery* 34: 840-845.
- Chopp M, Portnoy HD (1980) Systems analysis of intracranial pressure. *J Neurosurg* 53: 516-527.
- Chunyu T, XP, Li N, Qin L, Tian Z (2014) The correlation between intracranial pressure and intraocular pressure after brain surgery. *Int J Ophthalmol Eye Res* 2: 54-8.

- Couret D, Boumaza D, Grisotto C, Triglia T, Pellegrini L, Ocquidant P, Bruder NJ, Velly LJ (2016) Reliability of standard pupillometry practice in neurocritical care: an observational, double-blinded study. *Crit Care* 20: 99.
- Cserr HF (1971) Physiology of the choroid plexus. *Physiol Rev* 51: 273-311.
- Cushing H (1902) Some experimental and clinical observations concerning states of increased intracranial tension.1: the mutter lecture for 1901. *The American Journal of the Medical Sciences* 124: 375.
- Cushing H (1903) The blood-pressure reaction of acute cerebral compression, illustrated by cases of intracranial hemorrhage: a sequel to the mutter lecture for 1901. *The American Journal of the Medical Sciences* 125: 1017.
- Czigler B, Csikós D, Hidasi Z, Anna GZ, Csibri E, Kiss E, Salacz P, Molnár M (2008) Quantitative EEG in early Alzheimer's disease patients-power spectrum and complexity features. *Int J Psychophysiol* 68: 75-80.
- Czosnyka M, Czosnyka Z, Pickard JD (1996a) Laboratory testing of three intracranial pressure microtransducers: technical report. *Neurosurgery* 38: 219-224.
- Czosnyka M, Guazzo E, Whitehouse M, Smielewski P, Czosnyka Z, Kirkpatrick P, Piechnik S, Pickard JD (1996b) Significance of intracranial pressure waveform analysis after head injury. *Acta Neurochir (Wien)* 138: 531-542.
- Czosnyka M, Smielewski P, Piechnik S, Schmidt EA, Al-Rawi PG, Kirkpatrick PJ, Pickard JD (1999) Hemodynamic characterization of intracranial pressure plateau waves in head-injured patients. *J Neurosurg* 91: 11-19.
- Czosnyka M, Pickard JD (2004) Monitoring and interpretation of intracranial pressure. *J Neurol Neurosurg Psychiatry* 75: 813-821.

- Czosnyka M, Czosnyka Z, Keong N, Lavinio A, Smielewski P, Momjiam S, Schmidt EA, Petrella G, Owler B, Pickard JD (2007) Pulse pressure waveform in hydrocephalus: what it is and what it isn't. *Neurosurg Focus* 22: E2.
- Dardenne G, Dereymaeker A, Lacheron M (1969) Cerebrospinal fluid pressure and pulsatility: an experimental study of circulatory and respiratory influences in normal and hydrocephalic dogs. *Europ Neurol* 2: 193-216.
- Davanzo JR, Sieg EP, Timmons SD (2017) Management of traumatic brain injury. *Surg Clin N Am* 97: 1237–1253.
- Davidoff LM, Chamlin M (1959) The “fontanometer”: adaptation of the Schiotz tonometer for the determination of intracranial pressure in the neonatal and early periods of infancy. *PEDIATRICS* 24: 1065-1068.
- Davies DJ, Su Z, Clancy MT, Lucas SJ, Dehghani H, Logan A, Belli A (2015) Near-infrared spectroscopy in the monitoring of adult traumatic brain injury: a review. *J Neurotrauma* 32: 933-941.
- Decimo I, Fumagalli G, Berton V, Krampera M, Bifari F (2012) Meninges: from protective membrane to stem cell niche. *Am J Stem Cells* 1: 92-105.
- Dereymaeker A, Stevens A, Rombouts JJ, Lacheron JM, Pierquin A (1971) Study on the influence of the arterial pressure upon the morphology of cisternal CSF pulsations. *Europ Neurol* 5: 107-114.
- Donnelly L (2014) The brain: functional divisions. *Anaesthesia & Intensive Care Medicine* 15: 195-200.
- Donnelly J, Czosnyka M, Harland S, Varsos GV, Cardim D, Robba C, Liu X, Ainslie PN, Smielewski P (2016) Cerebral haemodynamics during experimental intracranial hypertension. *Journal of Cerebral Blood Flow & Metabolism* 37: 694-705.

- Driessen C, Eveleens J, Bleyen I, Van Veelen ML, Joosten K, Mathijssen I (2014) Optical coherence tomography: a quantitative tool to screen for papilledema in craniosynostosis. *Childs Nerv Syst* 30: 1067-1073.
- Dronkers CJ (2011) The estimation of intracranial pressure using blood pressure signals. Master's Thesis. University of Twente, Netherlands.
- Drummond JC (2000) Monitoring depth of anaesthesia: with emphasis on the application of the Bispectral Index and the middle latency auditory evoked response to the prevention of recall. *Anaesthesiology* 93: 876-882.
- Du R, Meeker M, Bacchetti P, Larson MD, Holland MC, Manley GT (2005) Evaluation of the portable infrared pupillometer. *Neurosurgery* 57: 198-203.
- Dunn LT (2002) Raised intracranial pressure. *J Neurol Neurosurg Psychiatry* 73(Suppl I): i23-i27.
- Eide PK (2003) The relationship between intracranial pressure and size of cerebral ventricles assessed by computed tomography. *Acta Neurochir (Wien)* 145: 171-179.
- Eide PK (2006) A new method for processing of continuous intracranial pressure signals. *Med Eng Phys* 28: 579-587.
- Eide PK, Brean A (2006) Lumbar cerebrospinal fluid pressure waves versus intracranial pressure waves in idiopathic normal pressure hydrocephalus. *Br J Neurosurg* 20: 407-414.
- Eide PK, Sorteberg W (2007) Association among intracranial compliance, intracranial pulse pressure amplitude and intracranial pressure in patients with intracranial bleeds. *Neurol Res* 29: 798-802.
- Eide PK (2008) Comparison of simultaneous continuous intracranial pressure (ICP) signals from ICP sensors placed within the brain parenchyma and the epidural space. *Med Eng Phys* 30: 34-40.

- Eide PK (2016) The correlation between pulsatile intracranial pressure and indices of intracranial pressure-volume reserve capacity: results from ventricular infusion testing. *J Neurosurg* 125: 1493-1503.
- Eisenberg HM, Gary HE Jr, Aldrich EF, Saydjari C, Turner B, Foulkes MA, Jane JA, Marmarou A, Marshall LF, Young HF (1990) Initial CT findings in 753 patients with severe head injury: a report from the NIH Traumatic Coma Data Bank. *J Neurosurg* 73: 688-698.
- Esper SA, Pinsky MR (2014) Arterial waveform analysis. *Best Practice & Research Clinical Anaesthesiology* 28: 363-380.
- Evensen KB, O'Rourke M, Prieur F, Holm S, Eide PK (2018) Non-invasive estimation of the intracranial pressure waveform from the central arterial blood pressure waveform in idiopathic normal pressure hydrocephalus patients. *Scientific Reports* 8: 4714.
- Fan BJ-Y, Kirkness C, Vicini P, Burr R, Mitchell P (2008) Intracranial pressure waveform morphology and intracranial adaptive capacity. *Am J Crit Care* 17:545-554.
- Figaji AA, Zwane E, Fieggen AG, Siesjo P, Peter JC (2009) Transcranial Doppler pulsatility index is not a reliable indicator of intracranial pressure in children with severe traumatic brain injury. *Surgical Neurology* 72: 389-394.
- Firsching R, Schütze M, Motschmann M, Behrens-Baumann W (2000) Venous ophthalmodynamometry: a non-invasive method for assessment of intracranial pressure *J Neurosurg* 93: 33-6.
- Firsching R, Muller C, Pauli SU, Voellger B, Rohl FW, Behrens-Baumann W (2011) Noninvasive assessment of intracranial pressure with venous ophthalmodynamometry. *Clinical article. J Neurosurg* 115: 371-374.
- Fountas KN, Sitkauskas A, Feltes CH, Kapsalaki EZ, Dimopoulos VG, Kassam M, Grigorian AA, Robinson JS, Ragauskas A (2005) Is non-invasive monitoring of intracranial

pressure waveform analysis possible? Preliminary results of a comparative study of non-invasive versus invasive intracranial slow-wave waveform analysis monitoring in patients with traumatic brain injury. *Med Sci Monit* 11: CR58-CR63.

Fountas KN, Kapsalaki EZ, Machinis TG, Boev AN, Robinson JS, Troup EC (2006) Clinical implications of quantitative infrared pupillometry in neurosurgical patients. *Neurocrit Care* 5: 55-60.

Frigieri-Vilela GH, Cabella B, Mascarenhas S, Czosnyka M, Smielewski P, Dias C, Cardim DA, Mascarenhas YM, Wang CC, Andrade R, Tanaka K, Silva-Lopes L, Colli BO (2016) Validation of a New Minimally Invasive Intracranial Pressure Monitoring Method by Direct Comparison with an Invasive Technique. In: Ang BT. (eds) *Intracranial Pressure and Brain Monitoring XV. Acta Neurochirurgica Supplement*, vol 122. Springer, Cham.

Gaab MR, Heissler HE, Ehrhardt K (1989) Physical characteristics of various methods for measuring ICP. *Intracranial Pressure VII* (Berlin: Springer) pp 16-21.

Ganslandt O, Mourtzoukos S, Stadlbauer A, Sommer B, Rammensee R (2017) Evaluation of a novel non-invasive ICP monitoring device in patients undergoing invasive ICP monitoring: preliminary results. *J Neurosurg*, DOI: 10.3171/2016.11.JNS152268.

Galloon S (1969) The volume of the intracranial contents. *International Anesthesiology Clinics*: 7: 663-686.

Gao M, Rose WC, Fetics B, Kass DA, Chen C-H, Mukkamala R (2016) A simple adaptive transfer function for deriving the central blood pressure waveform from a radial blood pressure waveform. *SCIENTIFIC RepoRts* 6:33230, DOI: 10.1038/srep33230.

Gardner AJ, Shih SL, Adamov EV, Zafonte RD (2017) Research frontiers in traumatic brain injury: defining the injury. *Phys Med Rehabil Clin N Am* 28: 413-431.

- Gass A, Barker GJ, Riordan-Eva P, MacManus D, Sanders M, Tofts PS, McDonald WI, Moseley IF, Miller DH (1996) MRI of the optic nerve in benign intracranial hypertension. *Neuroradiology* 38: 769-773.
- Gastfriend BD, Palecek SP, Shusta EV (2017) Modeling the blood-brain barrier: Beyond the endothelial cells. *Current Opinion in Biomedical Engineering* DOI: 10.1016/j.cobme.2017.11.002.
- Geeraerts T, Newcombe VF, Coles JP, Abate MG, Perkes IE, Hutchinson PJ, Outtrim JG, Chatfield DA, Menon DK (2008) Use of T2- weighted magnetic resonance imaging of the optic nerve sheath to detect raised intracranial pressure. *Crit Care* 12: R114.
- Giraudet F, Longeras F, Mulliez A, Thalamy A, Pereira B, Avan P, Sakka L (2017) Noninvasive detection of alarming intracranial pressure changes by auditory monitoring in early management of brain injury: a prospective invasive versus non-invasive study. *Critical Care* 21-35, DOI: 10.1186/s13054-017-1616-2.
- Giron-Sierra JM (2017a) *Digital Signal Processing with Matlab examples, Volume 1: Signals and Data, Filtering, Non-stationary Signals, Modulation. Signals and Communication Technology*, Springer, DOI: 10.1007/978-981-10-2534-1.
- Giron-Sierra JM (2017b) *Digital Signal Processing with Matlab Examples, Volume 2: Decomposition, Recovery, Data-Based Actions. Signals and Communication Technology*, Springer, DOI: 10.1007/978-981-10-2537-2.
- Giulioni M, Ursino M (1996) Impact of cerebral perfusion pressure and autoregulation on intracranial dynamics: a modeling study. *Neurosurgery* 39: 1005-1014.
- Glick RP, Niebruegge J, Lee SH, Egibor O, Lichtor T, Alperin N (2006) Early experience from the application of a noninvasive magnetic resonance imaging-based measurement of intracranial pressure in hydrocephalus. *Neurosurgery* 59: 1052-1061.

- Golan S, Kurtz S, Mezd-Koursh D, Waisbourd M, Kesler A, Halpern P (2013) Poor correlation between intracranial pressure and intraocular pressure by hand-held tonometry. *Clin Ophthalmol* 7: 1083-1087.
- Golzan SM, Mikaili M, Sedighi A, Avolio A, Karimi M (2009) Non-invasive intracranial pressure measurement using transcranial doppler sonography and support vector machines. In Dössel O, Schlegel WC (eds.): WC, IFMBE Proceedings 25/IV, pp. 1752-1755.
- Golzan SM, Kim MO, Seddighi AS, Avolio A, Graham SL (2012) Non-invasive estimation of cerebrospinal fluid pressure waveforms by means of retinal venous pulsatility and central aortic blood pressure. *Ann Biomed Eng* 40: 1940-1948.
- Greitz D (2004) Radiological assessment of hydrocephalus: new theories and implications for therapy. *Neurosurg Rev* 27: 145-167.
- Grubb RL, Raichle ME, Phelps ME, Ratcheson RA (1975) Effects of increased intracranial pressure on cerebral blood volume, blood flow, and oxygen utilization in monkeys. *J Neurosurg* 43: 385-398.
- Gwer S, Sheward V, Birch A, Marchbanks R, Idro R, Newton C, Kirkham F, Lin J-P, Lim M (2013) The tympanic membrane displacement analyser for monitoring intracranial pressure in children. *Child's Nerv Syst* 29: 927-933.
- Hamer J, Alberti E, Hoyer S, Wiedemann K (1977) Influence of systemic and cerebral vascular factors on the cerebrospinal fluid pulse waves. *J Neurosurg* 46: 36-45.
- Han Y, McCulley TJ, Horton JC (2008) No correlation between intraocular pressure and intracranial pressure. *Ann Neurol* 64: 221-224.
- Hanlo PW, Peters RJA, Gooskens RHJM, Heethaar RM, Keunen RWM, van Huffelen AC, Tulleken AF, Willemsse J (1995) Monitoring intracranial dynamics by transcranial Doppler—a new Doppler index: trans systolic time *Ultrasound Med Biol* 21: 613-621.

- Hansen HC, Helmke K (1997) Validation of the optic nerve sheath response to changing cerebrospinal fluid pressure: ultrasound findings during intrathecal infusion tests. *J Neurosurg* 87: 34-40.
- Heckmann JG, Weber M, Jünemann AG, Neundörfer B, Mardin CY (2004) Laser scanning tomography of the optic nerve vs CSF opening pressure in idiopathic intracranial hypertension. *Neurology* 62: 1221-1223.
- Hee MR, Izatt JA, Swanson EA, Huang D, Schuman JS, Lin CP, Puliafito CA, Fujimoto JG (1995) Optical coherence tomography of the human retina. *Arch Ophthalmol* 113: 325-332.
- Helmke K, Hansen HC (1996) Fundamentals of transorbital sonographic evaluation of optic nerve sheath expansion under intracranial hypertension. I. Experimental study. *Pediatr Radiol* 26: 701-705.
- Hiler M, Czosnyka M, Hutchinson P, Balestreri M, Smielewski P, Matta B, Pickard JD (2006) Predictive value of initial computerized tomography scan, intracranial pressure, and state of autoregulation in patients with traumatic brain injury. *J Neurosurg* 104: 731-737.
- Huang-Link YM, Al-Hawasi A, Oberwahrenbrock T, Jin YP (2015) OCT measurements of optic nerve head changes in idiopathic intracranial hypertension. *Clin Neurol Neurosurg* 130: 122-127.
- Iencean SM, Ciurea AV (2008) Intracranial hypertension: classification and patterns of evolution. *J Med Life* 1: 101-107.
- Jacks AS, Miller NR (2003) Spontaneous retinal venous pulsation: aetiology and significance. *J Neurol Neurosurg Psychiatry* 74: 7-9.
- Jerin C, Wakili R, Kalla R, Gürkov R (2015) The effect of increasing intracranial pressure on ocular vestibular-evoked myogenic potential frequency tuning. *Ear Hear* 36: e336-e341.

- John JS (2015) Pupillometry: Cutting edge biometrics for early intervention in increased intracranial pressure. *J Contin Educ Nurs* 46: 431-432.
- Johnston IH, Rowan JO, Harper AM, Jennett WB (1972) Raised intracranial pressure and cerebral blood flow: I. Cisterna magna infusion in primates. *JNNP* 35: 285-296.
- Jonas J B, Wang N and Yang D (2012) Retinal vein pulsation is in phase with intracranial pressure and not intraocular pressure. *Invest Ophthalmol Vis Sci* 53: 6045.
- Kalmar AF, Aken JV, Caemaert J, Mortier EP, Struys MMRF (2005) Value of Cushing reflex as warning sign for brain ischaemia during neuroendoscopy. *British Journal of Anaesthesia* 94: 791-799.
- Kao Y-H, Guo W-Y, Liou AJ-K, Chen T-Y, Huang C-C, Chou C-C, Lirng J-F (2013) Transfer function analysis of respiratory and cardiac pulsations in human brain observed on dynamic magnetic resonance images. *Computational and Mathematical Methods in Medicine*, DOI: 10.1155/2013/157040.
- Karamanoglu M, O'Rourke MF, Avolio AP, Kelly RP (1993) An analysis of the relationship between central aortic and peripheral upper limb pressure waves in man. *Eur Heart J* 14: 160-167.
- Kashif FM, Verghese GC, Novak V, Czosnyka M, Heldt T (2012) Model-Based non-invasive estimation of intracranial pressure from cerebral blood flow velocity and arterial pressure. *Sci Transl Med* 4: 129ra44.
- Kasuga Y, Nagal H, Hasegawa Y, Nitta M (1987) Transmission characteristics of pulse waves in the intracranial cavity of dogs. *J Neurosurg* 66: 907-914.
- Kellie G (1824) On death from cold, and on congestions of the brain. *Transac Medico Chir Soc Edinb* 1: 84-169.
- Kemp DT (1978) Stimulated acoustic emissions from within the human auditory system. *J Acoust Sci Am* 64: 1386-1391.

- Khan MN, Shallwani H, Khan MU, Shamim MS (2017) Noninvasive monitoring intracranial pressure – a review of available modalities. *Surgical Neurology International* 8: 51, DOI: 10.4103/sni.sni_403_16.
- Kim MO, Li J, Qasem A, Graham SL, Alberto AP (2012) Frequency dependent transmission characteristics between arterial blood pressure and intracranial pressure in rats. 34th annual international conference of the IEEE EMBS, San Diego, California USA, 28 August – 1 September 2012.
- Kim MO (2014) Obligatory role of central aortic blood pressure in pulsatile cerebral haemodynamics. PhD Thesis. Macquarie University, Australia.
- Kim MO, Adji A, O'Rourke MF, Avolio AP, Smielewski P, Pickard JD, Czosnyka M (2015b) Principles of cerebral haemodynamics when intracranial pressure is raised: lessons from the peripheral circulation. *Journal of Hypertension* 33: 1233-1241.
- Kim MO, Eide PK, O'Rourke MF, Adji A, Avolio AP (2016b) Intracranial pressure waveforms are more closely related to central aortic than radial pressure waveforms: implications for pathophysiology and therapy. In B-T Ang (ed.) *Intracranial pressure and brain monitoring XV. Acta Neurochirurgica Supplement, Vol. 122*, Springer International Publishing Switzerland, DOI: 10.1007/978-3-319-22533-3_12.
- Kim MO, O'Rourke MF, Adji A, Avolio A (2016b) Central pulsatile pressure and flow relationship in the time and frequency domain to characterize hydraulic input to the brain and cerebral vascular impedance. In B-T Ang (ed.) *Intracranial pressure and brain monitoring XV. Acta Neurochirurgica Supplement, Vol. 122*, Springer International Publishing Switzerland, DOI: 10.1007/978-3-319-22533-3_61.
- Kim MO, Li Y, Wei F, Wang J, O'Rourke MF, Adji A, Avolio AP (2017) Normal cerebral vascular pulsations in humans: changes with age and implications for microvascular disease. *Journal of Hypertension* 35: 2245-2256.

- Kimberly HH, Shah S, Marill K, Noble V (2008) Correlation of optic nerve sheath diameter with direct measurement of intracranial pressure. *Acad Emerg Med* 15: 201-204.
- Kirkness CJ, Mitchell PH, Burr RL, March KS, Newel DW (2000) Intracranial pressure waveform analysis: clinical and research implications. *J Neurosci Nurs* 32: 271-277.
- Koeppen BM, Stanton BA (2013) 6 - Regulation of extracellular fluid volume and NaCl balance. *Renal Physiology (fifth edition)*: 93-114.
- Kongstad L, Grände PO (2001) Arterial hypertension increases intracranial pressure in cat after opening of the blood-brain barrier. *J Trauma*. 51: 490-496.
- Koskinen L-O, Malm J, Zakelis R, Bartusis L, Ragauskas A, Eklund A (2017) Can intracranial pressure be measured non-invasively bedside using a two-depth Doppler-technique? *J Clin Monit Comput* 31: 459-467.
- Krejza J, Mariak Z, Babikian V (2001) Importance of angle correction in the measurement of blood flow velocity with transcranial Doppler sonography. *Am J Neuroradiol* 22: 1743-1747.
- Krille L, Zeeb H, Jahnen A (2012) Computed tomographies and cancer risk in children: a literature overview of CT practices, risk estimations and an epidemiologic cohort study proposal. *Radiat Environ Biophys* 5: 103-111.
- Kruse FE, Burk RO, Völcker HE, Zinser G, Harbarth U (1989) Reproducibility of topographic measurements of the optic nerve head with laser tomographic scanning. *Ophthalmology* 96: 1320-1324.
- Lang EW, Mehdorn HM, Dorsch NWC, Czosnyka M (2002) Continuous monitoring of cerebrovascular autoregulation: a validation study. *J Neurol Neurosurg Psychiatry* 72: 583-586.
- Lang EW, Paulat K, Witte C, Zolondz J, Mehdorn HM (2003) Noninvasive intracranial compliance monitoring: technical note and clinical results. *J Neurosurg* 98 :214-218.

- Langfitt TW, Weinstein JD, Kassell NF, Simeone FA (1964) Transmission of increased intracranial pressure. I. Within the craniospinal axis *J. Neurosurg.* 21: 989-997.
- Larson MD, Muhiudeen I (1995) Pupillometric analysis of the 'absent light reflex'. *Arch Neurol* 52: 369-72.
- Lashutka MK, Chandra A, Murray HN, Phillips GS, Hiestand BC (2004) The relationship of intraocular pressure to intracranial pressure. *Ann Emerg Med* 43: 585-591.
- Lavinio A, Menon DK (2011) Intracranial pressure: why we monitor it, how to monitor it, what to do with the number and what's the future? *Curr Opin Anaesthesiol* 24: 117-123.
- Liefeld PH, Gooskens RH, Peters RJ, Tulleken CAF, Kappelle LJ, Han KS, Regli L, Hanlo PW (2009) New transcranial Doppler index in infants with hydrocephalus: transsystolic time in clinical practice. *Ultrasound Med Biol* 35: 1601-1606.
- Levin BE (1978) The clinical significance of spontaneous pulsations of the retinal vein. *Arch Neurol* 35: 37-40.
- Levinsky A, Papyan S, Weinberg G, Stadheim T, Eide PK (2016) Non-invasive estimation of static and pulsatile intracranial pressure from transcranial acoustic signals. *Medical Engineering and Physics* 38: 477-484.
- Lewis PM, Smielewski P, Rosenfeld JV, Pickard JD, Czosnyka M (2016) The correlation between intracranial pressure and cerebral blood flow velocity during ICP plateau waves. In B-T Ang (ed.) *Intracranial pressure and brain monitoring XV*. *Acta Neurochirurgica Supplement*, Vol. 122, Springer International Publishing Switzerland, DOI: 10.1007/978-3-319-22533-3_16.
- Li Z, Luo Y (2010) Finite element study of correlation between intracranial pressure and external vibration responses of human head. *Adv Theor Appl Mech* 3: 139-149.

- Liebeskind DS, Marcinkevicius E, Pranevicius M, Pranevicius O (2013) Clinical assessment of non-invasive intracranial pressure absolute value measurement method. *Neurology* 80: 507-508.
- Luerssen TG (1997) Intracranial pressure: current status in monitoring and management. *Semin Pediatr Neurol* 4: 146-155.
- Lupetin AR, Davis DA, Beckham I, Dash N (1995) Transcranial Doppler sonography. Part 1. Principles, technique, and normal appearances. *Radiographics* 15: 179-191.
- Luria AR (1970) The functional organization of the brain. *Scientific American* 222: 66-79.
- Mack J, Squier W, Eastman JT (2009) Anatomy and development of the meninges: implications for subdural collections and CSF circulation. *Pediatric Radiology* 39: 200-210.
- Mack WJ, King RG, Ducruet AF, Kreiter K, Mocco J, Maghoub A, Mayer S, Connolly ES (2003) Intracranial pressure following aneurysmal subarachnoid hemorrhage: monitoring practices and outcome data. *Neurosurg Focus* 14: 1-5.
- Manwaring P, Wichern D, Manwaring M, Manwaring J, Manwaring K (2004) A signal analysis algorithm for determining brain compliance non-invasively. *Conf Proc IEEE Eng Med Biol Soc* 1: 353-356.
- Marchbanks RJ (1984) Measurement of tympanic membrane displacement arising from aural cardiovascular activity, swallowing, and intra-aural muscle reflex. *Acta Otolaryngol* 98: 119-129.
- Marshall I, MacCormick I, Sellar R, Whittle I (2008) Assessment of factors affecting MRI measurement of intracranial volume changes and elastance index. *Br J Neurosurg* 22: 389-397.
- Marmarou A, Shulman K, Lamorgese J (1975) Compartmental analysis of compliance and outflow resistance of the cerebrospinal fluid system. *J Neurosurg* 43: 523-34.

- Marmarou A, Shulman K, Rosende R (1978) Nonlinear analysis of the cerebrospinal fluid system and intracranial pressure dynamics. *J Neurosurg* 48: 332-344.
- Martin B, Loth K (2009) The influence of coughing on cerebrospinal fluid pressure in an in vitro syringomyelia model with spinal subarachnoid space stenosis. *Cerebrospinal Fluid Research* 6: 17, DOI: 10.1186/1743-8454-6-17.
- Martínez-Mañas RM, Santamarta D, Campos JM, Ferrer E (2000) Camino® intracranial pressure monitor: prospective study of accuracy and complications. *J Neurol Neurosurg Psychiatry* 69: 82-86.
- Mascarenhas S, Vilela GHF, Carlotti C, Damiano LEG, Seluque W, Colli B, Tanaka K, Wang CC, Nonaka KO (2012) The new ICP minimally invasive method shows that the Monro–Kellie doctrine is not valid. In: Schuhmann M, Czosnyka M (eds.) *Intracranial pressure and brain monitoring XIV. Acta Neurochirurgica Supplementum*, vol 114. Springer, Vienna.
- Meeker M, Du R, Bacchetti P, Privitera CM, Larson MD, Holland MC, Manley G (2005) Pupil examination: validity and clinical utility of an automated pupillometer. *J Neurosci Nurs* 37: 34-40.
- Melo JRT, Di Rocco F, Blanot S, Cuttaree H, Sainte-Rose C, Oliveira-Filho J, Zerah M, Meyer PG (2011) Transcranial Doppler can predict intracranial hypertension in children with severe traumatic brain injuries. *Childs Nerv Syst* 27: 979-984.
- Mertz K, Bencsik B, Büki B, Avan P (2004) Noninvasive testing of intracranial pressure changes due to body position in infants. *Orv Hetil* 145: 1427-1430.
- Michaeli D, Rappaport ZH (2002) Tissue resonance analysis: a novel method for non-invasive monitoring of intracranial pressure. Technical note. *J Neurosurg* 96: 1132-1137.

- Mick EC (1991) Method and apparatus for the measurement of intracranial pressure. US Patent 5,074,310.
- Mick EC (1992) Method and apparatus for the measurement of intracranial pressure. US Patent 5,117,835.
- Miller JD, Garibi J, Pickard JD (1973) Induced changes of cerebrospinal fluid volume: effects during continuous monitoring of ventricular fluid pressure. *Arch Neurol* 28: 265-269.
- Milhorat TH, Hammock MK, Fenstermacher JD, Rall DP, Levin VA (1971) Cerebrospinal Fluid Production by the Choroid Plexus and Brain. *Science* 173: 330-332.
- Momjian S, Czosnyka Z, Czosnyka M, Pickard JD (2004) Link between vasogenic waves of intracranial pressure and cerebrospinal fluid outflow resistance in normal pressure hydrocephalus. *British Journal of Neurosurgery* 18: 56-61.
- Monro A (1783) *Observations on the structure and function of the neural system*. Edinburgh: Creech and Johnson, London.
- Morgan WH, Lind CR, Kain S, Fatehee N, Bala A, Yu DY (2012) Retinal vein pulsation is in phase with intracranial pressure and not intraocular pressure. *Invest Ophthalmol Vis Sci* 53: 4676-4681.
- Morris (1997) *Practical neuroangiography*, Baltimore, Williams and Wilkins.
- Muehlmann M, Koerte IK, Laubender RP, Steffinger D, Lehner M, Peraud A, Heinen F, Kiefer M, Reiser M, Ertl-Wagner B (2013) Magnetic resonance-based estimation of intracranial pressure correlates with ventriculoperitoneal shunt valve opening pressure setting in children with hydrocephalus. *Invest Radiol* 48: 543-547.
- Nair S (2016) Clinical review of non-invasive intracranial pressure measurement in medical cases. *Journal of Neuroanaesthesiology and Critical Care* 3: 9-14.

- Nayak S, Soni MK, Bansal D (2012) Filtering techniques for ECG signal processing. *IJREAS* 2: 671-679.
- Nichols WW, Denardo SJ, Wilkinson IB, McEniery CM, Cockcroft J, O'Rourke MF (2008) Effects of arterial stiffness, pulse wave velocity, and wave reflections on the central aortic pressure waveform. *The Journal of Clinical Hypertension* 10: 295-303.
- North B (1997) Intracranial pressure monitoring. In Reilly P, Bullock R (eds.) *Head injury*. Chapman & Hall, London. ISBN 0 412 58540 5.
- Olzowy B, von Gleichenstein G, Canis M, Mees K (2008) Distortion product otoacoustic emissions for assessment of intracranial hypertension at extreme altitude? *Eur J Appl Physiol* 103: 19-23.
- O'Rourke MF, Yaginuma T (1984) Wave reflections and the arterial pulse. *Arch Intern Med* 144: 366-371.
- Oswal A, Toma AK (2017) Intracranial pressure and cerebral haemodynamics. *Anaesthesia & Intensive Care Medicine* 18: 259-263.
- Otto KA (2008) EEG power spectrum analysis for monitoring depth of anaesthesia during experimental surgery. *Lab Anim* 42: 45-61.
- Padayachy LC (2016) Non-invasive intracranial pressure assessment. *Childs Nerv Syst* 32:1587-1597.
- Partington T, Farmery A (2014) Intracranial pressure and cerebral blood flow. *Anaesthesia and Intensive Care Medicine* 15: 189-194.
- Pauwels EK, Bourguignon MH (2012) Radiation dose features and solid cancer induction in pediatric computed tomography. *Med Princ Pract* 21: 508-515.
- Perfetto JC, Sirne RO, Ruiz A, D'Attellis CE (2012) Arterial blood pressure waveform analysis and its applications in the assessment of vasovagal syncope*. In Kamath MV, Watanabe M, Upton A (eds.) *Heart Rate Variability (HRV) Signal Analysis: Clinical*

Applications. CRC Press, Taylor & Francis Group, an informa business. Boca Raton, USA.

Peters RJA, Hanlo PW, Gooskens RHJ, Braun KPJ, Tulleken CAF, Willemse J (1995) Non-invasive ICP monitoring in infants: the Rotterdam Teletransducer revisited. *Childs Nerv Syst* 11: 207-213.

Petkus V, Ragauskas A, Jurkonis R (2002) Investigation of intracranial media ultrasonic monitoring model. *Ultrasonics* 40: 829-833.

Pettorossi VE, Rocco CD, Caldarelli M, Mancinelli R, Velardi F (1978) Influences of phasic changes in systemic blood pressure on intracranial pressure. *Eur Neurol* 17: 216-225.

Pindrik J, Ye X, Ji BG, Pendleton C, Ahn ES (2014) Anterior fontanelle closure and size in full-term children based on head computed tomography. *Clinical Pediatrics* 53: 1149-1157.

Pitlyk PJ, Piantanida TP, Ploeger DW (1985) Noninvasive intracranial pressure monitoring. *Neurosurgery* 17: 581-584.

Piper IR, Miller JD, Dearden NM, Leggate JRS, Robbertson I (1990) Systems analysis of cerebrovascular pressure transmission: an observational study in head-injured patients. *J Neurosurg* 73: 871-880.

Popovic D, Khoo M, Lee S (2009) Noninvasive monitoring of intracranial pressure. *Recent Pat Biomed Eng* 2: 165-179.

Portnoy HD, Chopp M, Branch C, Shannon MB (1982) Cerebrospinal fluid pulse waveform as an indicator of cerebral autoregulation. *J Neurosurg* 56: 666-678.

Powers WJ, Zazulia AR, Videen TO, Adams RE, Yundt KD, Aiyagari V, Grubb RL, Diringer MN (2001) Autoregulation of cerebral blood flow surrounding acute (6 to 22 hours) intracerebral haemorrhage. *Neurology* 57: 18-24.

- Pranevicius O, Pranevicius M, Pranevicius H, Marcinkevicius E, Liebeskind DS (2012) Noninvasive method to measure intracranial and effective cerebral outflow pressure. US Patent 8,109,880.
- Querfurth HW, Arms SW, Lichy CM, Irwin WT, Steiner T (2004) Prediction of intracranial pressure from noninvasive transocular venous and arterial hemodynamic measurements a pilot study. *Neurocrit Care* 1: 183-194.
- Querfurth HW, Lieberman P, Arms S, Mundell S, Bennet M, van Horne C (2010) Ophthalmodynamometry for ICP prediction and pilot test on Mt. Everest. *BMC Neurology* 10: 106.
- Raabe A, Totzauer R, Meyer O, Stöckel R, Hohrein D and Schöche J (1998) Reliability of epidural pressure measurement in clinical practice: behavior of three modern sensors during simultaneous ipsilateral intraventricular or intraparenchymal pressure measurement. *Neurosurgery* 43: 306-311.
- Raboel PH, Bartek J, Andresen M, Bellander BM, Romner B (2012) Intracranial pressure monitoring: invasive versus non-invasive methods—a review. *Crit Care Res Pract* 950393.
- Ragauskas A, Daubaris G (1995) Method and apparatus for non-invasively deriving and indicating of dynamic characteristics of the human and animal intracranial media. US Patent 5,388,583.
- Ragauskas A, Daubaris G, Ragaisis V, Petkus V (2003) Implementation of non-invasive brain physiological monitoring concepts. *Med Eng Phys* 25 667-678.
- Rajajee V, VanamanM, Fletcher JJ, Jacobs TL (2011) Optic nerve ultrasound for the detection of raised intracranial pressure. *Neurocrit Care* 15: 506-515.
- Raksin Pb, Alperin N, Sivaramakrishnan A, Surapanenis, Lichtor T (2003) Noninvasive intracranial compliance and pressure based on dynamic magnetic resonance imaging of

blood flow and cerebrospinal fluid flow: review of principles, implementation, and other non-invasive approaches. *Neurosurg Focus* 14: e4.

Reid A, Marchbanks RJ, Burge DM, Martin AM, Bateman DE, Pickard JD, Brightwell AP (1990) The relationship between intracranial pressure and tympanic membrane displacement. *Br J Audiol* 24: 123-129.

Rich PM, Cox TC, Hayward RD (2003) The jugular foramen in complex and syndromic craniosynostosis and its relationship to raised intracranial pressure. *Am J Neuroradiol* 24: 45-51.

Robba C, Bacigaluppi S, Cardim D, Donnelly J, Bertuccio A, Czosnyka M (2016) Non-invasive assessment of intracranial pressure. *Acta Neurol Scand* 2016: 134: 4–21.

Robba C, Cardim D, Tajsic T, Pietersen J, Bulman M, Donnelly J, Lavinio A, Gupta A, Menon DK, Hutchinson PJA, Czosnyka M (2017) Ultrasound non-invasive measurement of intracranial pressure in neurointensive care: a prospective observational study. *PLOS Medicine* 14: e1002356, DOI: 10.1371/journal.pmed.1002356.

Rohrschneider K, Burk RO, Kruse FE, Völcker HE (1998) Reproducibility of the optic nerve head topography with a new laser tomographic scanning device. *Ophthalmology* 101: 1044-1049.

Rosenberg JB, Shiloh AL, Savel RH, Eisen LA (2011) Non-invasive methods of estimating intracranial pressure. *Neurocrit Care* 15:599–608.

Rosner MJ, Becker DP (1984) Origin and evolution of plateau waves: experimental observations and a theoretical model. *J Neurosurg* 60: 312-324.

Ross N, Eynon CA (2005) Intracranial pressure monitoring. *Current Anaesthesia & Critical Care* 16: 255–261.

- Roytowski D, Figaji A (2013) Raised intracranial pressure: what it is and how to recognise it. *Continuing Medical Education* 31: 85-90.
- Ryder HW, Espey FF, Kristoff FV, Evans JP (1950) Observations on the interrelationships of intracranial pressure and cerebral blood flow*. Presented at the Meeting of the Harvey Cushing Society, Colorado Springs, Colorado, April 16, 1950.
- Sajjadi SA, Harirchian MH, Sheikhabahaei N, Mohebbi MR, Malekmadani MH, Saberi H (2006) The relation between intracranial and intraocular pressures: study of 50 patients. *Ann Neurol* 59: 867-870.
- Sakka L, Coll G, Chazal J (2011) Anatomy and physiology of cerebrospinal fluid. *Head and Neck diseases* 128: 309-316.
- Saladino A, White JB, Wijdicks EF, Lanzino G (2009) Malplacement of ventricular catheters by neurosurgeons: a single institution experience. *Neurocrit Care* 10: 248-252.
- Salman MS (1997) Can intracranial pressure be measured noninvasively? *Lancet* 350(9088): 1367.
- Salmon JH, Hajjar W, Bada HS (1977) The fontogram: a noninvasive intracranial pressure monitor. *PEDIATRICS* 60: 721-725.
- Savini G, Zanini M, Carelli V, Sadun AA, Ross-Cisneros FN, Barboni P (2004) Correlation between retinal nerve fibre layer thickness and optic nerve head size: an optical coherence tomography study. *Br J Ophthalmol* 89: 489-492.
- Schmidt B, Klingelhofer J, Schwarze JJ, Sander D, Wittich I (1997) Noninvasive prediction of intracranial pressure curves using transcranial doppler ultrasonography and blood pressure curves. *Stroke* 28: 2465-2472.
- Schmidt B, Czosnyka M, Raabe A, Yahya H, Schwarze JJ, Sackerer D, Sander D, Klingelhofer J (2002) Adaptive non-invasive assessment of intracranial pressure and cerebral autoregulation. *Stroke* 34: 84-89.

- Schmidt EA, Despas F, Traon AP-L, Czosnyka Z, Pickard JD, Rahmouni K, Pathak A, Senard JM (2018) Intracranial pressure is a determinant of sympathetic activity. *Front Physiol* 9: 11.
- Scott CJ, Kardon RH, LeeAG, Frisen L, Wall M (2010) Diagnosis and grading of papilledema in patients with raised intracranial pressure using optical coherence tomography vs clinical expert assessment using a clinical staging scale. *Arch Ophthalmol* 128: 705-711.
- Scremin OU (2012) Chapter 39: Cerebral Vascular System. In Mai JK & Paxinos G (eds.) *The Human Neural System, Third Edition*. Elsevier Science & Technology, DOI: 10.1016/B978-0-12-374236-0.10039-2
- Serlin Y, Shelef I, Knyazer B, Friedman A (2015) Anatomy and physiology of the blood–brain barrier. *Seminars in Cell & Developmental Biology* 38: 2-6.
- Shafi S, Diaz-Arrastia R, Madden C, Gentilello L (2008) Intracranial pressure monitoring in brain-injured patients is associated with worsening of survival. *Journal of Trauma and Acute Care Surgery* 64: 335-340.
- Sheeran P, Bland J, Hall G (2000) Intraocular pressure changes and alterations in intracranial pressure. *Lancet* 355: 899.
- Shimbles S, Dodd C, Banister K, Mendelow AD, Chambers IR (2005) Clinical comparison of tympanic membrane displacement with invasive intracranial pressure measurements. *Physiol Meas* 26: 1085.
- Silva GJJ, Ushizima MR, Lessa PS, Cardoso L, Drager LF, Atala MM, Consolim-Colombo FM, Lopes HF, Cestari IA, Krieger JE, Krieger EM (2009) Critical analysis of autoregressive and fast Fourier transform markers of cardiovascular variability in rats and humans. *Braz J Med Biol Res* 42: 386-396.

- Sinha DN (2000) Method for non-invasive intracranial pressure measurement. US Patent 6,117,089.
- Skau M, Yri H, Sander B, Gerds TA, Milea D, Jensen R (2013) Diagnostic value of optical coherence tomography for intracranial pressure in idiopathic intracranial hypertension. *Graefe Arch Clin Exp* 251: 567-574.
- Soldatos T, Karakitsos D, Chatzimichail K, Papathanasiou M, Gouliamos A, Karabinis A (2008) Optic nerve sonography in the diagnostic evaluation of adult brain injury. *Crit Care* 12: R67.
- Speck V, Staykov D, Huttner H B, Sauer R, Schwab S, Bardutzky J (2011) Lumbar catheter for monitoring of intracranial pressure in patients with post-hemorrhagic communicating hydrocephalus. *Neurocrit Care* 14: 208-215.
- Spentzas T, Henricksen J, Patters AB, Chaum E (2010) Correlation of intraocular pressure with intracranial pressure in children with severe head injuries*. *Pediatr Crit Care Med* 11: 593-598.
- Spiegelberg A, Preu M, Kurtcuoglu V (2016) B-waves revisited. *Interdisciplinary Neurosurgery* 6: 13-17.
- Spiegelberg A, Krause M, Meixensberger J, Seifert B, Kurtcuoglu V (2018) Significant association of slow vasogenic ICP waves with normal pressure hydrocephalus diagnosis. *Acta Neurochir Suppl* 126: 243-246.
- Steinborn M, Friedmann M, Hahn H, Hapfelmeier A, Macdonald E, Warncke K, Salej A (2015) Normal values for trans bulbar sonography and magnetic resonance imaging of the optic nerve sheath diameter (ONSD) in children and adolescents. *Ultraschall Med* 36: 54-58.

- Stendel R, Heidenreich J, Schilling A, Akhavan-Sigari R, Kurth R, Picht T, Pietilä T, Suess O, Kern C, Meisel J, Brock M (2003) Clinical evaluation of a new intracranial pressure monitoring device. *Acta Neurochir* 145: 185-193.
- Stone MB, Tubridy CM, Curran R (2010) The effect of rigid cervical collars on internal jugular vein dimensions. *Acad Emerg Med* 17: 100-102.
- Swanson JW, Aleman TS, Xu W, Ying GS, Pan W, Liu GT, Lang SS, Heuer GG, Storm PB, Bartlett SP, Katowitz WR, Taylor JA (2017) Evaluation of optical coherence tomography to detect elevated intracranial pressure in children. *JAMA Ophthalmol* 135: 320-328.
- Takahashi S, Mugikura S (2010) Intracranial arterial system: the main trunks and major arteries of the cerebrum. In Takahashi S (ed.) *Neurovascular Imaging*, Springer-Verlag London Limited 2010, DOI: 10.1007/978-1-84882-134-7_1.
- Tameem A, Krowidi H (2013) Cerebral physiology. *Continuing Education in Anaesthesia, Critical Care & Pain* 13: 113-118.
- Tan I, Butlin M, Liu YY, Ng K, Avolio AP (2012) Heart rate dependence of aortic pulse wave velocity at different arterial pressures in rats. *Hypertension* 60: 528-533.
- Tasker RC (2013) Brain vascular and hydrodynamic physiology. *Seminars in Pediatric Surgery* 22: 68-173.
- Taylor WR, Chen JW, Meltzer H, Gennarelli TA, Kelbch C, Knowlton S, Richardson J, Lutch MJ, Farin A, Hults KN, Marshall LF (2003) Quantitative pupillometry, a new technology: normative data and preliminary observations in patients with acute head injury. *J Neurosurg* 98 :205-213.
- Trick GL, Vesti E, Tawansy K, Skarf B, Gartner J (1998) Quantitative evaluation of papilledema in pseudotumor cerebri. *Invest Ophthalmol Vis Sci* 39: 1964-1971.

- Tomycz LD, Hale AT, George TM (2017) Emerging insights and new perspectives on the nature of hydrocephalus. *Pediatr Neurosurg* 52: 361-368.
- Toutant SM, Klauber MR, Marshall LF (1984) Absent or compressed basal cisterns on first CT scan: ominous predictors of outcome in severe head injury. *J Neurosurg* 61: 691-694.
- Tuettenberg J, Czabanka M, Horn P, Woitzik J, Barth M, Thomé C, Vajkoczy P, Schmiedek P, Muench E (2009) Clinical evaluation of the safety and efficacy of lumbar cerebrospinal fluid drainage for the treatment of refractory increased intracranial pressure: clinical article. *J Neurosurg* 110: 1200-1208.
- Tumani H (2015a) Anatomy of CSF-related spaces and barriers between blood, CSF, and brain. In Deisenhammer F, *et al.* (eds.) *Cerebrospinal Fluid in Clinical Neurology*. Springer International Publishing Switzerland, DOI 10.1007/978-3-319-01225-4_2.
- Tumani H (2015b) Physiology and constituents of CSF. In Deisenhammer F, *et al.* (eds.) *Cerebrospinal Fluid in Clinical Neurology*. Springer International Publishing Switzerland, DOI 10.1007/978-3-319-01225-4_3.
- Uludag K, Blinder P (In Press) Linking brain vascular physiology to hemodynamic response in ultra-high field MRI. *NeuroImage*
- van Beek AH, Claassen JA, Rikkert MGO, Jansen RW (2008) Cerebral autoregulation: an overview of current concepts and methodology with special focus on the elderly. *Journal of Cerebral Blood Flow & Metabolism* 28, 1071-1085.
- Verweij BH, Muizelaar JP, Vias FC (2001) Hyper acute measurement of intracranial pressure, cerebral perfusion pressure, jugular venous oxygen saturation, and laser Doppler flowmetry, before and during removal of traumatic acute subdural hematoma. *J Neurosurg* 95: 569-72.

- Voss SE, Horton NJ, Tabucchi TH, Folowosele FO, Shera CA (2006) Posture-induced changes in distortion-product otoacoustic emissions and the potential for noninvasive monitoring of changes in intracranial pressure. *Neurocrit Care* 4: 251-257.
- Voulgaris SG, Partheni M, Kaliora H, Haftouras N, Pessach IS, Polyzoidis KS (2005) Early cerebral monitoring using the transcranial Doppler pulsatility index in patients with severe brain trauma. *Ann Transplant* 11: CR49-CR52.
- Wagshul ME, Kelly EJ, Yu HJ, Garlick B, Zimmerman T, Egnor MR (2009) Resonant and notch behavior in intracranial pressure dynamics: laboratory investigation. *J Neurosurg Pediatrics* 3: 354-364.
- Wagshul ME, Eide PK, Madsen JR (2011) The pulsating brain: A review of experimental and clinical studies of intracranial pulsatility. *Fluids and Barriers of the CNS* 8: 5.
- Wan WH, Ang BT, Wang E (2008) The Cushing Response: A case for a review of its role as a physiological reflex. *J Clin Neurosci* 15: 223-228.
- Wang YX, Jonas JB, Wang N, You QS, Yang D, Xie XB, Xu L (2014) Intraocular pressure and estimated cerebrospinal fluid pressure: the Beijing eye study 2011. *PLOS ONE* 9: e104267.
- Wang L, Feng L, Yao Y, Wang Y, Chen Y, Feng J, Xing Y (2015) Optimal optic nerve sheath diameter threshold for the identification of elevated opening pressure on lumbar puncture in a Chinese population. *PLoS One* 10: e0117939.
- Weerakkody RA, Czosnyka M, Zweifel C, Castellani G, Smielewski P, Keong N, Haubrich C, Pickard J, Czosnyka Z (2010) Slow vasogenic fluctuations of intracranial pressure and cerebral near infrared spectroscopy—an observational study. *Acta Neurochir* 152: 1763-1769.

- Weerakkody RA, Czosnyka M, Zweifel C, Castellani G, Smielewski P, Brady K, Pickard JD, Czosnyka Z (2012) Near infrared spectroscopy as possible non-invasive monitor of slow vasogenic ICP waves. *Acta Neurochir Suppl* 114: 181-185.
- Wiegand C, Richards P (2007) Measurement of intracranial pressure in children: a critical review of current methods. *Developmental Medicine & Child Neurology* 49: 935-941.
- Wilkinson IB, Mohammad NG, Tyrrell S, Hall IR, Webb DJ, Paul VE, Levy T, Cockcroft JR (2002) Heart rate dependency of pulse pressure amplification and arterial stiffness. *American Journal of Hypertension* 15: 24-30.
- Williams MA, Malm J, Eklund A, Horton NJ, Voss SE (2016) Distortion product otoacoustic emissions and intracranial pressure during CSF infusion testing. *Aerospace Medicine and Human Performance* 87: 844-851.
- Wilson MH (2016) Monroe-Kellie 2.0: the dynamic vascular and venous pathophysiological components of intracranial pressure. *J Cereb Blood Flow Metab* 36: 1338-1350.
- Wu X, Ji Z (2007) Non-invasive detection for intracranial high pressure with FVEP picked-up by independent component analysis. *Sheng Wu Yi Xue Gong Cheng Xue Za Zhi* 24: 1015-1018.
- Xu P, Kasprowicz M, Bergsneider M, Hu X (2010) Improved non-invasive intracranial pressure assessment with nonlinear kernel regression. *IEEE Trans Inf Technol* 14: 971-978.
- York DH, Pulliam MW, Rosenfeld JG, Watts C (1981) Relationship between visual evoked potentials and intracranial pressure. *J Neurosurg* 55: 909-916.
- Yan X, Su XG (2009) *Linear regression analysis: theory and computing*. World Scientific, Singapore 348 pp.
- Yue X, Wang L (2009) Deformation of skull bone as intracranial pressure changing. *Afr J Biotechnol* 8: 745-750.

- Zhang X, Burstein R, Levy D (2012) Local action of the proinflammatory cytokines IL-1 β and IL-6 on intracranial meningeal nociceptors. *Cephalalgia* 32: 66-72.
- Zhang X, Medow JE, Iskandar BJ, Wang F, Shokouejinejad M, Koueik J, Webster JG (2017) Invasive and non-invasive means of measuring intracranial pressure: a review. *Physiol. Meas.* 38 R143.
- Zhao YL, Zhou JY, Zhu GH (2005) Clinical experience with the non-invasive ICP monitoring system. *Acta Neurochir Suppl* 95: 351-355.
- Zou R, Park E-H, Kelly EM, Egnor M, Wagshul ME, Madsen JR (2008) Intracranial pressure waves: characterization of a pulsation absorber with notch filter properties using systems analysis: laboratory investigation. *J Neurosurg Pediatrics* 2: 83-94.
- Zweifel C, Castellani G, Czosnyka M, Helmy A, Manktelow A, Carrera E, Brady KM, Hutchinson PJ, Menon DK, Pickard JD, Smielewski P (2010) Noninvasive monitoring of cerebrovascular reactivity with near infrared spectroscopy in head-injured patients. *J Neurotrauma* 27: 1951-1958.

Appendix A: ethics approval form



MACQUARIE ANIMAL RESEARCH AUTHORITY (ARA) University

AEC Reference No.: 2016/005

Date of Expiry: 29 March 2017

Full Approval Duration: 29 March 2016 to 29 March 2017 (12 months)

This ARA remains in force until the Date of Expiry (unless suspended, cancelled or surrendered) and will only be renewed upon receipt of a satisfactory Progress Report before expiry (see Approval email for submission details).

Principal Investigator:

Doctor Mark Butlin
Department of Biomedical Sciences
Macquarie University, NSW 2109
mark.butlin@mq.edu.au
0422 908 895

Associate Investigators:

Alberto Avolio 0408 657 616
Stuart Graham 0416 060 862
Dana Georgevsky 0431 685 528

In case of emergency, please contact:

the Principal Investigator / Associate Investigator named above
or **Manager, CAF: 9850 7780 / 0428 861 163 or Animal Welfare Officer: 9850 7758 / 0439 497 383**

The above-named are authorised by MACQUARIE UNIVERSITY ANIMAL ETHICS COMMITTEE to conduct the following research:

Title of the project: Intracranial pressure estimation from cardiovascular inputs

Purpose: 4 - Research: Human or Animal Biology

Aims: To investigate whether mean and pulse intracranial pressure can be accurately estimated from cardiovascular inputs and outputs such as the arterial pressure waveform and intra-ocular pulsations.

Surgical Procedures category: 2 - Animal Unconscious without Recovery

All procedures must be performed as per the AEC-approved protocol, unless stated otherwise by the AEC and/or AWO.

Maximum numbers approved (for the Full Approval Duration):

Species	Strain	Age/Weight/Sex	Total	Supplier/Source
02 - Rat	Sprague Dawley	12-20 weeks/any/any	25	ARC Perth
TOTAL			25	

Location of research:

Location	Full street address
Faculty of Medicine and Health Sciences	Level 1, F10A, 2 Technology Place, Macquarie University, NSW 2109
Central Animal Facility	Building F9A, Research Park Drive, Macquarie University, NSW 2109

Amendments approved by the AEC since initial approval: N/A

Conditions of Approval: N/A

Being animal research carried out in accordance with the Code of Practice for a recognised research purpose and in connection with animals (other than exempt animals) that have been obtained from the holder of an animal suppliers licence.

Professor Mark Connor (Chair, Animal Ethics Committee)

Approval Date: 18 February 2016